The thickness effect in adhesive bonded joints

THESIS REPORT

by

Cristina Mestre Rodriguez

in partial fulfillment of the requirements for the degree of

Master of Science
in Civil Engineering

at the Delft University of Technology,
to be defended publicly on 12 January 2018

Thesis committee:	Prof. dr. M. Veljkovic,	TU Delft, chair
	Dr. M. Pavlovic	TU Delft, supervisor
	Dr. ir. I. Schipperen	TNO, supervisor
	Dr. S. Teixeira de Freitas	TU Delft

TU Delft TNO innovation for life

ABSTRACT

Adhesive bonded joints are commonly used in structural applications. The thickness of the bondline has an important influence in the resistance of the joint. Information on this topic is mostly available for thin bondlines; up to 1 mm. However, little information is known about the effect of increasing the bondline thickness. This study consists of a literature study to analyze the trends on the mechanical properties such as shear strength, peel strength and fracture toughness due to increasing bondline thickness; an experimental part that studies the shear strength of double lap joints loaded in tension using one brittle and one ductile adhesive; and a numerical part that assesses whether the experimental results can be reproduced using Finite Element techniques. From the experiments, thickness dependency on multiple parameters such as the lap shear strength, the deformation capability and the strains at failure is proven. For both adhesives, the lap shear strength decreased with thickness. The Finite Element Analysis are able to accurately predict the failure initiation for the thick joints and the deformation capability up to yield for all the thicknesses.

Keywords: Thickness effect, adhesive, bonded joint, lap shear strength, cohesive failure mode

ACKNOWLEDGEMENTS

This work was supported by the Structural Dynamics department of TNO, which provided the sources to carry out the experiments. By doing my thesis at TNO I was able to make the most of the time spent during this project by being in a great environment. I would like to thank specially Dr. ir. Ingrid Schipperen, my daily supervisor at TNO, for her good guidance and transfer of knowledge in Finite Element modelling. I would like to thank also Sander and Lisa, who gave me tips and valuable sources to gain a better insight to the adhesive bonding.

Secondly, I would like to thank Dr. Marko Pavlovic for supervising my thesis and connecting students working on similar projects so that we could share points of view and knowledge on certain topics.

I would also like to thank Prof. dr. Veljkovic of Civil Engineering Faculty at TU Delft, chair of the committee, and Dr. Sofia Teixeira de Freitas of Aerospace Faculty at TU Delft for their valuable feedback and suggestions given at the progress meetings.

Last but not least, many thanks to my family and friends for being always supportive.

CONTENTS

LIST OF FIGURES

LIST OF TABLES

1 FRAME

1.1 INTRODUCTION

The use of composite materials is progressively increasing due to their high strength-to-weight ratio, low maintenance, high quality of the finished structure and excellent corrosion resistance. Composite materials have many applications. They have been used in the automotive and aerospace industries over the past 70 years and are becoming more popular in the civil engineering and infrastructure applications [3].

Often large structures are not composed of one part, or even one material. Among the different types of joining techniques, adhesive bonding is an inexpensive method commonly used in civil engineering applications [3]. This method has many advantages with respect to mechanical fastening techniques including low weight, more uniform stress distribution, elimination of notch effects and low fabrication costs [4]. Although it is widely used in the automotive and aerospace industries, adhesively bonded joints in civil engineering applications have essential differences, including the fabrication processes, loading, the bond geometries (adhesive and adherent thicknesses), curing conditions and service environments. In the automotive and aerospace industries, adhesive bonds are thin ($0.1 - 1$ mm) whereas in civil engineering applications adhesives are much thicker ($2 - 20$ mm) [4]. Although a lot is known already on the thinner bond lines, the effect of thicker bond lines is still unknown.

Furthermore, adhesively bonded joints are usually combined with bolts or rivets for safety reasons. However, this double fastening leads on one hand to a higher price per joint and on another hand, bolts create an interruption in the continuous fibres compromising the mechanical properties of the composite. Therefore, if both required stiffness and strength of the bonded joint can be ensured, bolts as a safety solution of the adhesive would be no longer necessary.

Composite-to-steel joints are important components in structures. The strength of composite-to-steel joints is influenced by different factors: the type of adhesive, the surface preparation and the adhesive bond line. The adhesive bond line is usually the weakest link in bonded joints. The load transfer from one structural member to another occurs in a localized region; hence it has a relatively low efficiency [5].

The main failure modes of bonded joints are cohesive failure, which occurs inside the adhesive, interfacial or adhesive failure, along the interface between the adhesive and the adherend, or adherend failure, known as plate failure for structural applications (Figure 1.1). [2] Plate failure occurs outside the bonded area possibly as a consequence of an inappropriate design. Therefore, this type of failure will not be the point of interest in this thesis and it will be avoided by choosing plates with high enough thickness.

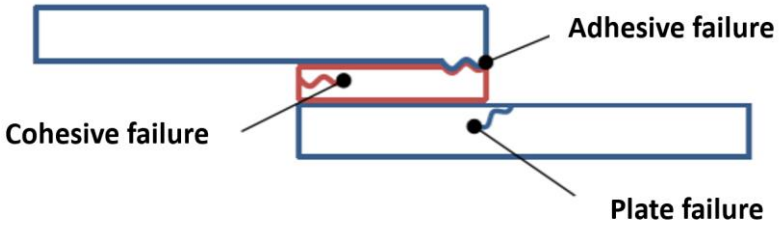

Figure 1.1 Side view of a single lap joint defining the failure modes

1.2 AIM AND OBJECTIVES

The aim of this thesis is to investigate the effect of increasing the thickness of bond lines on the mechanical behavior of adhesively bonded joints. The main objective is first, to analyze both experimentally and numerically what are the changes of the mechanical properties of the bond line when increasing the layer thickness. Secondly, compare the results obtained with both methods to see the feasibility to predict the failure mechanisms with finite element analyses.

The main research objectives intend to answer the following research questions.

1. What is the mechanical behavior of increasingly thicknesses bond lines up to 10 mm?
   1.1 What is the effect of the increasingly thickness on these parameters: Young's modulus, the failure strength and the failure strain.
   1.2 What is the expected failure mode for bond lines of thicknesses between 2 and 10 mm.

2. Is the strength of a thick bonded joint predictable?
   This means that if the critical element of the joint is the bond line and we know how it is expected to fail, there will be no need to include mechanical fasteners for safety reasons.

3. Can the mechanical behavior of thick bond lines be modelled using finite element methods?
   3.1 How can we model the mechanical behavior of thick bond lines.
   3.2 Do the finite element analyses recreate the failure mechanisms found in the experiments? Is it a reliable analysis method?

1.3 METHODOLOGY

A description of the approach and procedures followed in this project are explained below.

1. Literature study

In the first stage of the thesis, a literature study was carried out into the thickness effects in adhesively bonded structural joints. The literature study had two main focuses.

1.1 The range of thicknesses for which information is available.
1.2 The trends on the mechanical properties due to an increasing bond thickness.

The literature study is reported in Chapter 2.

2. Experiments

The experimental part studied the shear strength resistance of double lap joints loaded in tension under static loading. For this, two different adhesives were used, one used for civil applications and the other for maritime applications. The reason behind the choice of these two particular adhesives is because they are also material of study in the JIP project composite joints, the project to which this thesis is related.

Based on the literature review a few adhesive thicknesses were determined, which were to be used in the design of the specimens. The details of the properties and layouts of the specimens are given in a chapter that includes all the experimental procedure and results (Chapter 3).

In total, five different sets of samples were prepared, each with a different bondline thickness, thus addressing the thickness effect for a range between 1 and 10 mm.

The double lap joint specimens were tested up to failure to capture a complete force displacement curve. The parameters that were determined from the curve are the failure strength and the displacement at failure. It was studied if derived parameters could be obtained that would provide information on the material properties.

Finally, trends in the results were determined and empirical relations established.

3. Finite Element Analyses

Finite Element Analyses were performed to assess whether the experimental results could be reproduced using Finite Element techniques. Finite Element models were created in Abaqus. For this, different material parameters and failure models had to be considered in order to run the analyses. For the representation of the adhesive behavior, it was decided to use elasto-plastic models.

Special attention was given to the prediction of the change in the stress fields due to increasing thickness and the different failure modes seen in the experiments.

The Finite Element Analyses are reported in Chapter 4. A comparison between the experimental results and the Finite Element results is given in Chapter 5. Chapter 6 gives an insight to probabilistic models to determine the design resistance from the experimental results and includes information of the safety factors that should be used in the design of adhesively bonded joints. The final two chapters provide conclusions and recommendations, respectively.

1.4 LIMITATIONS

In this research the author faced a few limitations. First of all, the modifications in initial plan of studying the thickness effect of hybrid bonded joints. This was changed for the study of adhesively bonded steel-to-steel joints. The reason behind was to avoid the influence of having two different materials, which would have added an extra factor to take into consideration and would also have difficulted the understanding of this effect in the results.

In the experimental part of this study, there was also a limitation in the sample size. It was set to five samples per set-up, which is in accordance with the standards and gives enough idea on the spreading in the results. However, a higher sample size would have given a better approximation of the deviation in the geometrical parameters of the samples such as the width, thickness or overlap length, used in the determination of the safety factors (see Chapter 6). Hence, it would have resulted in no need of making use of Monte Carlo to extend the test results.

In the numerical part, there were also multiple limitations. The material parameters that were used as an input for the FE analysis were obtained in literature and in some cases they might not represent the actual material parameters. In some other cases the information required could not be found in literature, for instance the tensile or shear stress - strain curves of the adhesives. For that, it would

have been necessary to perform additional bulk tests. However, due to economical and time limitations, these additional material tests were not performed in this project.

Furthermore, an even more difficult limitation in terms of the FE analysis came when trying to apply the cohesive zone modelling, which is used to represent the behavior of the interface between two materials. In order to use this method, multiple material parameters of the adhesive are required, which are obtained performing different bulk tests and more important, are dependent on the thickness of the adhesive in every particular test. However, in the FE analysis the interface can be assigned with a zero thickness, which makes difficult then to compare with the material data that has to be given as input. Therefore, the understanding of how the different parameters affect the field outputs and how these outputs can be correlated to the experimental results, is of high complexity. A further explanation on this topic is given in the recommendations.

Another aspect to be highlighted is the fact that only two materials models were studied for the adhesive, whereas there might be many more (that required even more parameters that were unknown and as such would bring more uncertainties into the equation) that might be better suited to also study failure propagation. However, since the aim of this study was the study of the applicability of FE up to failure initiation, other models were not studied. Furthermore, seeing that the stress strain curve of Araldite, which is seen as a more brittle adhesive in this study, shows a plastic behavior, however short, the choice of plasticity based models seemed to be fair.

2 LITERATURE REVIEW

A literature review was first conducted in order to get a better understanding of adhesively bonded joints and collect the information available in literature about the adhesive thickness effect on the different mechanical properties. Section 2.1 is dedicated to the state of art of the adhesive bonding and explains the main engineering applications. Sections 2.2 compares this type of fastening among other types. Section 2.3 includes definitions used for the joint components and the types of loadings. Section 2.4 describes the parameters that affect the strength of a bonded joint, the different failure mechanisms and the durability of this type of joints. Section 2.5 explains the different types of joint configurations and the different stress distributions in the bondline. Section 2.6 describes the manufacturing process and the importance of the surface preparation. Section 2.7 includes the classification of adhesives and their properties. Furthermore, it also explains the different tests that describe the bulk properties of the adhesives. The next section, Section 2.8, includes the information available on the effect of adhesive thickness on the different mechanical properties. Section 2.9 includes a table with all the test methods and the corresponding properties to be tested, either for adhesives or for bonded joints. In Section 2.10 it is explained what is the effect of bondline thickness on the fracture of bonded joints. The last section, Section 2.11, is a proposal for the experiments that will be further explained in Section 3.

2.1 STATE OF ART

The adhesive bonding technology has been applied within many industries. Adhesively bonded FRP or steel joints have been used in composite profiles for aerospace and automotive industries over the past 70 years. However, they have been used for structural applications only for the last few decades. Differences between these applications include bond geometries (adhesive and adherend thicknesses), the fabrication processes, the loading conditions, the curing conditions and the service environments.

An adhesively bonded joint is fabricated by placing an adhesive between the two components that have to be joined [8]. After introducing the adhesive, it solidifies to produce the adhesive bond. The two other components, which are made of steel or FRP or one each of a different material, are known as adherend, substrate or in the particular case of structural applications, it is often referred as plate (see Figure 2.1).

In reference to the thickness of the adhesive layer; adhesive layers are usually thin in aerospace and automotive industries ($0.1 - 1$ mm), whereas in buildings and bridge structures adhesive layers are much thicker ($2 - 20$ mm), and can be up to 50 mm locally [4, 5].

There are different reasons why thicknesses differ considerably from one application to another. For instance, the joint geometry, production accuracies, the loading conditions and the operating environment are different [4]. The environmental conditions at which the joints are submitted condition the environmental durability, which is affected by the hot and wet (moisture) conditions. Other factors influencing the long-term performance are fatigue and ultraviolet radiation [4].

The curing temperatures also differ and are highly dependent on the type of adhesive. In the civil engineering industry ambient temperatures are usual because adhesives are commonly applied in-situ, whereas for aerospace applications, temperatures reach more than 100^{o}C, thus the adhesives are handled in laboratories. The longer exposure to high temperatures lead to an increase of curing

degree, higher glass transition temperatures and as a consequence, joints tend to be more durable [4].

2.2 COMPARISON WITH OTHER MECHANICAL TECHNIQUES

Adhesive bonding is a joining method that has many advantages with respect to mechanical fastening techniques. Some of these advantages are [7]:

- Lower overall weight;
- The ability to make almost invisible connections (aesthetics);
- The ability to design and produce any type of complex configurations;
- More uniform stress distribution;
- The elimination of notch effects;
- The better control of the tolerances;
- Properties of adherends (cross section area, straightness, material behaviour) are unaffected;
- Lower fabrication costs
- Galvanic corrosion between dissimilar adherends is avoided
- The advantageous properties of the adhesive layer against electricity, heat and sound;
- The advantageous sealing properties of the adhesive layer against gases, moisture or chemicals.

There are also several disadvantages that have to be considered:

- The complexity of the manufacturing process (surfaces preparation, preparation of the adhesive, pressure and humidity conditions, control of the process and use of equipment);
- The curing time and temperature during which the adherends are joined;
- High influence of the environmental conditions on the durability;
- The properties of the adhesive are affected by temperature and are time dependent (durability);
- The difficulty to effectively dissemble the joints for repair purposes or re-use of the materials;
- The possibility of toxicity with respective effect on environment and labor conditions.

The design of adhesive bonded joints must take into account the advantages of using this type of joint but also to overcome disadvantages.

2.3 CLASSIFICATIONS AND DEFINITIONS

2.3.1 Important parameters

For structural applications joints in which load is to be transferred from one adherend to the other are referred to as structural adhesively bonded joints [7].

The typical connection layout between the adherends (plates, profiles) and the adhesive and their parameter definition is shown in the figure below.

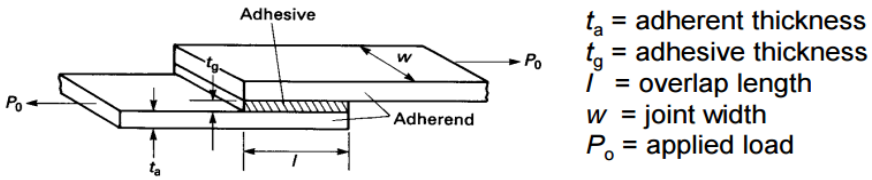

Figure 2.1 Parameters of a single-lap bonded joint under tension [24]

The overlap length is one of the most important parameters determining the strength of the joint. Figure 2.1 shows the fracture load and fracture average stress of a single lap joint as a function of overlap length.

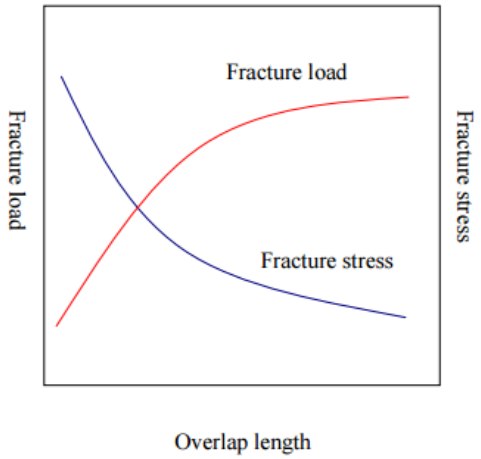

Figure 2.2 Relationship between overlap length, fracture load and fracture stress [9]

2.3.2 Loading modes of bonded joints

There are four main types of loading of adhesive bonded joints [24]; see Figure 2.3.

- Tensile stresses produced by out-of-plane tensile loads.
- Shear stresses caused by tensile-shear, torsional or pure shear loads imposed on the adherends.
- Cleavage loading caused by out-of-plane tensile loads acting on stiff and thick adherends at the ends of the joint.
- Peel loading caused by out-of-plane loads acting on thin adherends.

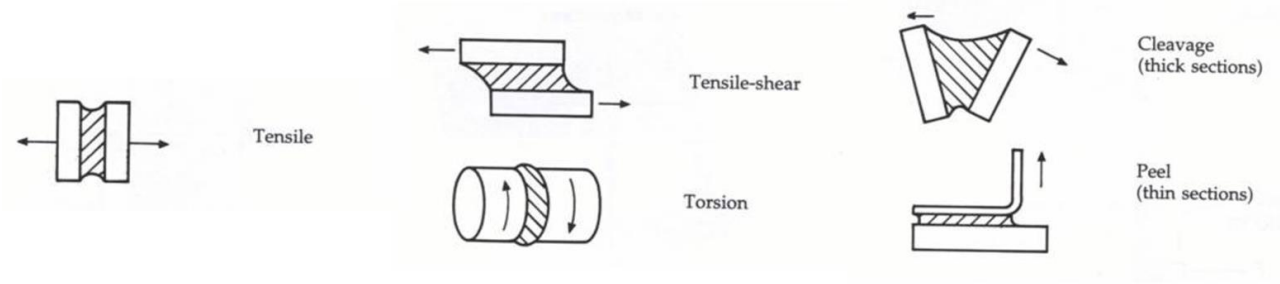

Figure 2.3 Loading modes of bonded joints [24]

2.4 STRUCTURAL BEHAVIOR OF ADHESIVELY BONDED JOINTS

2.4.1 Mechanical properties. Strength of the joint

The strength of a joint depends, for a given type of load, on the stress distribution within the joint. The stress distribution in turn is conditioned by the joint geometry and the mechanical properties of the adhesive and the adherends.

The surface preparation (see point 5.1) can improve the bonding quality between the adherends and the adhesive. Another important factor in the strength of the joint is the bondline itself. It is known from literature that the strength of a joint increases with decreasing bond line thickness. Next to bonding quality and bondline, the adherends could determine the bond strength. However, the adhesive bondline is usually the weakest link in bonded joints because the load is transferred from one adherend to another within a very localized region [5].

2.4.2 Failure modes

The failure modes of bonded joints can be classified in three main types:

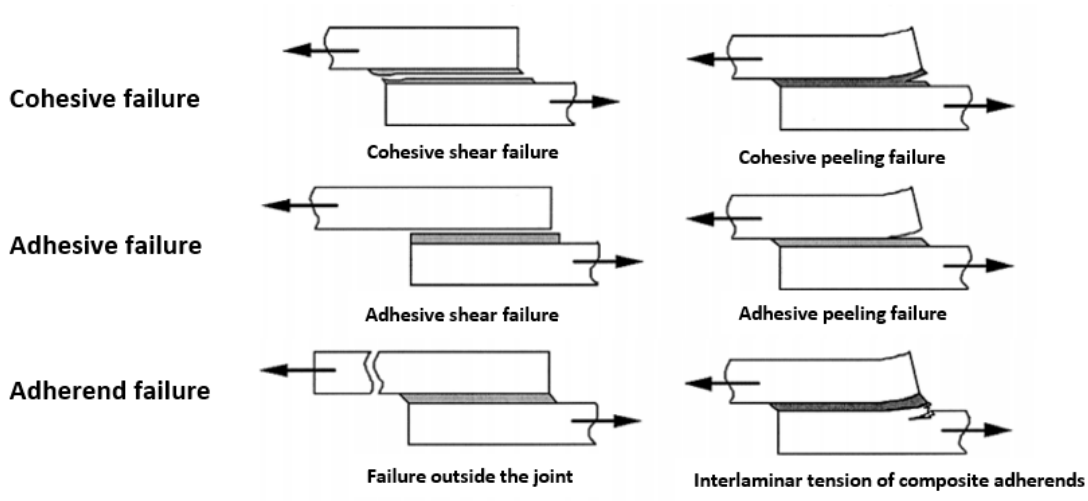

Figure 2.4 Classification of failure modes [11]

- **Cohesive failure**; failure of the adhesive. It is a localised effect, occurring due to excessive shear or peeling strains at points of high stress concentrations (i.e. at the end of the overlap

for a single-lap joint). The development of cohesive failure is influenced by the adhesive type; in case the adhesive is brittle, cohesive failure will mostly be caused by brittle fracture [11].

- **Adhesive or interface failure**, occurring along the interface between the adhesive and the adherend due to insufficient adhesion. The excessive stain/stress concentrations at the interface can be caused either because the chosen adhesive and/or adherend material combination is not suitable or because the preparation of the surfaces was not appropriate [13].

- **Adherend failure**, known as plate failure for structural applications. Adherend failure occurs outside the bonded area most possibly because of an inappropriate design. The adherend fails in tension or in the form of delamination within the FRP laminas. This would be the preferred failure mode in terms of maximum capacity of the joint being utilised; however, it occurs very rare occasions [11].

Cohesive failure is of high interest for this thesis because it is a preferred failure mode due to its more predictable bulk characteristic. Adhesive failure instead, is less predictable because of the effect of surface preparation which might influence considerably the failure behaviour.

Depending on which stresses are the cause of the failure, shear or peel, each type of failure can be subdivided in two failures, so in total there are six failure modes, shown in Figure 2.4.

Some rules and regulations define even more types of failure. However, those can be classified in the ones mentioned above, which are most commonly used.

2.4.3 Durability

The effectiveness of the joint depends on the quality, integrity and durability of the adhesive bond. There are several properties (see Figure 2.5) that determine the environmental durability of adhesive bonded joints, which also determine the entire life time of the structure [3]. For the joint applications relevant to this thesis, temperature, moisture content and ultraviolet radiation are the main environmental degrading phenomena.

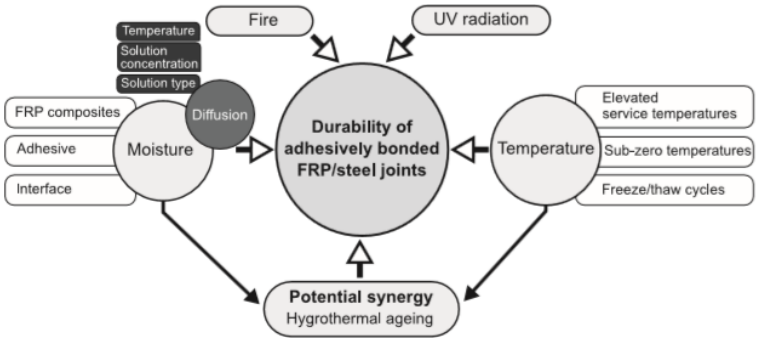

Figure 2.5 Environmental factors influencing the durability of adhesively FRP/steel joints [3]

For example, moisture can attack the FRP composites by one or a combination of the following mechanisms: alteration of the resin matrix, damage of the fibre/matrix interface, fibre-level degradation. As shown in Figure 2.6, moisture content reduces the strength and the elastic modulus of adhesives [3].

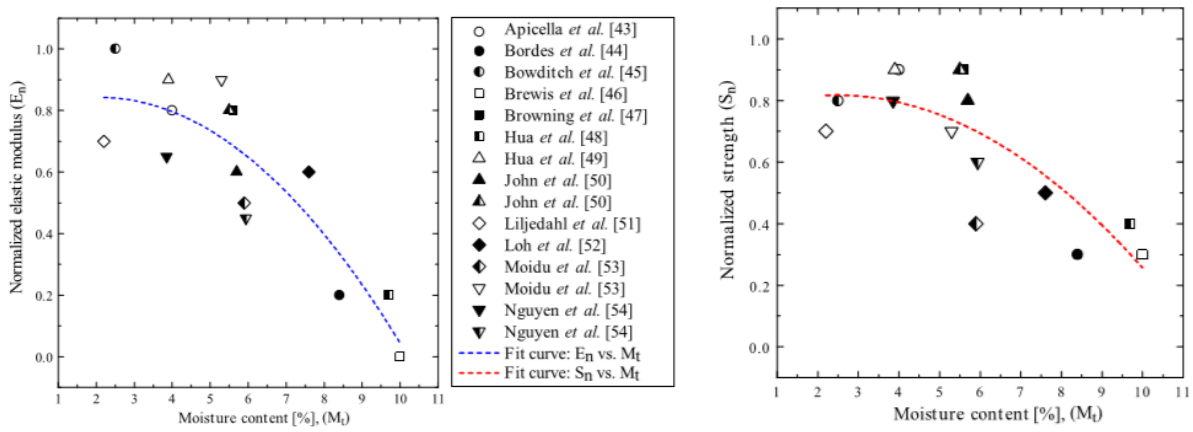

Figure 2.6 Influence of moisture content in the elastic modulus and the strength. Adhesive: multiple; Test method: multiple vapor and liquid sorption tests [3]

For the aim of this thesis, the study of the thickness effect of adhesively bonded joints, these factors affecting the durability are excluded from the subject of study to avoid the mixing of several effects.

2. 5 DESIGN OF ADHESIVE BONDED JOINTS

The development of reliable design and methodologies to predict failure can be expected to result in more efficient use of the composites and the adhesives. In order to predict the structural behavior of the adhesively bonded joints it is necessary to analyze them [8]. The two main objectives are:

- To determine the stresses and strains under a given loading;
- To predict the probable points of failure.

Adhesives can carry higher compressive and shear forces than tensile and peeling. Thus, the design of adhesively bonded joints has to ensure that the joint is subjected primarily to shear and compression and creates minimal out-of-plane, cleavage and direct tensile peeling forces [11].

2.5.1 Joint configuration

A wide range of joints are available in structural design. The common configurations that were analyzed in the literature are single-lap, double-lap, stepped-lap and scarf joints (See Figure 2.7).

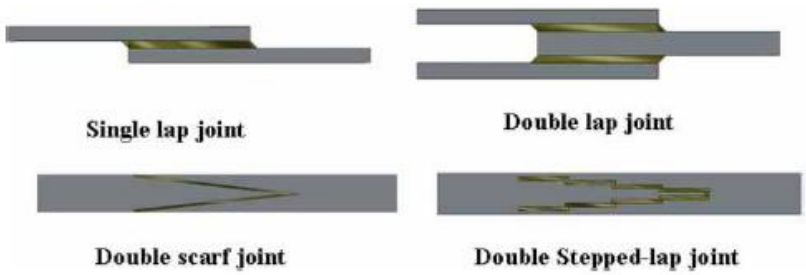

Figure 2.7 Adhesively bonded joint configurations [8]

Every configuration has a particular stress distribution within the joint, which also depends on the mechanical properties of the adhesives and the adherend [8]. For a single-lap joint, both shear and peeling stresses are concentrated at the end of the bonded joint (see Figure 2.8, left). Also note the

constant stress along the central part of the overlap length. For a double-lap joint, the shear stress distribution is similar to a single-lap joint, with peak shear stresses at both ends. However normal stresses show a different trend. On Figure 2.8, right, it is shown a comparison of the peel stresses for these two configurations.

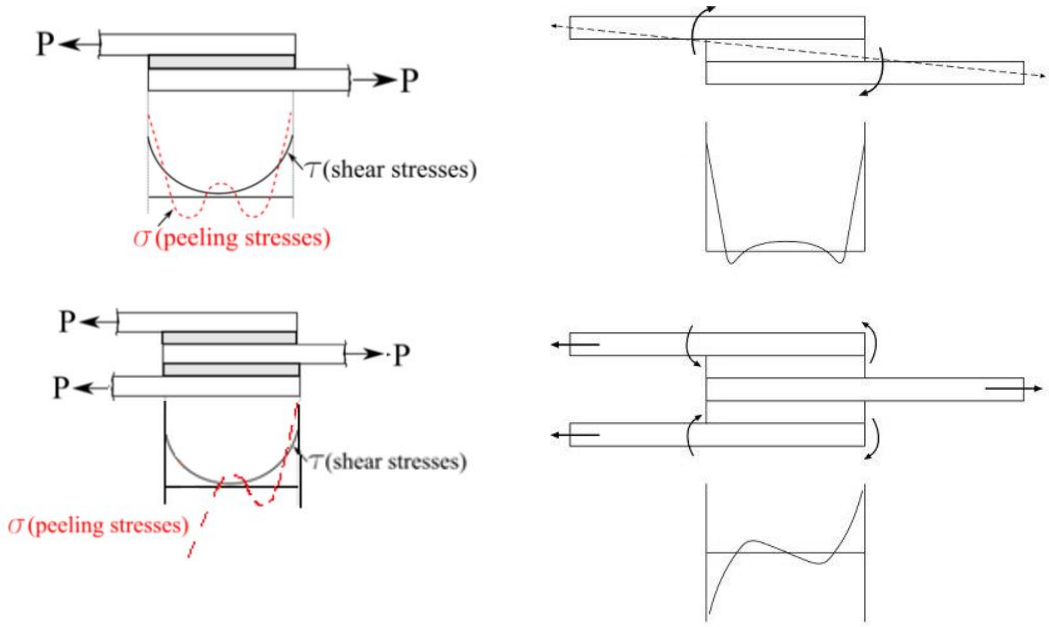

Figure 2.8 Shear and peel stresses of a single-lap joint (left) [8]. Comparison of peeling stresses for a SLJ and a DLJ (right)

For FRP composite adherends, it is important to underline the high through-thickness stresses at the overlap ends, due to the relatively low through-thickness strength of most composite materials. Therefore, joints with high strength adhesives are more likely to fail in the adherend before failure occurs in the adhesive (See Figure 2.9) [8].

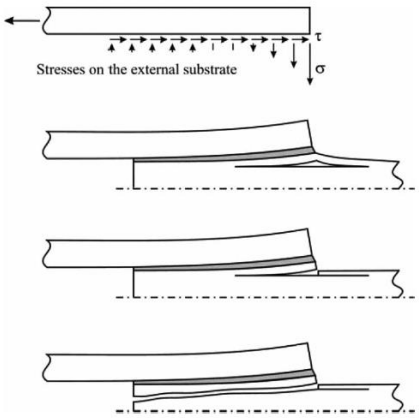

Figure 2.9 Failure in the adherend due to the application of a high strength adhesive [8]

The joint must be designed to reduce the stress concentrations. However, stresses from peel and cleavage should be minimized. Shaping of the adherend edges is also a common practice to decrease the peel stresses in this type of joints [8]. Furthermore, it limits the stress concentrations. This is the reason the specimens used in this thesis have a curved edge, which is the optimal shape to reduce the stress concentrations.

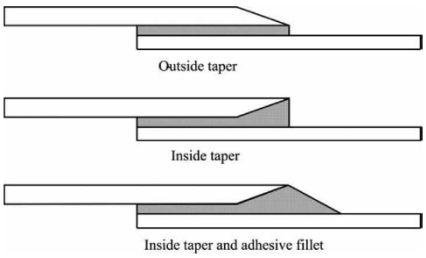

Figure 2.10 Peel stresses reduction by applying adherend shaping [8]

Double lap joint is a symmetric configuration where failure occurs due to shear stresses. Since it is symmetric, bending moment is not or only limited produced on the adherends; thereby excluding or limiting peel. Hence, shear failure will occur before peel failure. This is not the case of the asymmetric single lap joints design.

2.5.2 Peeling and shear strains

Haghani [13] performed a numerical and experimental study of adhesively bonded double-lap specimens consisting of one steel plate in the middle and two FRP laminates bonded on both sides. Two different epoxy adhesives were used in this study, a Sika system (Sika carbodur S624 laminate and Sikadur 330 epoxy) and a STO system (StoBPE primer 50 super BPE 4014 UHM laminate and StoBPE lim 567 epoxy). The stress-strain curve for these two different adhesive types for a thickness of 3.4 mm and 2 mm, respectively, as shown in Figure 2.11.

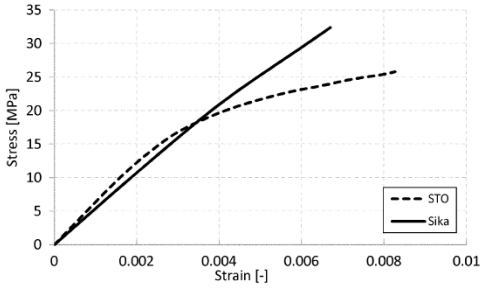

Figure 2.11 Stress-strain curves of two adhesives used in a study by Haghani [13]

In the stated study, FE models were used for both orthotropic and isotropic FRP laminates. By means of optic measurement techniques, the distribution of strain in the adhesive was investigated resulting in the following curves (see Figure 2.12) [13]. Please note that these curves represent only 35 mm distance from the edge and not the complete overlap length. Thus, they are meant to explain the distribution of the strains near the edge but not along the complete overlap length.

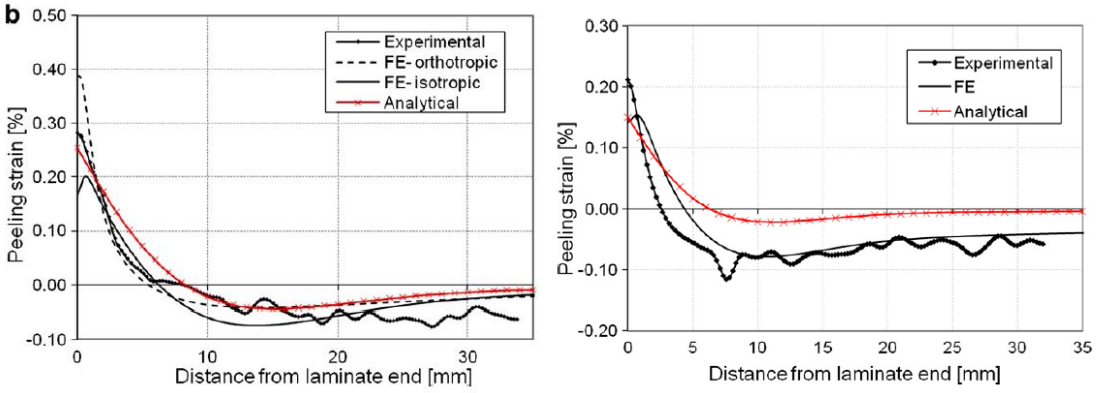

Figure 2.12 Comparison of FE, experimental and analytical results for peeling strain at 80 kN for STO specimen (left) and for Sika specimen (right) [13]

When studying the load-transfer mechanism in bonded joints it is very important to examine the distribution of strains through the adhesive thickness. One of the locations of more interest along the bond line where the strain distribution should be checked is the area near to the end of the laminate. In this location shear lag effect is observed and it is likely that failure initiates [13].

The following figures show the distribution of shear and peeling strains through the adhesive thickness (plotted from 0.5 mm from the end of the laminate to end; 2 mm thickness) for a constant load.

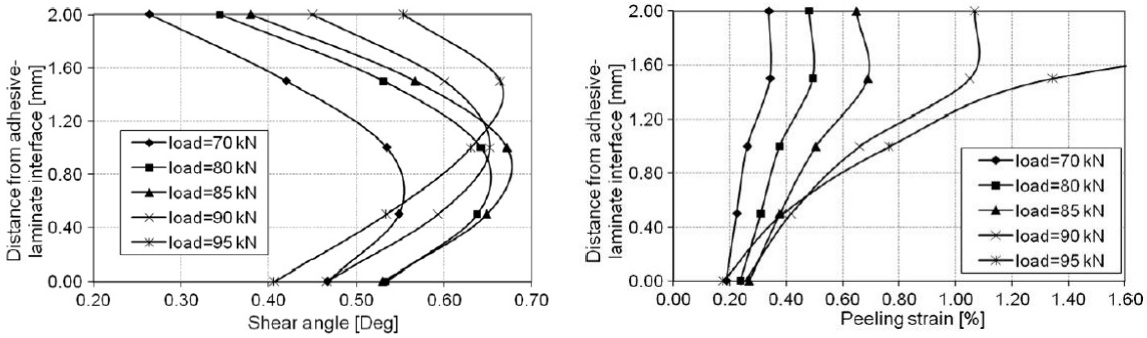

Figure 2.13 Shear (left) and peeling (right) strain distributions along thickness (t= 2 mm) [13]

Note that for the lower load levels the shear strain at the adhesive-FRP laminate interface is larger than that at the steel-adhesive interface. This fact is due to the adhesive is more restrained when in contact to the steel interface than to the laminate interface. The FRP laminate has a small E-modulus in the direction perpendicular to the fibres, which allows the transverse translational displacement of the laminate and also a higher shear deformation, compared to the steel plate. However, this is valid up to a certain load level (90kN), after which the strains at the steel-adhesive interface will also reach high values.

When comparing both graphs we can see that the shear strain distribution follows the same pattern when increasing the load, with a maximum value at around half-thickness. Furthermore, the peeling strain distribution shows a high concentration at the steel-adhesive interfece when increasing the loading.

Figure 2.14 proves that strain distribution for both peeling and shear components at a fixed load (80 kN) tend to become more uniform when increasing the distance from the interface of the laminate, due to the reduction of the shear lag effect.

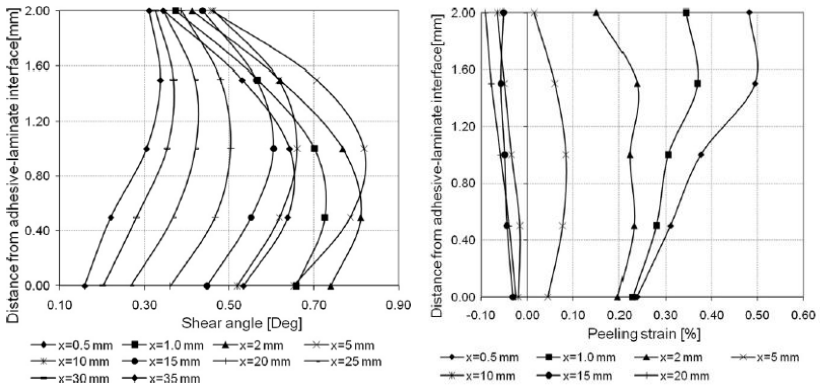

Figure 2.14 Distribution of shear(left) and peeling(right) strain through the thickness at different locations (load=80 kN) [13]

2.6 MANUFACTURING PROCESS

Thick adhesive layers usually lead to more defects in the joint, due to the fact that the manufacturing process is more complicated. For this reason, special attention has to be paid to the manufacturing of specimens, which has to be followed by a quality control. Defects can be either in the adhesive itself or in the surface. The defects in the adhesive are thickness-related because the relative displacement of the adherends is higher for thicker adhesive layers, resulting in more voids in the adhesive as well as higher thermal shrinkage during curing [42]. However, the surface defects have no relation with the adhesive thickness and can be minimized with a good surface preparation before the bonding takes place (See Section 6.1).

2.6.1 Surface preparation

The preparation of the surfaces prior to bonding is one of the most important processes determining the quality of the adhesively bonded joint [9]. The application of a pretreatment on the surfaces can even provide additional beneficial properties to the surfaces. It is a recommended procedure in order to achieve maximum mechanical strength [8].

As suggested by Davis and Bond [10], the most important step in the surface preparation process is the formation of a suitable surface chemistry because the integrity of the durability of the adhesive bond is directly influenced by the integrity of the adherends' surface. They investigated the factors affecting the durability of adhesively bonded joints and found that a "clean surface" is a necessary condition for adhesion but not sufficient for bond durability.

The structural adhesives create a chemical bonding between the adherend surface atoms and the atoms of the adhesive. These chemical links are the mechanism used to transfer the loads between the adherends. The failures in the adhesive bond (causing adhesive failure) are mostly attributed to poor processes during the fabrication, where the lack of surface preparation is the most relevant deficiency [8]. Possible composite surface treatments include abrasion/solvent cleaning techniques for thermosets composites and surface chemistry and surface topographical changes for thermoplastic composites, so that durable and strong bond can be ensured [8]. In case of steel surface treatment, possible treatments are sandblasting and solvent cleaning, for instance with Acetone.

The effects of surface treatment are the decrease of water contact angle, increase surface tension, increase surface roughness and change surface chemistry, which lead to an increase of the bond strength and durability [8].

2.7 ADHESIVES

2.7.1 Types and properties of adhesives

Many types of adhesives are used for structural applications including epoxies, acrylics, polyurethanes, silicones and high-temperature adhesives (phenolics, polymides and bismaleimides); see table below.

Adhesive type	Properties	Service temp. (ºC)	Tensile strength at Break [MPa]	Shear strength [MPa]	Tensile Modulus (Young's Modulus) [MPa]
Epoxy	High strength and temperature resistance, easy to use and low cost.	-40 to +100	13.4 to 246.8	3.9 to 53.4	186 to 18409
Acrylics	Versatile adhesives with capabilities of fast curing and tolerate dirtier and less prepared surfaces	-40 to +120	18.6 to 75.2	-	806.3 to 3530
Polyurethanes (PU)	Good flexibility at low temperatures, resistant to fatigue, impact resistance and durability.	-200 to +80	16.8 to 62	-	4.8 to 2193
Silicones	Excellent sealant for low stress applications, high degree of flexibility and very-high temperature resistance.	-60 to +300	2.6 to 9	-	0.3 to 0.4
Phenolics	Good strength for short-time, limited resistance to thermal shocks.	-40 to +175	34.5 to 69	-	2.7 to 17237
Polymides	Thermal stability, many factors dependent, difficult processability.	-40 to +250	96 to 156	-	3392 to 3882
Bismaleimides (BMI)	Very rigid, low peel properties.	-50 to +200	90 to 554		

Table 2.1 Properties of adhesives. Nominal values obtained from test methods ASTM [8, 34, 35]

Table 2.1 was created with information from multiple commercial brochures and one paper [8]. However, the shear strength of most of these adhesives is not specified by the producer and was left blank.

Manufacturers generally define an adhesive as structural if it can withstand a force of at least 6.9 MPa in a lap shear coupon test, when bonding metal and testing it at room temperature.

Adhesives can be classified as brittle or ductile, depending on their capacity to undergo plastic deformation and their energy absorption before fracture. The adhesive behaviour is dependent on the temperature, being generally brittle at low temperatures and ductile at high temperatures (200 ºC or higher) [21]. It is important to highlight that the same adhesive can behave both as ductile or brittle depending on the actual temperature at which it is submitted during use.

To determine the stresses and strains of the adhesives it is necessary to determine their mechanical properties; in particular the stress-strain curves and the modulus of elasticity. As it can be seen in Figure 2.15, the stress-strain curves are non-linear. This is a common behaviour for both tension and shear. Brittle adhesives show a slight non-linearity before final fracture [11]. As observed by Haghani [13], the non-linearity of an adhesive, even at low load levels, might contribute to the large redistribution of strain along the bond line.

As a general rule, adhesives that are less rigid than their adherends are chosen in order to minimise the stress concentrations within the joint.

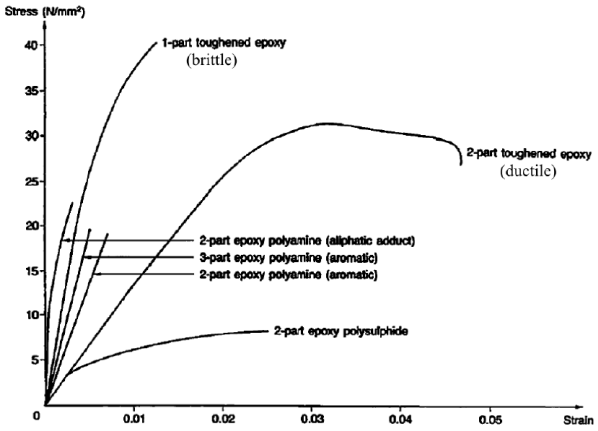

Figure 2.15 Tension strain-stress relationship for different adhesives [11]

2.7.2 Bulk material properties of adhesives

A list of standards issued by the American Society for Testing Materials (ASTM), the British Standards Institution (BSI) and the International Organization for Standardization (ISO) establishes different approaches to measure the properties of bulk adhesive specimens.

Bulk specimens can be cast and machined to the required shape; machining is not needed for many liquid and film adhesives which can easily be cast into bulk specimens [23]. This section briefly explains the specimen preparation, test methods and standards. Further details of the presented methods can be found in the referenced standards (see Table 2.2).

Mechanical properties of adhesives are dependent on the temperature. Thus it is necessary to select first different temperatures at which strength properties will be measured in order to obtain a strength profile over the temperature range [21].

The standard ISO 15166 includes the methods of preparing bulk specimens. It differentiates between two-part systems with adhesives cured at ambient or higher temperature (Part 1) and single component systems that require elevated temperature for the curing of the adhesive (Part 2). The importance of the specimen surface should be highlighted. This must not contain defects or damages such as scratches and nicks, which may affect the results of the tests. Specimens may be molded to shape or cut from plates and then polished in case of surface defects which have to be removed [25].

The three main bulk material properties that are presented below are tension, shear and compression.

2.7.2.1. Tension

The tensile properties (modulus of elasticity, Poisson's ratio, tensile strength and failure strain) can be determined by monotonic loading of a waisted specimen in tension. Specimens are waisted to ensure that the maximum strain occurs at the middle of the gauge-length. Geometries and test specifications for tensile properties are determined by the standard ISO 527-2 [26]. Tensile testing of bulk adhesive may be performed by casting or machining either straight-sided or tapered specimens [22]. Longitudinal and transversal strains are measured with gauges, contacting extensometers or video extensometers (non-contact technique). Contact techniques are recommended for accurate measurements of small strains, modulus of elasticity and Poisson's ratio determination; whereas non-

contact extensometers are preferred when determining the failure strains. Tensile tests are designed to be performed at any temperature conditions and they are also compatible with long-term testing such as fatigue or creep under non-ambient temperatures [24].

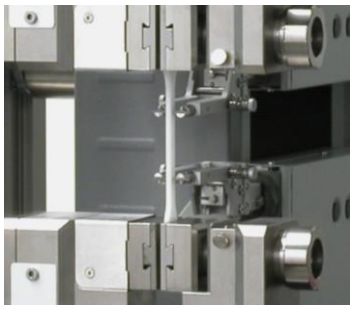

Figure 2.16 Tensile test set-up for molding and extrusion plastics according to standard ISO 527-2 [26]

2.7.2.2. Shear

The shear properties determination of bulk adhesives may be accomplished through several methods. For instance, the V-notched beam test specified by the standard ASTM D5379 [27], which can be used to determine through-thickness shear properties such as shear strength and shear modulus. The specimen used for the V-notched beam test is a rectangular beam with a two-sided 90 degrees angle notch in the middle of the beam. It is mounted in two specially designed test fixtures (see Figure 2.17).

Figure 2.17 V-notched beam test, fixture and specimen according to standard ASTM D 5379 [24]

Due to the complexity of the clamping system, this test is only suited for quasi-static loading, at loading rates under a certain limit. The specimen is monotonically loaded in compression, resulting in a nearly uniform shear stress in the notched section of the specimen. The strain field can be calculated based on the measured crosshead displacement of the loading device. Alternatively, it can be directly obtained either with two bonded strain gauges or by use of DIC measurements. In Figure 2.18, the black rectangles, centered about the loading axis, show the location of the strain gauges. For this test the failure of the specimen is highly dependent on the microstructure of the material [24].

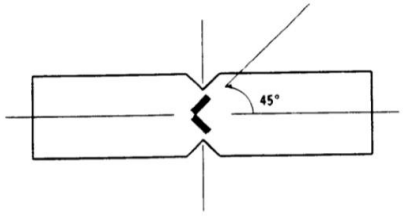

Figure 2.18 Side view of V-notched beam specimen [27]

The shear bondline properties can also be measured with the Thick Adherend Shear Test (TAST) according to the standard ISO 11003-2. This method is widely used because the specimens are easier to prepare and to test than with the V-notched beam [41]. When performing the TAST there is an extensometer that measures not only the adhesive displacement but also the adherend displacement. For this reason, it is necessary to apply a correction factor to the measured displacements in order to obtain only the adhesive displacement. According to the standard, this correction factor should be deducted from the measurement of the shear strain on a "dummy" specimen consisting of the adherend material alone [41]. For the fabrication of the specimens the standard recommends the machining (cutting) of two plates bonded together [28].

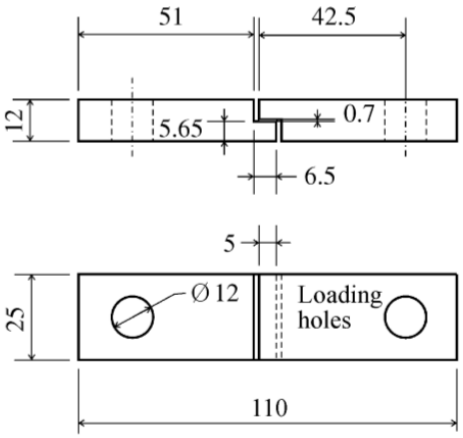

Figure 2.19 TAST specimen layout (dimensions in mm) [41]

2.7.2.3. Compression

Current methods for determining compression properties of adhesives are limited. ISO 604 [29] includes a method to measure elastic properties of thick square cross-sections. ASTM D695 [30] is suitable for measuring strength and elastic properties of adhesives.

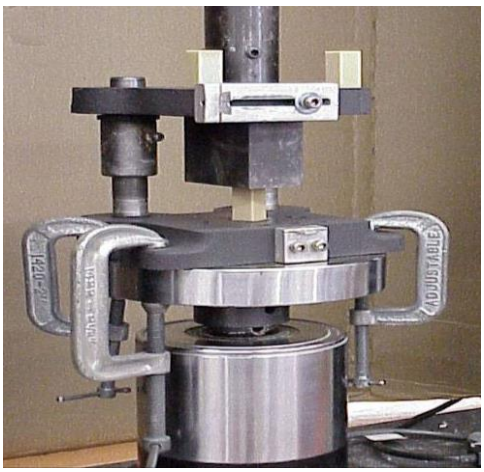

Figure 2.20 Compression test set-up according to standard ASTM D695 [30]

For this test method, specimens can either be blocks or cylinders. According to ASTM D695, the typical dimensions of the blocks are 12.7 by 12.7 by 25.4 mm and cylinders dimensions are 12.7 mm in diameter by 25.4 mm. Specimens are loaded under direct compression. Longitudinal and transversal strains are measured by making use of strain gauges [24].

2.8 TRENDS OF THE MECHANICAL PROPERTIES WHEN INCREASING BOND THICKNESS

From all the literature we will focus on the effect of adhesive thickness on these parameters:

- Shear strength (7.1)
- Peel strength (7.2)
- Fracture toughness / fracture energy (7.3)

It was seen that the shear modulus and the tensile (or Young's) modulus are not dependent on the thickness. They remain constant for every adhesive thickness. For this reason, these two parameters will not be discussed further.

2.8.1 Shear strength

- Experimental analysis (Single-lap joints)

Multiple investigations have been made in order to provide the thickness effect on the resistance of a single-lap joint using analytical models, finite element methods and/or experiment tests. However, the relationship between the strength of a single-lap joint and the adhesive thickness is still not well understood. Whereas the classical elastic analyses predict high strength for increasingly adhesive thicknesses, experimental results show the opposite results [15].

Performed experiments using epoxy as adhesive have found that for adhesive thicknesses up to 1 mm, the highest lap shear strength occurs for a thickness of 0.4 mm. After this value (0.6 to 1 mm), the shear strength decreases significantly, most probably due to the change of the adhesive from ductile to brittle because of its elastic-plastic behavior. The increase of adhesive thickness from 0.4 to 1 mm is inversely proportional to the value of the joint strength. The decrease in the lap strength is explained by the fact that with increasing thickness the bond line is affected by voids and microcracks in larger amount, thus reducing the bonding capacity [14].

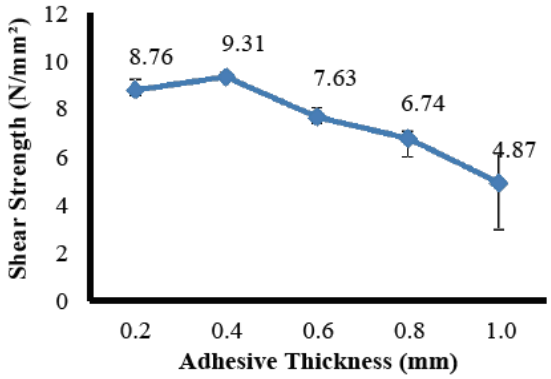

Figure 2.21 Relationship between lap shear strength and adhesive thickness (up to 1 mm). Adhesive: epoxy; Adherend: Aluminium A1 2024; Test method: ASTM D 1002 [14]

By means of experiments and statistical analyses based on Weibull distribution the influence of the adhesive thickness was studied on the mechanical behavior of the joint, proposing then an "optimal" thickness combining both reliability and best mechanical performance [15].

Experiments with adhesive thickness between 0.4 and 0.8 mm proved again that the shear failures are essentially cohesive and the average value of the shear strength decreases when the thickness of the

adhesive is increased (see Figure 2.22). In this figure also the minimum shear strength is shown; an important parameter when designing the joints [15].

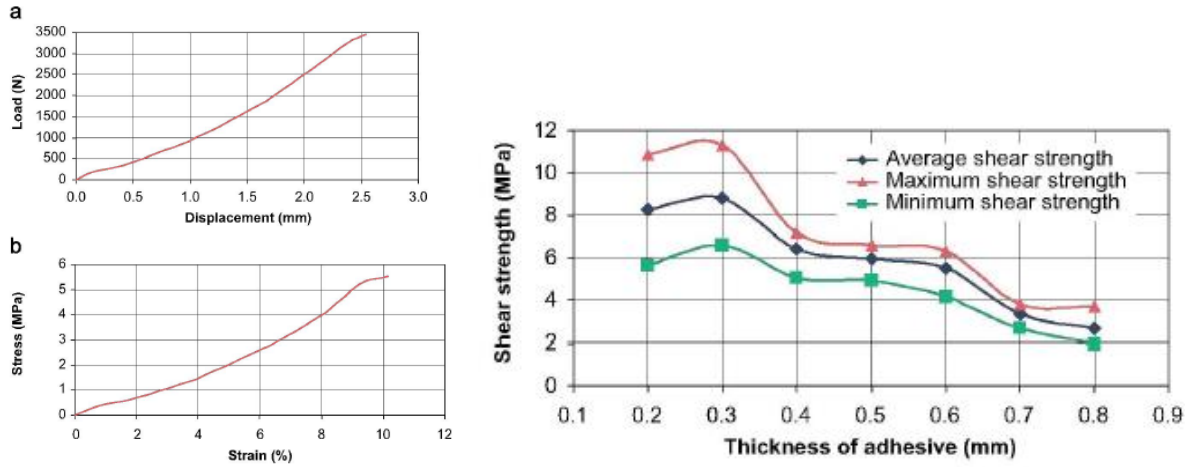

Figure 2.22 Shear strength as a function of the adhesive thickness (up to 0.8 mm). Adhesive: Acrylic ; Adhered: 6160 Aluminium alloy ; Test method: Shear tensile strength test UNE-EN 1465 [15]

The use of Weibull distribution brings to the most suitable thickness for this specific adhesive between 0.4 and 0.5 mm, setting 0.5 mm as the optimum (See Figure 2.23). This methodology is applicable for an easier design of more reliable adhesive joints [15].

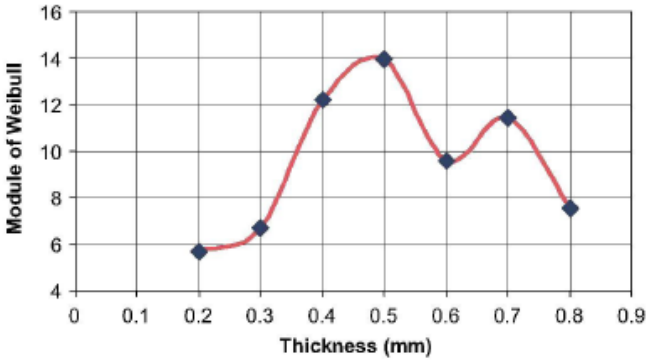

Figure 2.23 Weibull module variation depending on adhesive thickness (up to 0.8 mm). Adhesive: Acrylic; Test method: Weibull distribution [15]

A report from the U.S. Department of Transportation [19] uses different test matrices to determine the dimensions of the single-lap specimens that are tested with variable thickness, up to 0.14 inches (3.6 mm) [19]. The Figure 2.24 shows the results from using both ASTM D3165 and ASTM D5656, the later leading to a higher apparent shear strength.

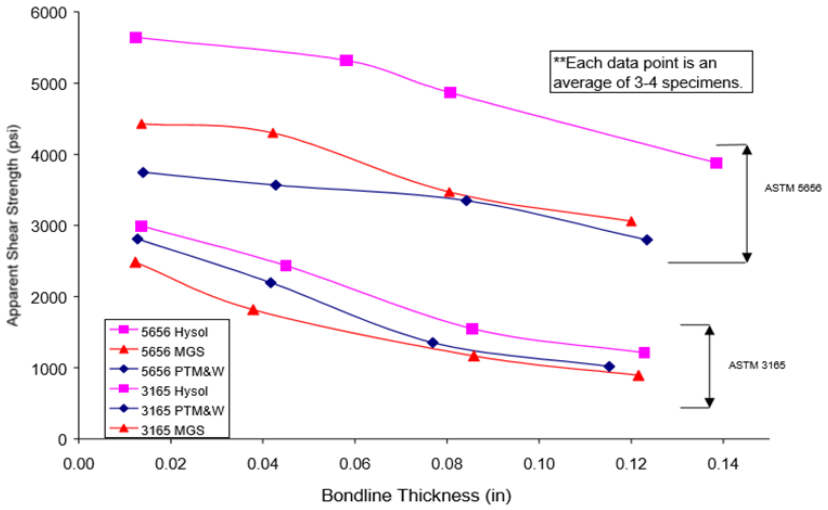

Figure 2.24 Apparent lap shear strength versus bondline thickness (up to 3.6 mm) for 3 different adhesive systems. Adhesives: epoxies, Adherends: Aluminium; Test methods: ASTM D 3165 and ASTM D 5656 [19]

The following figures show the layout of the specimens and the deformed shape corresponding to both tests. On the left, the specimen of ASTM D3165; on the right, specimens corresponding to ASTM D5656.

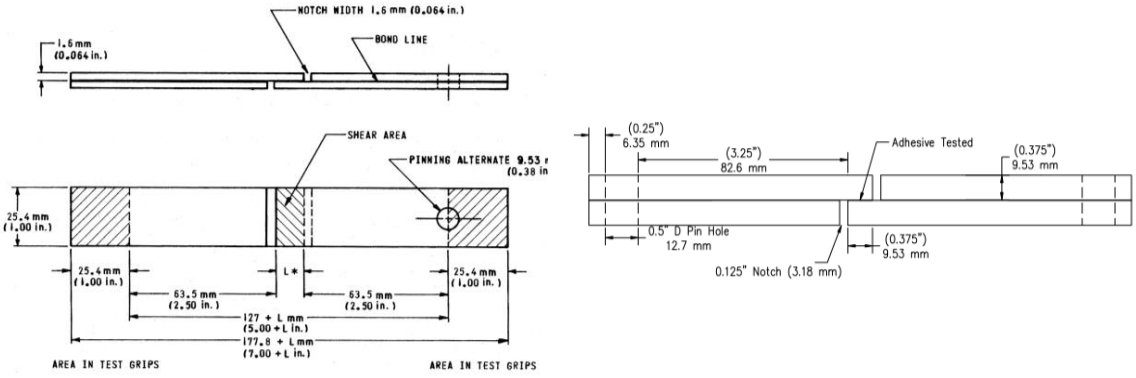

FIGURE 2. ASTM D 3165 TEST SPECIMEN PROFILE [6]

Figure 2.25 ASTM D 3165 (Left) ; ASTM D 5656 (Right) [19]

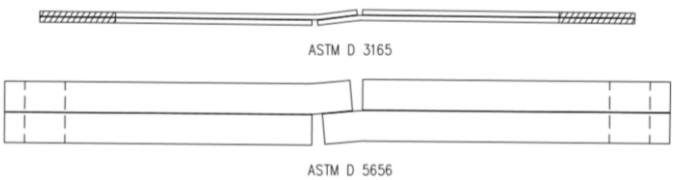

Figure 2.26 Test specimen deformation under loading [19]

Standard method ASTM D3165 is applied for thin adherends whereas standard ASTM D5656 is used; for thick adherends. In the first case, specimens show a combined state of shear and high peel stresses which results in a much lower measured lap shear strength as shown in Figure 2.24. Therefore, ASTM D5656 can provide more reliable information of the shear strength and it is used to determine the stress-strain behavior of adhesives in shear by tension loading. However, this standard is valid only for aluminum adherends.

Once more, it was confirmed that the apparent shear strength decreases when increasing the adhesive thickness. It was also found that for thick-adherend specimens, systems were largely

cohesive in nature even for large adhesive thicknesses [19]. Figure 2.27 shows the variation in the apparent shear strength for different adherend materials when increasing the bond line thickness Thus we can state that the apparent shear strength is highly dependent on the adherend bending stiffness. Therefore, the use of a proper thick-adherend configuration will ensure that the adhesive shear strength is not influenced by the properties of the adherend [19].

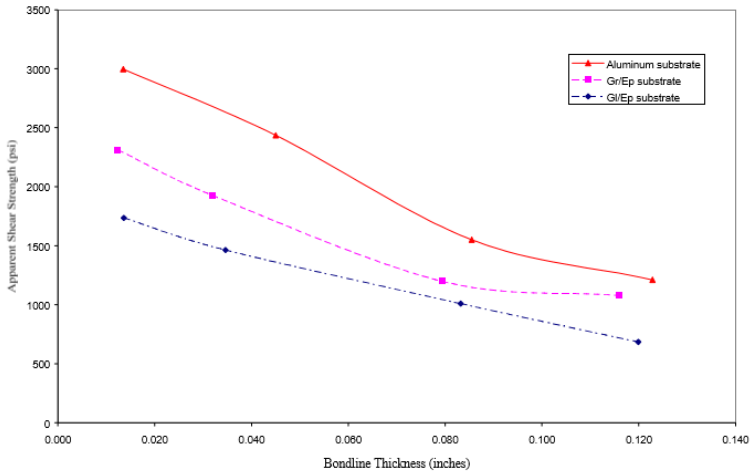

Figure 2.27 Apparent shear strength versus bondline thickness (up to 3.6 mm) for 3 different adherend types. Adhesive: Hysol EA9343 paste adhesive (epoxy), Adherends: Aluminum, Glass fiber, Carbon fiber; Test method: ASTM D 3165 [19]

The following figure collects all the different sources analyzed in the literature referring to the thickness effect on the shear strength. The general trend of linear decrease for increasing adhesive thickness remains valid for all epoxies and polyurethanes.

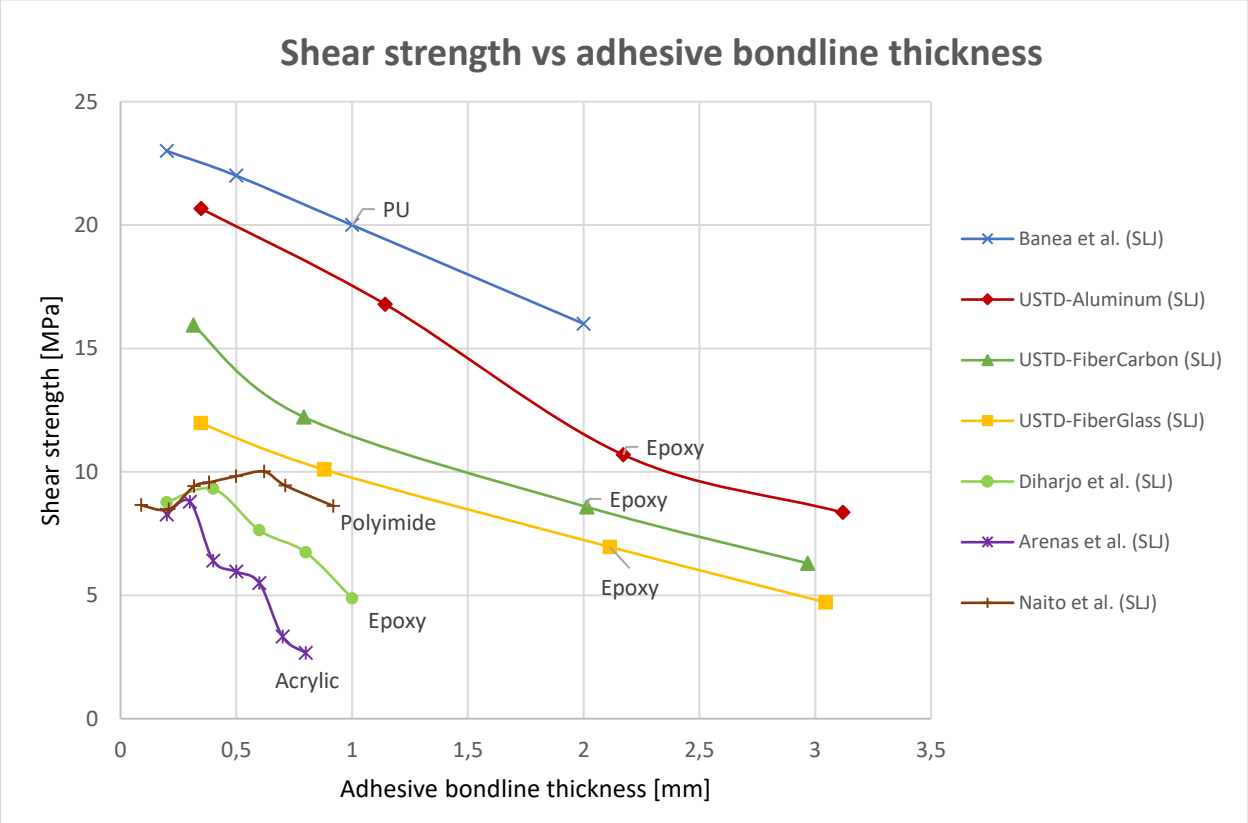

Figure 2.28 Shear strength versus bondline thickness (up to 3.2 mm) for different adherend and adhesive types. Test method: Shear tensile strength test

- FEA (Double-lap joints)

As suggested by Belnoue and Hallett [16] cohesive and adhesive failure modes can be treated separately, unlike other FE methods. They developed a smeared-crack model for cohesive failure. A similar model is used by the authors for the cohesive element modelling of adhesive failure. The proposed methodology was used to model a double lap-joint specimen and the interaction between cohesive and adhesive was studied in more detail [16]. The tested specimens had an adhesive layer of 0.25 mm, 0.5 mm, 1 mm and 1.5 mm. Once more, all the specimens with a thick adhesive layer (all the specimens with 1.5 mm adhesive layer) failed in the adhesive.

2.8.2 Peel strength

There is a large variety of tests to assess the peel strength of adhesively bonded joints. There exist multiple test configurations, which determine how the adherends are peeled-off. Some typical peel tests are the floating roller peel test, the climbing drum peel test, the T-peel test and the lever-arm peel test, which can be at an angle of peeling of 180 degrees as shown in the figure or at any certain angle.

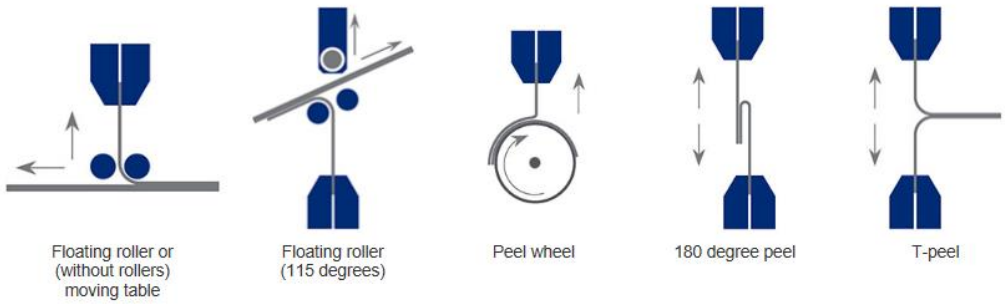

Figure 2.29 Types of peel test [49]

In most of the tests, the peel strength is obtained by measuring the average force per unit width of the specimen [N/mm] that is required to separate progressively the two adherends of the bonded joint. In case of hybrid bonded joints, the most flexible adherend is the one to be peeled off from the rigid adherend.

The adherend, either if it is aluminum, steel or a composite, its rigidity, the type of adhesive, the quality of the adhesion and the multiple test configurations are the cause of the big difference between the measured peel strengths from one test configuration to another [46].

In test standards, the thickness of the adherends and dimensions are specified. However, the adhesive layer thickness is not specified and it is determined once the specimen is ready to be tested, by subtracting the thicknesses of the adherends from the total thickness [44].

Due to the multiple test configurations and the fact that very little research on peel strengths for thick adhesives has been done yet, it is very complicated to define trends on peel strength with increasingly adhesive thickness. The following figure includes the expected ranges of values than can be expected for thicknesses up to 0.4 mm.

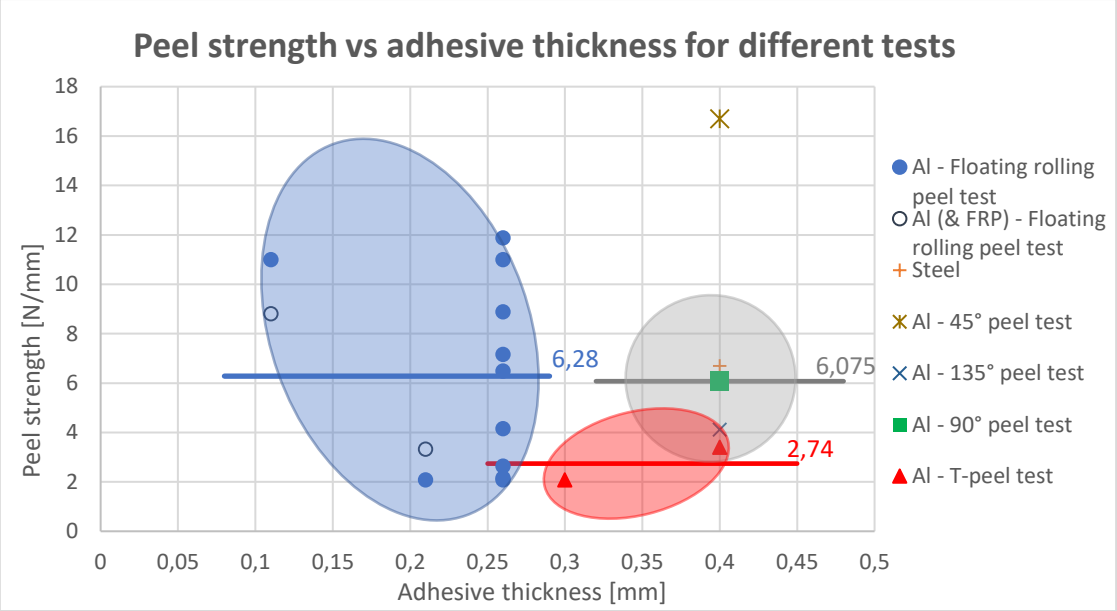

Figure 2.30 Peel strength versus bondline thickness (up to 0.45 mm) for different peel tests and adherends. Adhesive: epoxies

As stated by different authors, the peel load and peel strength can only be compared when using exactly the same flexible adhesives [44].

Furthermore, it is found that the failure mode is more important than the failure load. A good adhesion will result in cohesive failure or adherend failure, with cohesive failure preferred since it ensures that the adherends are properly bonded to each other and that the bond will endure. A bad adhesion will cause adhesive failure instead [45]. It is important to highlight the fact that in case cohesive failure is dominant with respect to the other failure modes, the comparison between adhesives' peel strength is consistent disregarding the type of peel-off adherend [45].

2.8.3 Fracture toughness

Belnoue and Hallett [16] used a high strength epoxy system, commonly used in structural applications, (light weight, gap filling properties and resistance to environmental degradation) to perform several tests (3ENF and DCB tests) and determine the thickness effect of a ductile adhesive on the shear strength and the critical fracture energy under pure shear (G_c^{ref}).

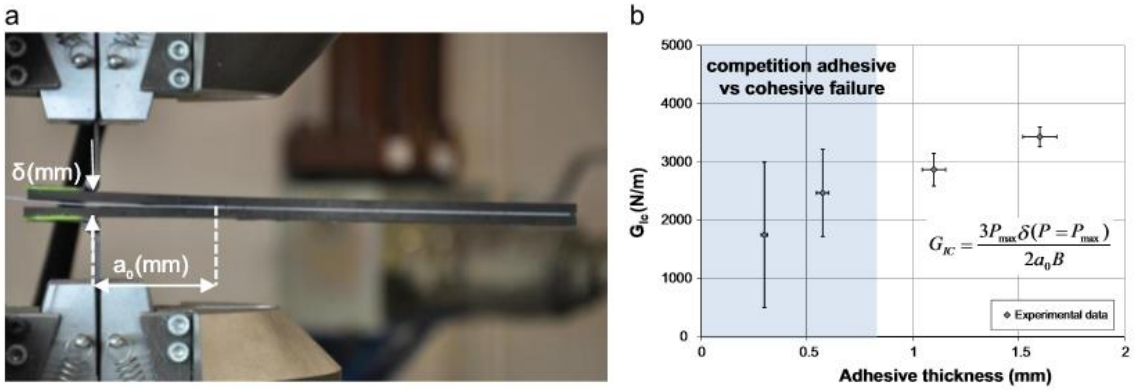

Figure 2.31 Mode I fracture toughness for different adhesive thicknesses. Experimental set-up DCB tests(a), Experimental measure of mode I fracture toughness as function of bond thickness (b) [16]

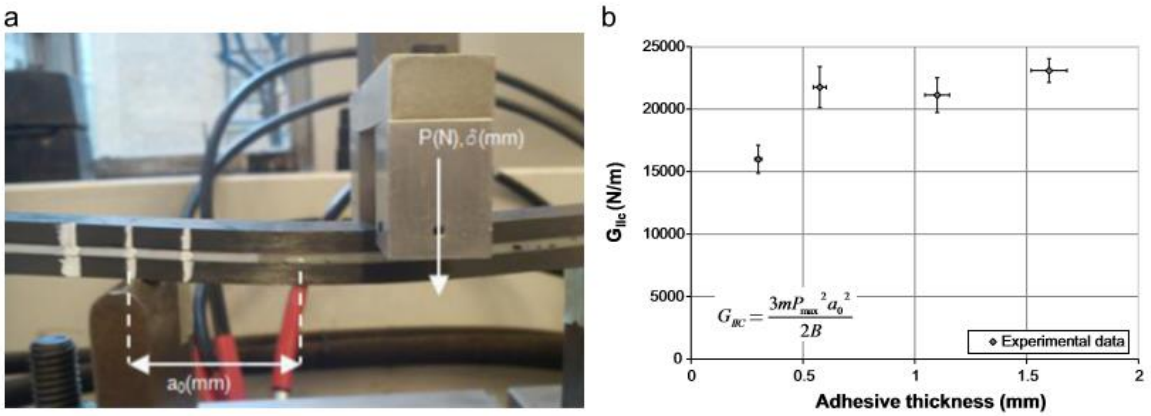

Figure 2.32 Mode II fracture toughness for different adhesive thicknesses. Experimental set-up 3ENF tests (a), Experimental measure of mode II fracture toughness as function of bond thickness (b) [16]

The correlation between the fracture toughness and the bond thickness for different adhesives is shown in Figure 2.33.

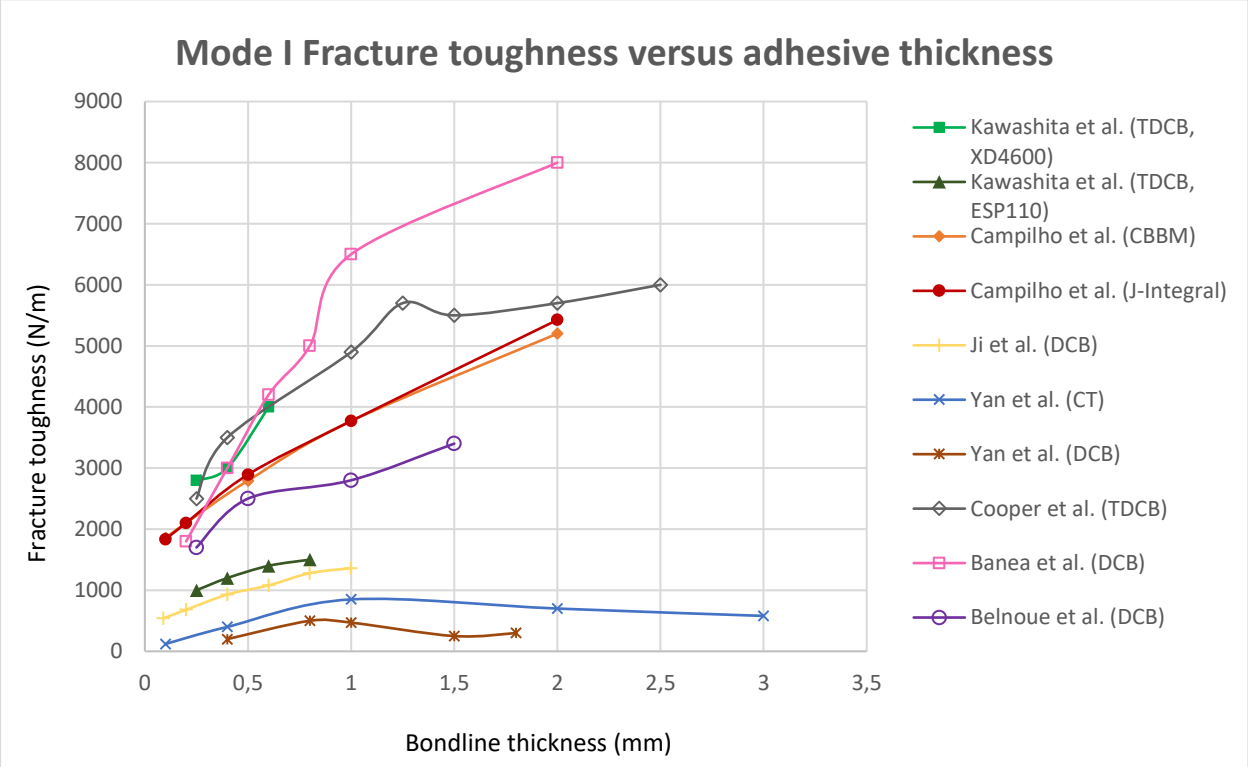

Figure 2.33 Mode I fracture toughness against bond thickness (up to 3 mm) for different bonded joints

Analyzing the previous Figure 2.33 and the type of adhesives we can see two patterns. Ductile adhesives show an increase of fracture toughness with adhesive bond thickness, whereas brittle adhesives reach a certain plateau after which the fracture toughness remains quite constant.

The studied fracture toughness are only for thicknesses up to 3 mm. However, it is not possible to define a trend for higher thicknesses. One assumption is that fracture toughness will keep increasing for ductile adhesive with thickness and it will remain constant in case of brittle adhesives. Thus, further research is required to investigate the trends for increasing thicknesses.

2.9 OVERVIEW TEST METHODS

Table 2.2 gives an overview of all test methods and corresponding standards that can be used for adhesive properties characterization.

Material property	Standard / Test method	Section
Elastic properties – adhesives		
- E, G, υ	Tensile test of plastics – ISO 527	7.2.1
	V-Notched Beam method – ASTM D5379	7.2.2
	Modified-Rail test method – ASTM D 4027	
Strength properties – adhesives		
- Tension	Tensile test of plastics – ISO 527 / ASTM D 638	7.2.1
	Tensile test of fibre-resin composites – ASTM D3039	
- Shear	V-Notched Beam method – ASTM D5379	7.2.2
	Thick Adherend Shear Test (TAST) – ISO 11003-2	7.2.2
- Compression	Compressive test of plastics – ISO 604 / ASTM D695	7.2.3
- Mixed mode (shear and tension)	V-notched plate test – N/A	
- Maximum principal strain	Tensile test of plastics – ISO 527	7.2.1
Fracture toughness		
- Mode I	Double Cantilever Beam (DCB) – ISO 25217 / ASTM D3433	
	Tapered Double Cantilever Beam (TDCB) – ISO 25217 / ASTM D3433	(8.3)
	Compact tension (CT) – N/A	
- Mode II	End-Notched Flexure (ENF) test – ASTM D7905	
	End-Loaded Split (ELS) test – ESIS protocol	
- Mixed mode (mode I and mode II)	Fixed Ratio Mixed Mode – N/A	
Peel strength (metal bonding)		
- Peel or stripping strength	180 degree peel test – ASTM D903	
	Climbing Drum Peel test – ASTM D1781	(8.2)
	T-peel test – ASTM D1876	
	Floating roller peel test – ASTM D3167	
	90 degree peel test – ASTM D6862	
Additional tests – adhesives		
- Tensile creep in shear	ASTM D 2294	
- Tensile shear strength at elevated temp.	ASTM D 2295	
- Tensile shear strength at subzero temp.	ASTM D 2557	
- Shear strength pin-and-collar specimen	ASTM D4562	
Strength properties – bond (Joint properties)		
- Tensile shear strength of DLJ	ASTM D 3528	
- Tensile shear bond strength of SLJ	Single Lap Shear (SLS) test – ASTM D1002 / ASTM D3165 / ASTM D5868 / ISO 4587	8.1
- Stress-strain behavior in tensile shear	Thick Adherend Metal Lap-Shear Joints test – ASTM D 5656	8.1
- Shear Interfacial bond strength	Thick Adherend Shear Test (TAST) – ASTM D 3983 / ISO 11003-2	7.2.2
Additional tests - joints		
- Time to rupture under static load	ISO 15109	
- Lap shear adhesion for FRP bonding	ASTM D5868	
- Shear strength by block-shear method	ASTM D4501	
- Shear strength of Sandwich shear LJ	ASTM D3164	

Table 2.2 Material properties and corresponding test and standards.

2.10 EFFECT OF ADHESIVE THICKNESS ON FRACTURE OF BONDED JOINTS

In the study of the failure of adhesively bonded joints, it is necessary to refer to two phases, the crack initiation and the crack propagation. It is expected that crack initiates where the maximum stresses develop. For this, it important to analyze the different parameters in the design of the joint.

As it has been seen, single-lap joints behave differently than double-lap joints because they present a higher peel stress concentration at the ends of the overlap, which drives to an initial adhesive failure in these regions [18]. Therefore, for the design of the joint it is necessary to do a comparison of maximum principal stress or strain at the mid-thickness of the adhesive layer to the characteristic strength of the adhesive used in the joint [13].

Another important factor in the design, which is of high interest for this thesis, is the adhesive thickness effect on the fracture development and the failure mode. One study developed by Belnoue and Hallett [16] states that the thinner the specimens, the more they are prone to fail in the interface (adhesive failure). For double lap joints, they found that in case of bond lines larger than 1.5 mm, failure occurred always in the adhesive (cohesive failure).

For adhesive thicknesses of less than 0.4 mm the adhesive failure mode increases considerably and it will not depend on the thickness as with the cohesive failure. In this case, the shear strength presents higher values but it starts to decrease after reaching a maximum. In this situation, shear will mainly depend on the adhesive resistance of the bonding along the interface [15].

2.11 PROPOSAL

One of the objectives of this thesis is to analyze the mechanical behavior of double lab joints. This type of joints is chosen as it is applied in real civil and maritime applications. One example can be seen in ship superstructure to hull connection, above the deck, as shown in the following figure. The section consists of a U-shaped adhesive bonded joint connecting a composite beam and the U-shaped steel deck (see Figure 2.34).

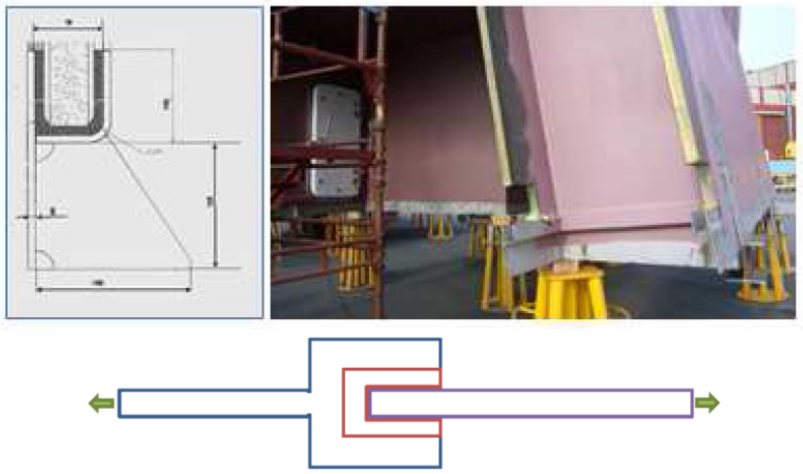

Figure 2.34 Example of a U-shaped hybrid (composite to steel) bonded joint used in the superstructure of a ship

In this thesis two adhesives will be used, representing both brittle and ductile behaviors. The chosen adhesives are Araldite 2015 (brittle) and Crestomer 1152PA (ductile).

- Urethane Acrylate Crestomer 1152PA (Civil specimen, used in civil infrastructure applications)

Crestomer 1152PA is a high performance structural adhesive with an urethane acrylate base. It is highly thixotropic and it has no sagging on vertical surfaces. Some of its benefits are an excellent retention of toughness, a controlled cure behavior, an excellent retention and high elongation at break, excellent fatigue and impact resistance. The typical gap filling of this adhesive is from 1 mm up to 25 mm [33]. No information of the stress-strain curve for this adhesive is available on literature.

- Epoxy Araldite 2015 (Maritime specimen)

Araldite 2015 is a two component epoxy paste adhesive, with curing room temperature. It is non-sagging up to 10 mm thickness and thixotropic (it has time-dependent viscosity). It consists of a toughened paste, ideal for bonding composites such as CFRP, GRP and SMC and dissimilar adherends; with excellent resistance for dynamic loading. This adhesive is also suitable as gap filling or in vertical applications [32].

The tensile strain-stress curve of Araldite displays both elastic and short plastic regions (see Figure 2.35), which will have to be considered in the finite element analysis, approximated by a bilinear curve.

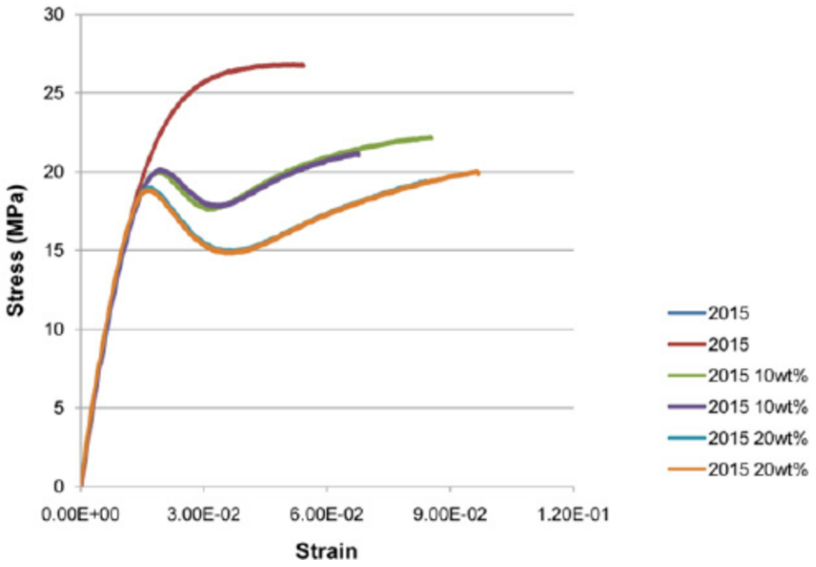

Figure 2.35 Tensile stress-strain curve for Araldite 2015 [43]

3 EXPERIMENTAL PROCEDURE AND RESULTS

This Chapter contains a brief explanation of the experimental investigations and the main results that were obtained. A set of experimental tests were performed in order to study the effect of the adhesive thickness of adhesively bonded double-lap joints under tension loading. The detailed test set up and the test plan can be found in the Appendix 1.

In Section 3.1 the main experiment objectives are presented. In Section 3.2 it is shown the geometry of the specimens tested and in section 3.3, the material characterization. In Section 3.4 it is presented how the specimens were classified. Section 3.5 contains the procedure followed to manufacture the specimens and Section 3.6, the test instrumentation. In Section 3.7 it is explained how the test data was processed. Section 3.8 contains the experimental results, from the different curves that were obtained to the analysis of the observed failure modes. At the end of the chapter there is Section 3.9, which contains a brief discussion of the experimental results. These experimental results were used to develop an analytical model for DLJ contained in Chapter 4 and also to validate the numerical finite element models explained in Chapter 5.

3.1 EXPERIMENT OBJECTIVES

This experiment has two main objectives:

- Determination of the load versus the applied displacement curve with special emphasis on the load at failure.
- Determination of the strain fields and displacements in the adhesive layer.

3.2 JOINT GEOMETRY

The tensile shear strength test for double lap joints was performed based on the Standard Test Method ASTM D 3528. The dimensions of the specimens were chosen in accordance with the dimensions of the joints tested in the Composite Joints JIP project. Where applicable, the dimensions chosen are equal to the dimensions suggested in the standard. However, not all the dimensions are given in the standard or are usable for thick adhesives. A general geometry is shown in Figure 3.1, which is defined as a function of the adhesive bondline thickness *t.*

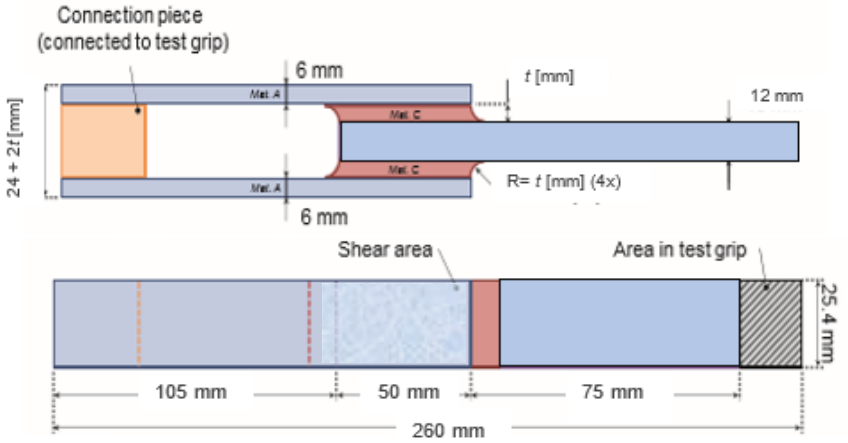

Figure 3.1 Front and side view of a small scale test specimen with a generic thickness t adhesive layer

3.3 MATERIAL CHARACTERIZATION

For all the specimens, steel plates S355 are used for the adherends, whose thicknesses are 12 mm for the inner and 6 mm for the outer adherends.

Two different adhesives were used in this investigation, Araldite 2015 and Crestomer 1152PA, , which were chosen to represent two different applications; maritime and civil. Furthermore, they also represent both brittle and ductile behaviors, respectively. The mechanical properties and general information of the adhesives is gathered in the following table.

	Araldite 2015	**Crestomer 1152PA**
General information		
Adhesive type	Epoxy	Urethane-acrylate
Application	Maritime	Civil
Producer	Huntsman	Scott Bader
Sources	2201 and 1701	Brochure
Curing type	2 component	2 component
Curing time [h]	4 to 21	10 (to gain 10% shear strength)
Working temperature [°C]		18 to 25
Temperature range [°C]		-30 to 80
Gap filling		1 to 25
Mechanical property		
Young's modulus, E [MPa]	1850	1400
Shear modulus, G [MPa]	560	
Poisson ratio, υ [-]	0.33	0.47
Tensile yield stress, σ_y [MPa]	12.63	
Shear yield stress, τ_y [MPa]	14.6	
Tensile failure strength, σ_f [MPa]	27.3	26
Shear failure strength, τ_f [MPa]	≈ 18	10 to 15
Tensile failure strain, ε_f [%]	4.77	
Shear failure strain, γ_f[%]	43.9	
Elongation at break [%]	4.40	100
Toughness in tension, G_{Ic} [N/mm]	0.43	
Toughness in shear, G_{IIc} [N/mm]	4.70	
Yield stress at 7% strain [MPa]		17
Viscosity	Thixotropic (*)	Thixotropic (*)

Table 3.1 Properties of adhesives Araldite 2015 and Crestomer 1152 PA [32, 33]

(*) Time-dependent decrease in apparent viscosity under shear stress, followed by gradual recovery when the stress is removed. This property allows adhesives to be spread readily and applied In thick layers without running or flowing out of the gap before bonding because the adhesive loses its fluidity immediately after application.

3.4 SPECIMENS CLASSIFICATION

A test matrix is designed to evaluate the effect of the adhesive thickness on the mechanical properties of the joint. The test matrix (see Table 3.2) includes the different adhesive thicknesses and materials that were chosen. It also includes the number of specimens per thickness that were tested; five of each type. This sample size was chosen so that in case one test is invalid, there will still be four valid samples, as recommended by the ASTM standard and therefore, enough indication of possible spreading of the results.

Adhesive	**Adherend**	**Test method**	**Bondline thickness [mm]**	**Number of tests**
Crestomer 1152PA	Steel S355	Tensile shear	1	5
			3	5
			5	5
Araldite 2015	Steel S355	Tensile shear	1	5
			3	5
			5	5
			8	5
			10	5
				40

Table 3.2 Test matrix

A general sample numbering was used such as "*c/a_bondline thickness[mm]_sample number*", with a first letter (*c* or *a*) referring to the adhesive, Crestomer or Araldite (civil or maritime application), respectively. For example, *C52* indicates the second Crestomer sample with 5 mm bondline thickness.

3.5 MANUFACTURING PROCESS

The steel plates were cut and holes were drilled by the steel supplier. The gluing of the specimens was done by MOCS. It is necessary to highlight the importance of applying a surface pretreatment. It prevents poor bonding due to contaminants on the steel surfaces such as dust, dirt or grease, which might also condition the strength of the interface. In this case, the applied surface preparation and surface pretreatment of the steel plates was as follows (see photographs below).

1) Sandblasting
2) Cleaning with air pressure
3) Cleaning with Acetone and cloth or tissue

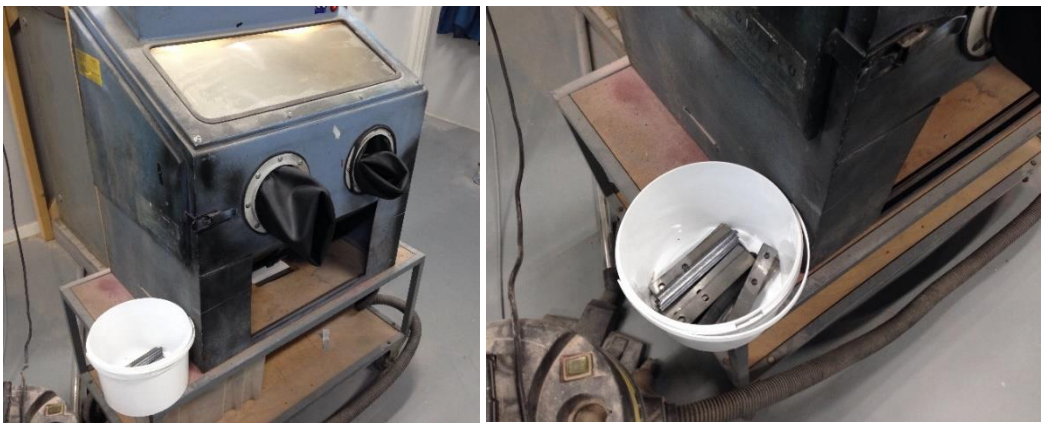

Figure 3.2 Surface preparation of plates. Left: Air pressure machine. Right: Plates after being cleaned with Acetone

Within 24 hours of the application of the pretreatment on the steel plates, the bonding is executed. To have an effective and accurate bonding, a special mold was designed. It consists of a steel plate with multiple holes in it. Pins are introduced in order to laterally position the plates. In this manner, five specimens with the same adhesive thickness can be produced in the same badge (see photographs below).

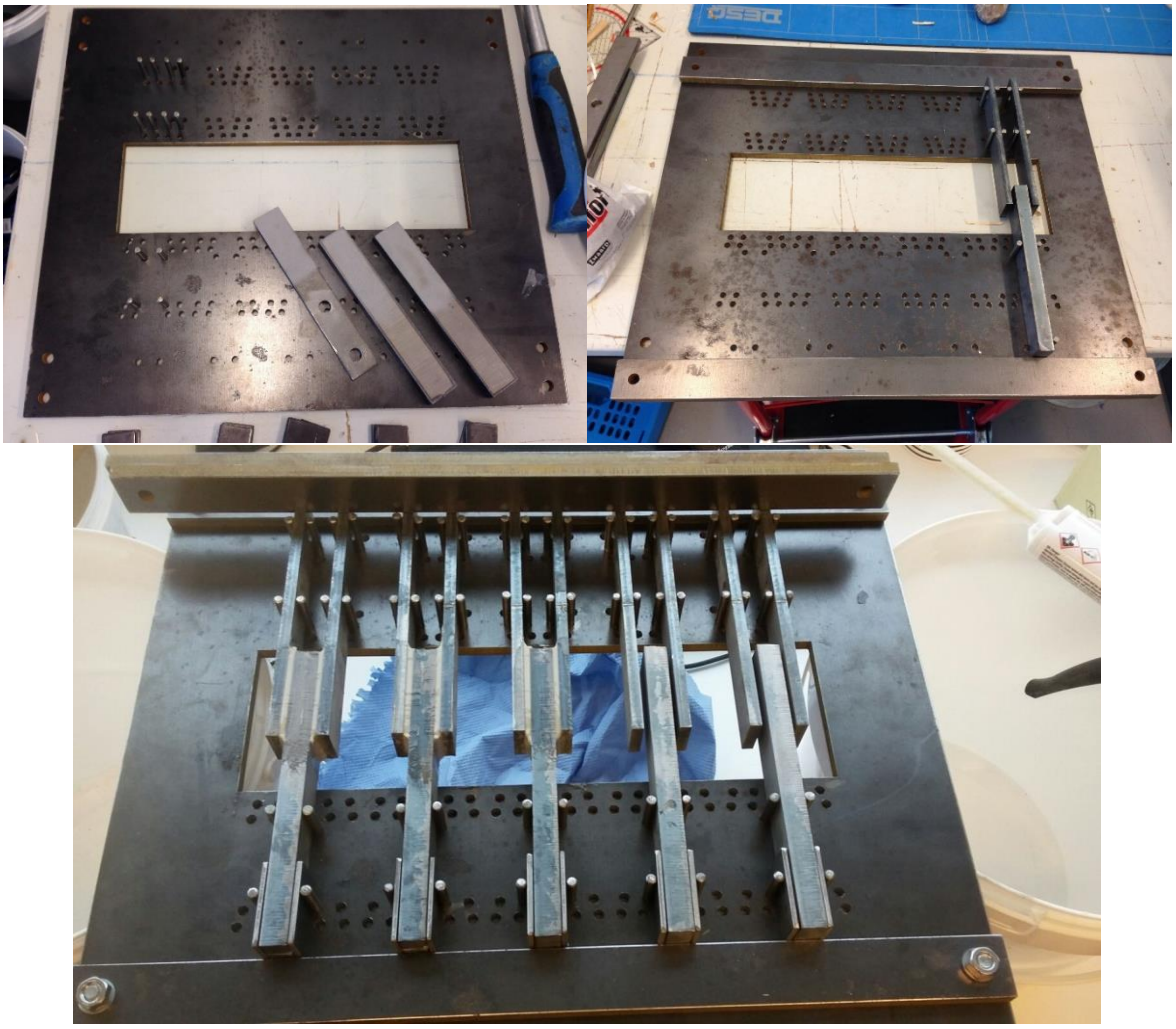

Figure 3.3 Mold used for the fabrication of the specimens and detailed manufacturing process

3.6 INSTRUMENTATION

All tests were conducted using a MTS 25 ton hydraulic Universal Testing Machine which applied a tensile static loading (See Figure 3.4). The specimens were placed in the set-up using a pair of self-aligning grips. On one end (upper end in the figure) the grip holds the specimen inside the load cell and has to move into alignment as soon as the load is applied. On the other end (lower end in figure) the adherends are held by another grip and also fixed by two bolts, used in combination with the connection piece. Thus, the adherends are perfectly aligned with the direction in which load is applied and any lateral displacement or rotation is avoided.

The load was applied at a constant displacement rate of 1.27 mm/min (0.05 inch/min) as prescribed by the ASTM D 3528 standard.

The specimen was connected with two LVDT (Linear Variable Differential Transducer) sensors, located in the positions showed in Figure 3.5, which measure the relative displacement of the adherends. A distance of 100 mm was taken between the two clamps that hold the sensors.

The applied load and the displacement of load cell and the front and back LVDTs sensors were measured by the testing machine transducers and forwarded to the computer where all the data was saved. Next to the load cell and the LVDTs high speed videos were made during the tests.

The tests and all the procedures prior and post testing were performed at the TNO laboratory.

Figure 3.4 25T hydraulic universal testing machine and loading direction

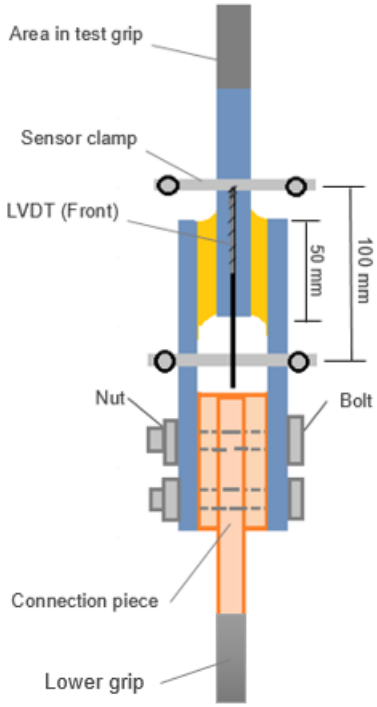

Figure 3.5 Instrumentation of specimens

The connection piece (Figure 3.6), which is used to connect the specimen to the lower test grip, consists of steel plates S355 of different thicknesses; a 12 mm thickness plate in the middle and multiple thin plates of 1, 2 or 4 mm at each side, combined for each test according to the adhesive bondline thickness to fill the gap between the two outer adherends.

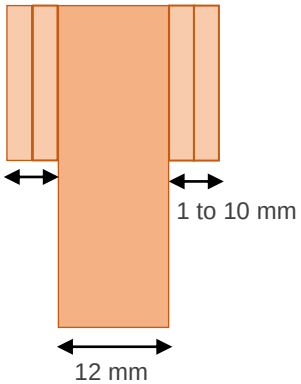

Figure 3.6 Connection piece detail, steel S355

3.7 DATA PROCESSING

The data obtained in the experiments was analyzed by making use of the Software MATLAB and filtered with the Low-pass Butterworth filter tool. Thus, it is possible to diminish the high-frequency fluctuations in the data, thereby creating figures with more smooth lines, without losing accuracy. The butter function reduces the sample size in a frequency domain with a 2nd, 4th or 8th order. Usually, the higher the order, the better the approximation. However, higher orders come at the expense of a more costly implementation. In this case, a second-order filter was chosen with a cutoff frequency of 10 Hz, which for data sampled at 600 Hz, corresponds to 0.03 π rad/sample.

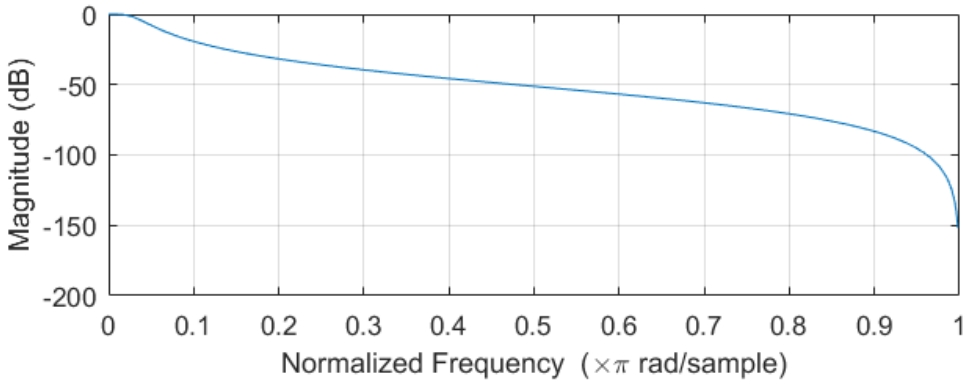

Figure 3.7 Magnitude of the 2nd order lowpass Butterworth filter. Experiment data (7 samples/sec) as signal

The following figure shows the comparison of the raw data, unfiltered and filtered, whose difference can be clearly observed by zooming in (Figure 3.8). As can be seen, filtering does not affect the accuracy of the phenomena of interest or the global behavior, but it makes the curves much smoother and easier to interpret.

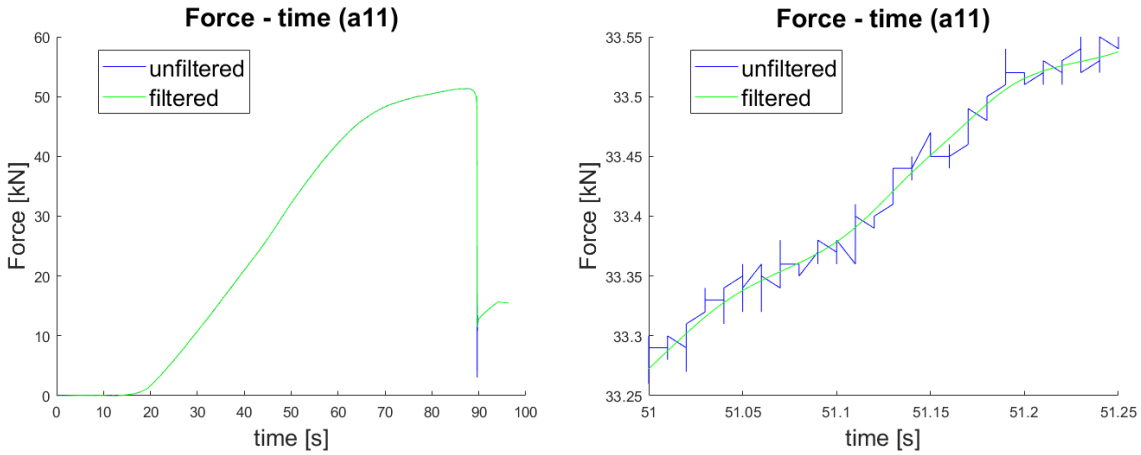

Figure 3.8 Comparison of Force – time, before and after filtering (a11)

This filter was applied to all the fields using time as the signal. Thus, the result is a new field for the force and two for the displacements of each LVDT, in which the high frequency data was eliminated. This new filtered data is stored and hereafter used to do the analyses and the plots.

Note that the data at the point of initiation still shows small fluctuations after filtering (see Figure 3.11). However, it is important to take into account the error in the calibration of the machine, which justifies these small fluctuations. The calibration machine was set on 5mm and the LVDT measured 5.01, thus it has a 0.2% deviation.

3.8 EXPERIMENTAL RESULTS

3.8.1 Force – displacement

The figures presented in this section (Figure 3.9 to 3.15) show the force displacement curve representing each test. The parameters used to create these plots are the force as registered by the load cell inside the testing machine and the displacement also measured in the load cell or the displacement over the LVDTs. The difference between both displacement measurements are clearly seen. It must be noted that, the displacement field given by the machine is not the actual displacement over the joint since it takes into account small initial displacements which are overcome by the joint and also displacements in the adherends and the set-up but not only by the adhesive (see Figure 3.9). The real displacements over the joint are determined by the two sensors (LVDTs), which are located at the back and front sides of the specimen and clamped at 100mm distance.

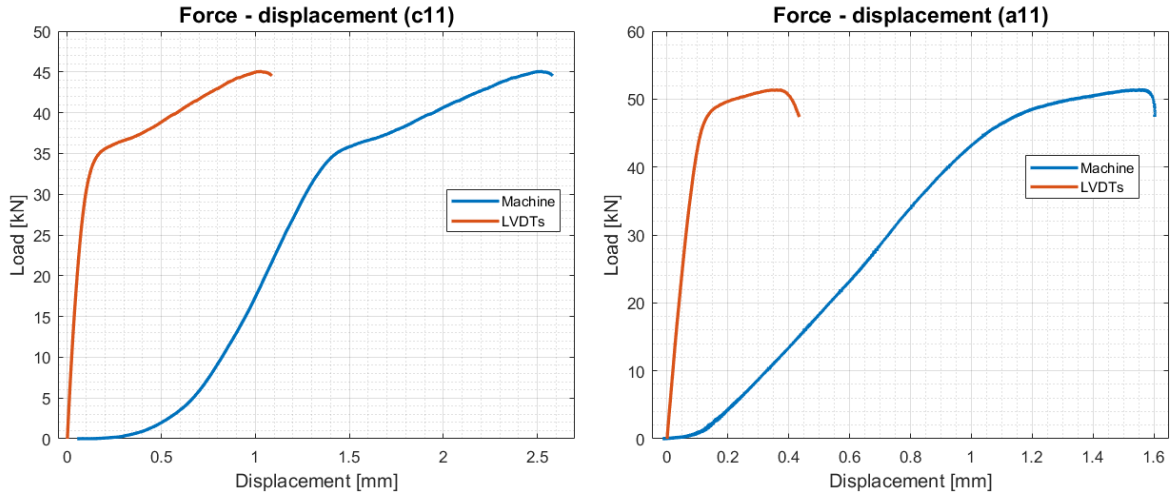

Figure 3.9 Comparison of Force – displacement, as given by the machine and as the mean of the LVDTs. Left: c11; right: a11

In all the figures the displacement over the joint (so from the LVDTs) is taken as the mean of the two respective displacements. As can be seen in Figure 3.10, the two LVDT lines show a reasonable agreement therefore, taking the average, for example to exclude some misalignment, is a good method.

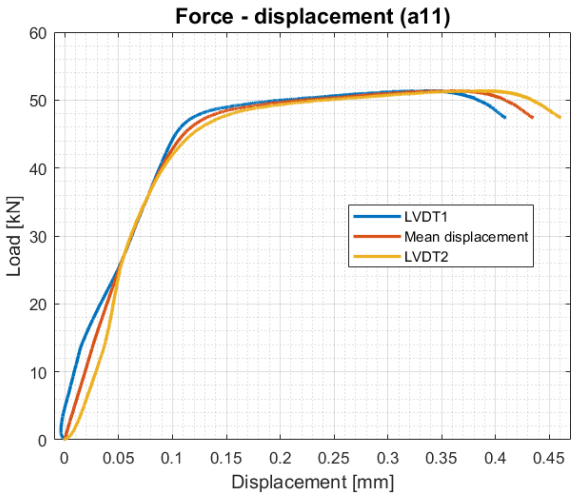

Figure 3.10 Force displacement curve for both LVDTs and mean displacement (a11)

Some modifications were done to adjust the raw curves to the final ones. The first step in order to determine these final curves is to set the initial force and displacement to zero. Since force might not

immediately act on the specimen when the test initiates, it was analyzed how the data points are distributed at the beginning of the test, so that it is possible to determine where exactly the force started acting on the specimen. As shown in Figure 3.11, the dots do not show an horizontal line at a certain force level but rather a cloud of data points. As a consequence, the initiation time was taken as the instant where the force becomes equal or larger than zero and then continues to be positive. This is set as the initiation point (see Figure 3.11).

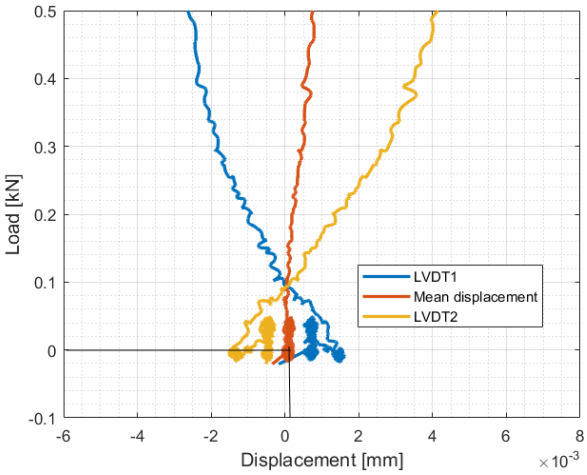

Figure 3.11 Data at initiation of test after filtering and setting of the initiation point (a11)

To determine the first data point it was defined in MATLAB the task of finding the last entry *i* with a negative force value. Thus, the first plotted point corresponds to the entry *i+1*, which should have a corresponding zero displacement. In case its mean displacement is not zero but *x mm*, then all the mean displacement entries were redefined by subtracting *x*. In Figure 3.12, the adjusted curve is shown, with initial zero force and displacement. When looking at the complete curve, both mean displacement and adjusted curve seem to coincide and the difference between them can only be observed when zooming in the figure (see Figure 3.12, left).

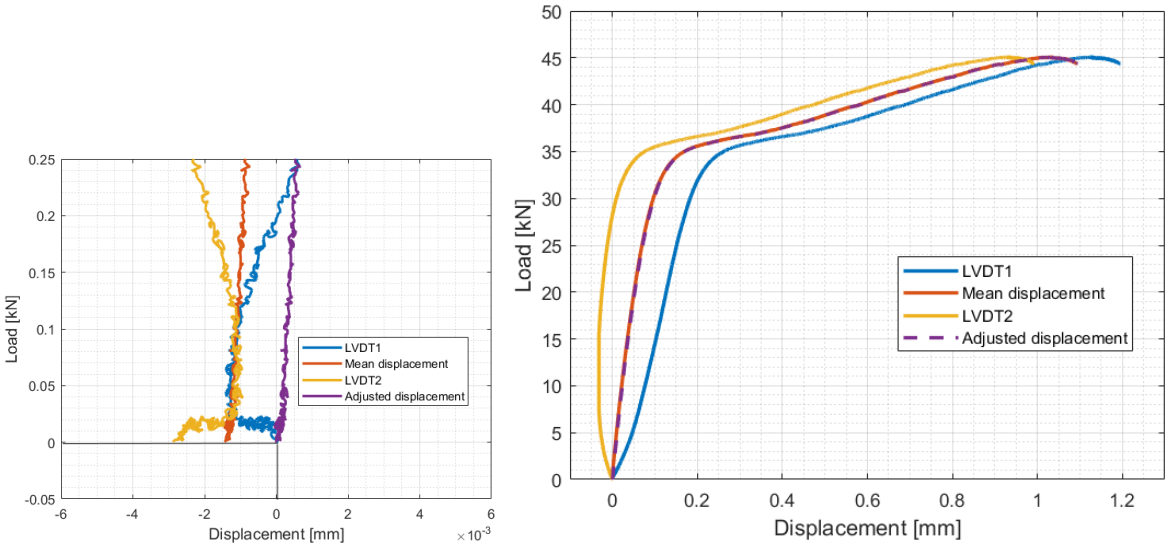

Figure 3.12 Force displacement curve adjustment to 0 initial displacement (c11)

The final data point where the curve ends is chosen as the point where a steep decrease in force towards zero begins. This steep decrease indicates that failure occurred at this point indicating the failure load, which is different from the maximum load. Moreover, the failure-time, i.e. the duration of the test till specimen failure, is calculated as the time between the initiation time and the time when failure load is reached.

Crestomer

Figure 3.13 shows the result of the double lap joint test for the Crestomer adhesive. Results are grouped per thickness and shown as adjusted (as described in the previous paragraph) force mean LVDT curves. Table 3.3 summarizes the average maximum force, time to failure and displacement at failure for each thickness. The individual results are given in the Appendix 2.

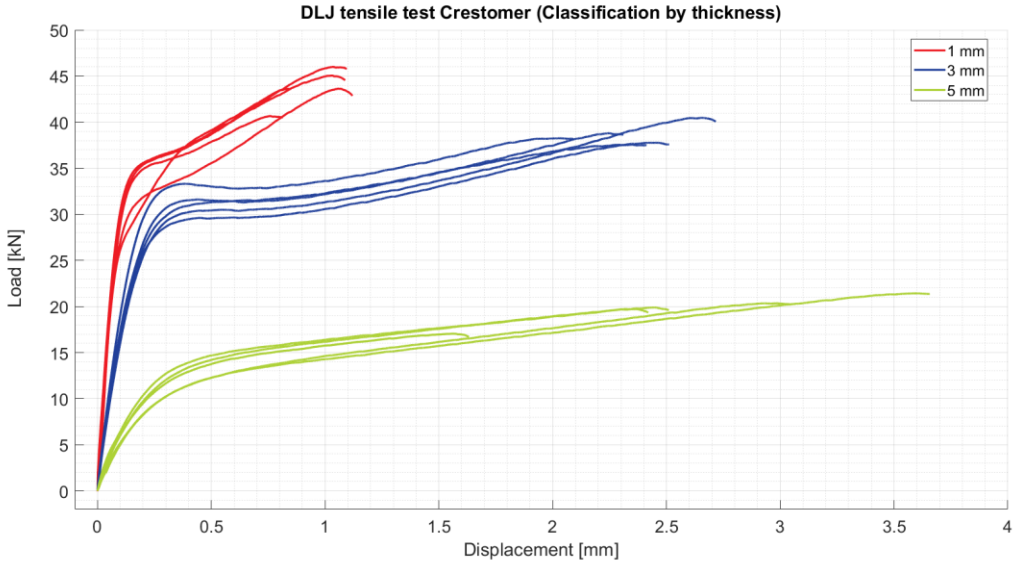

Figure 3.13 Crestomer Load – displacement curves. Classification by thickness

Sample group	Max. force [kN]	Time to failure [s]	Displacement at failure [mm]
1 mm	43.8 ± 2.01	111.6 ± 9.8	1.0 ± 0.1
3 mm	38.6 ± 1.16	178.0 ± 12.7	2.4 ± 0.2
5 mm	19.7 ± 1.61	180.7 ± 32.8	2.9 ± 0.6

Table 3.3 Average values of maximum force, failure-time and displacement at failure for Crestomer

A trend for Crestomer can be seen by analyzing Figure 3.13 and Table 3.3. The results show an increase of deformation capability with increasing thickness. Especially when looking at the increase of mean displacements with thickness, this trend is clear if the sample c55 is disregarded. Since this sample showed a much lower deformation (1.6 mm) and failed in a shorter time (106 seconds) than the other samples of the same group, it was disregarded when calculating the mean and the standard deviation.

The ductile behavior that characterizes the Crestomer is also noticeable in the Figure 3.13. It can be seen in the quick increase of the load at the initiation of the test, up to a certain plateau where the adhesive starts behaving plastically. This behavior can be assigned to the adhesive because the steel plates deform elastically, never reaching the yield, as it was established and checked during the design of the joints.

Furthermore, the load increases much slowly in time till failure after the plateau. In the High Speed videos no difference is visible between two frames because the change occurs relatively slowly (about 2 to 3 minutes till failure). However, the displacement downwards of the outer adherends due to the deformation of the adhesive is visible when comparing nonconsecutive frames (see Figure 3.14).

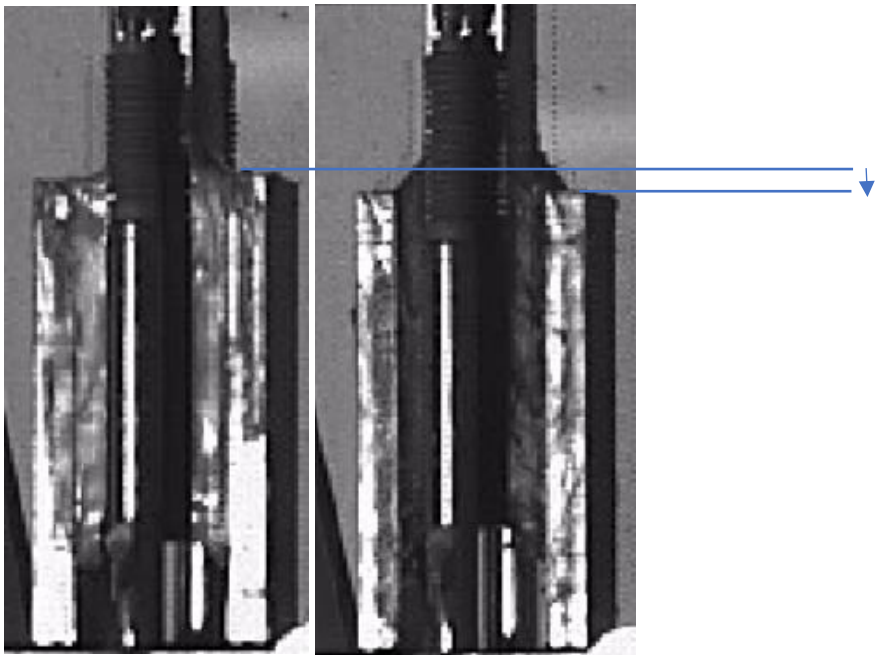

Figure 3.14 Increase of displacement in the plates due to increased deformation in the adhesive (c51). Frames 533 (left), 935 (right) at 60fps HS video.

Araldite

Also for the Araldite samples the per thickness grouped force displacement curves are shown in Figure 3.15 and summarized mean results in Table 3.4. The individual results can be found in the Appendix2.

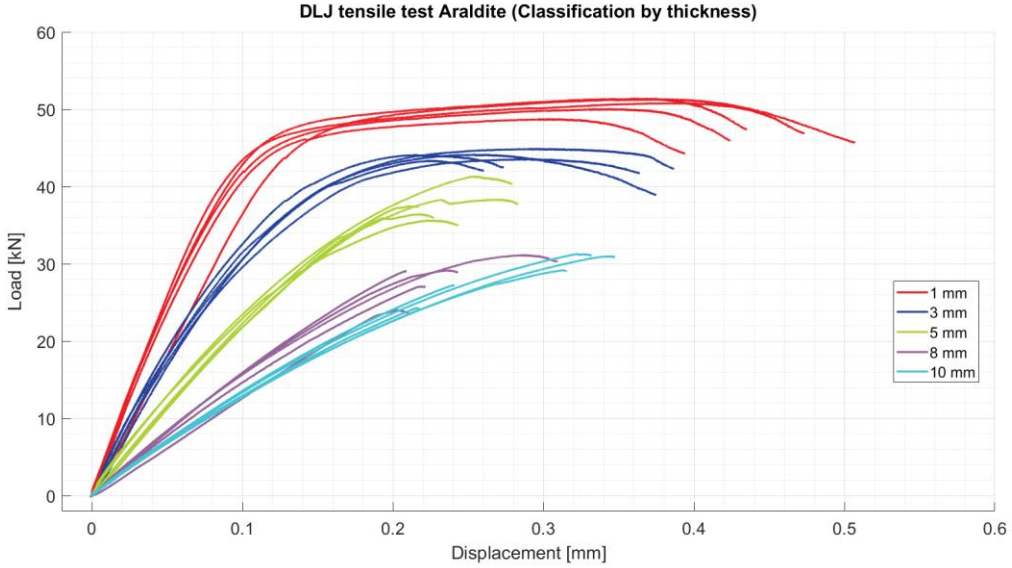

Figure 3.15 Araldite Load – displacement curves. Classification by thickness

Sample group	Max. force [kN]	Time to failure [s]	Displacement at failure [mm]
1 mm	50.4 ± 1.12	87.9 ± 8.1	0.4 ± 0.0
3 mm	44.0 ± 0.63	88.9 ± 8.6	0.3 ± 0.1
5 mm	37.8 ± 2.20	76.1 ± 13.3	0.3 ± 0.0
8 mm	28.1 ± 2.69	54.2 ± 9.1	0.2 ± 0.0
10 mm	28.6 ± 2.90	76.2 ± 17.9	0.3 ± 0.1

Table 3.4 Average values of maximum force, failure-time and displacement at failure for Araldite

Araldite samples showed two different behaviors. On one hand, samples with 1 and 3 mm bondline thicknesses showed a certain plasticity plateau with a more ductile behavior. On the other hand, samples with 8 and 10 mm bondline thickness showed a more brittle behavior. The 5 mm bondline thickness samples are clearly in between, showing only a very limited plateau. The plasticity plateau decreases with increasing bondline thickness.

For a further explanation on these two responses an analysis of the High Speed videos is done. For Araldite, in comparison to Crestomer where no crack was noticeable during the test, it is possible to see a crack that initiates on the top curved edge and, after one or two frames, the crack along the whole adhesive bondline, when failure has occurred (see Figure 3.16).

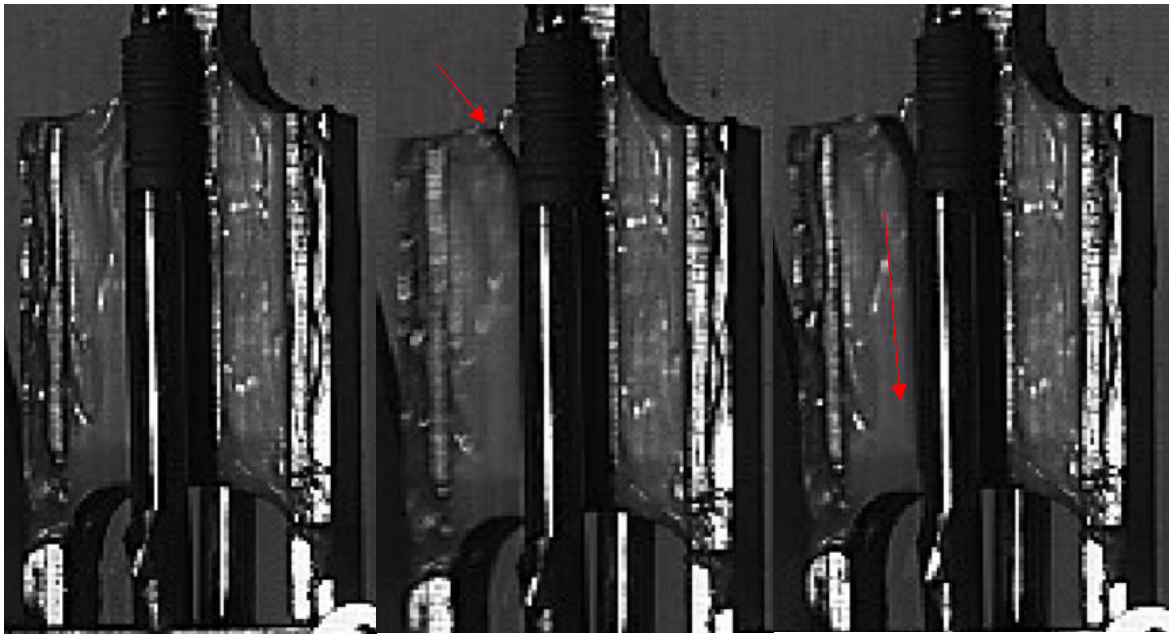

Figure 3.16 Crack initiation from the top curved edge (a101). Frames 89,90 and 91 (left to right) at 2000 fps HS video

Unfortunately, it is not possible to see in the HS videos any difference between the time that would correspond to the plateau and the initiation of the crack. Therefore, one assumption could be that after reaching the plateau some failure at micro-scale is occurring inside the adhesive, which is not visible with the naked eye. Following this hypothesis, the adhesive would enter in a region of damage growth up the final failure.

For samples with 8 and 10 mm bondline, this plateau is not reached. Therefore, the failure occurs at an elastic level. These two behaviors are explained with the respective failure modes in Section 3.8.6.

All samples (Crestomer and Araldite) classified by thickness

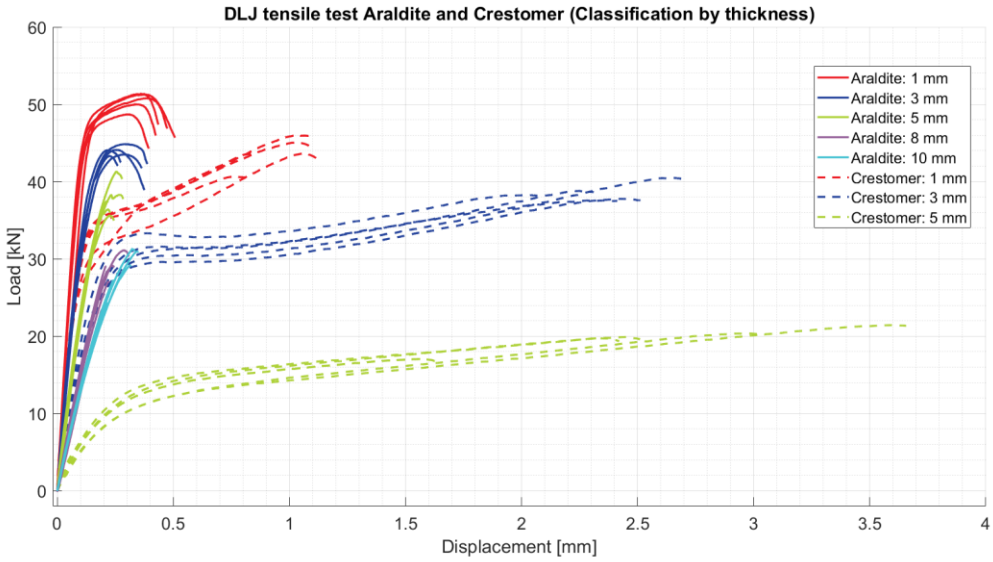

Figure 3.17 Araldite and Crestomer Load – displacement curves. Classification by thickness

Some conclusions one can draw from Figure 3.17 are that Crestomer shows more deformation capability than Araldite, which in turn shows a higher loading capability and as such, double lap shear strength. These conclusions are in agreement with the data provided by the manufacturer and found in literature.

3.8.2 Lap shear strength – shear strain

The average shear strain is calculated as the displacement in the force direction over the thickness of the bondline. The lap shear strength is calculated dividing the load by two times (DLJ) the ideal shear area specified in the geometry of the specimen, which varies with the thickness of the adhesive bondline (see equations).

Average shear strain: $$\gamma = \frac{\Delta y}{\Delta x} = \frac{\Delta y}{t} = \frac{(\Delta y_1 + \Delta y_2)/2}{t} \quad [-] \qquad (3.1)$$

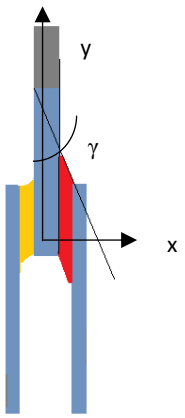

Figure 3.18 Detail of the coordinate system; average shear strain calculation

Average lap shear strength: $$\tau_s = \frac{F}{2A} = \frac{F}{2 \cdot 25.4(50+t)} \cdot 1000 \quad [MPa] \qquad (3.2)$$

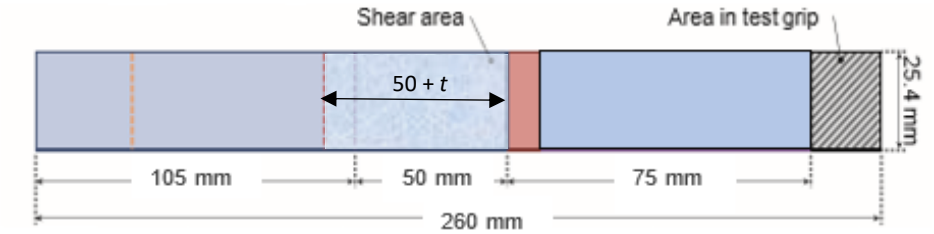

Figure 3.19 Detail of the shear area

One parameter that can be derived from a material shear stress – shear strain curve is the shear modulus (G), defined as the ratio of shear stress to the shear strain.

Shear modulus: $$G = \frac{\tau}{\gamma} \quad (3.3)$$

It is important to remark that the shear modulus is a material property. However, in Section 3.8.3 the possibility is studied to determine this parameter also for the joint to see how much this differs from the parameter of the bulk adhesive; value that can be found in literature.

Crestomer

Figure 3.20 shows the average strain and lap shear stress curves grouped per thickness for the Crestomer adhesive.

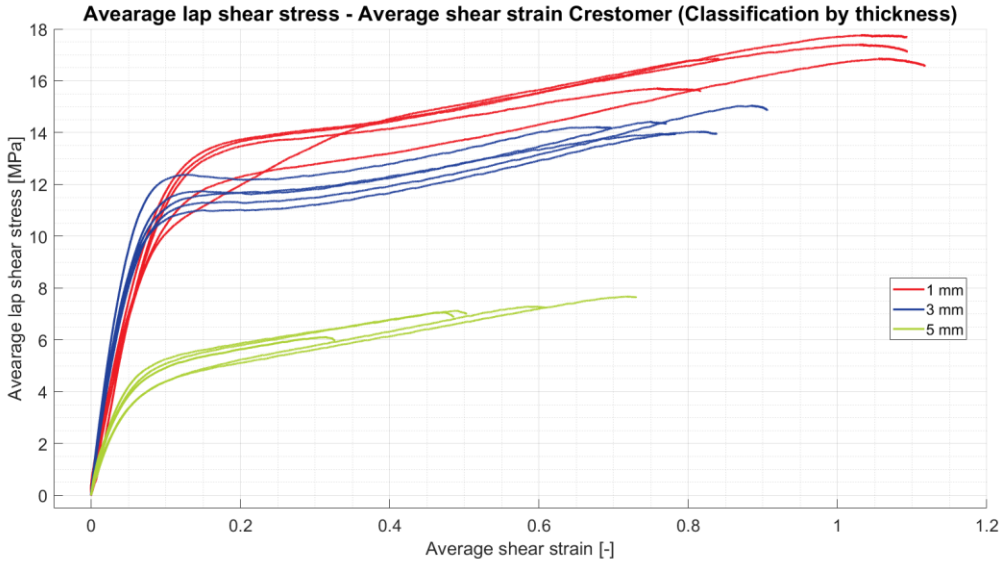

Figure 3.20 Crestomer Average lap shear stress – Average shear strain curves. Classification by thickness

Sample group	Max. lap shear stress [MPa]	Max. average shear strain [-]
1 mm	16.9 ± 0.8	1.00 ± 0.15
3 mm	14.3 ± 0.4	0.80 ± 0.08
5 mm	7.1 ± 0.6	0.53 ± 0.15

Table 3.5 Maximum lap shear stress and maximum average shear strain for Crestomer

The observed trend in Figure 3.20 is that the larger the thickness, the lower the maximum average shear strains in the adhesive. Even though the force-displacement curves showed increasing displacement with thickness, a thick bondline will decrease considerably the shear strains, modifying the trends. This means that the deformation and as such the average shear strain over the adhesive

at failure is thickness dependent. Note also the similarity in the curves and maximum parameters between groups 1 and 3 mm. The group 5mm, instead, shows much lower shear strains and lap shear strengths.

Araldite

The figure for all grouped Araldite shear strain versus average lap shear stress curves is given in Figure 3.21.

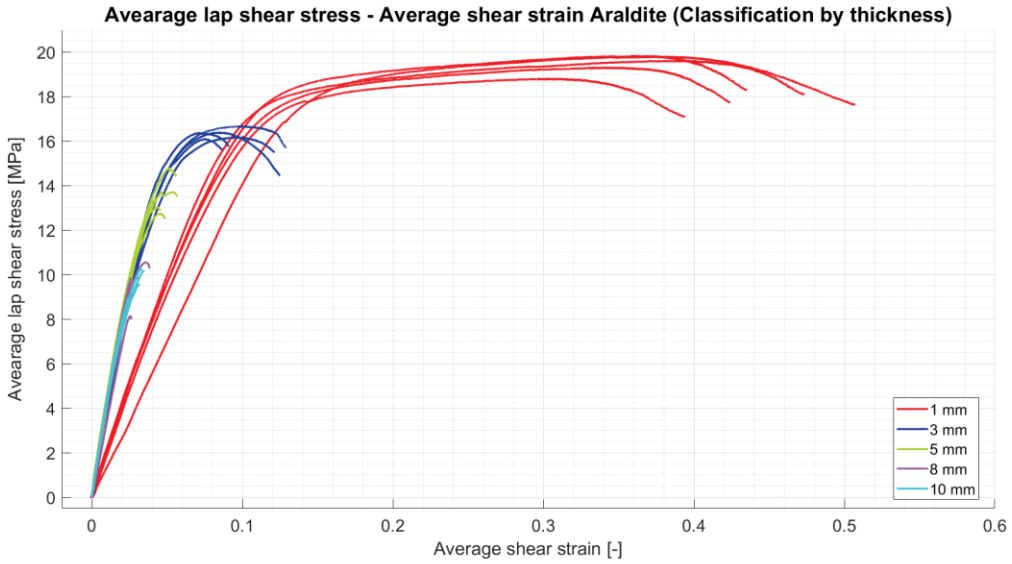

Figure 3.21 Araldite Average lap shear stress – Average shear strain curves. Classification by thickness

Sample group	Max. lap shear stress [MPa]	Max. average shear strain [-]
1 mm	19.5 ± 0.4	0.45 ± 0.04
3 mm	16.3 ± 0.2	0.11 ± 0.02
5 mm	13.5 ± 0.8	0.05 ± 0.01
8 mm	9.5 ± 0.9	0.03 ± 0.01
10 mm	9.4 ± 0.9	0.03 ± 0.01

Table 3.6 Maximum lap shear stress and maximum average shear strain for Araldite

Once more, there is a trend of decreasing lap shear strengths and shear strains with thickness (see Figure 3.21). Also note in this case the difference between group 1mm and all the other groups, which is due to the fact that, these curves are derived from the force – displacement curves which show only a small variation in displacement at failure. To determine the shear strain this displacement is divided by the thickness of the bondline, which acts as a "scale factor" of the original force – displacement curve (division by 1 for the 1 mm thickness adhesive and 10 for the 10 mm thickness adhesive).

All samples (Crestomer and Araldite) classified by thickness

The curves shown in Figure 3.22 corroborate once more that Araldite (solid line) is a brittle adhesive, whereas Crestomer (dashed line) shows a ductile behavior reaching much larger strains. The results are thickness dependent. As a general statement; for both materials the maximum lap shear strengths and maximum shear strains decrease with thickness. The maximum lap shear strength for Araldite is

of the order of 19.5 MPa for 1 mm adhesive bondline and 9.4 MPa for 10 mm. The maximum shear strains are in the order of 0.5, which is in agreement with literature. For Crestomer, it was obtained a maximum lap shear strength of 17.8 MPa for the 1mm bondline (c14) decreasing with thickness up to 6.1 MPa for 5 mm (c55). The maximum strains reached 1.1 for 1 mm bondline and over 0.7 for 5 mm.

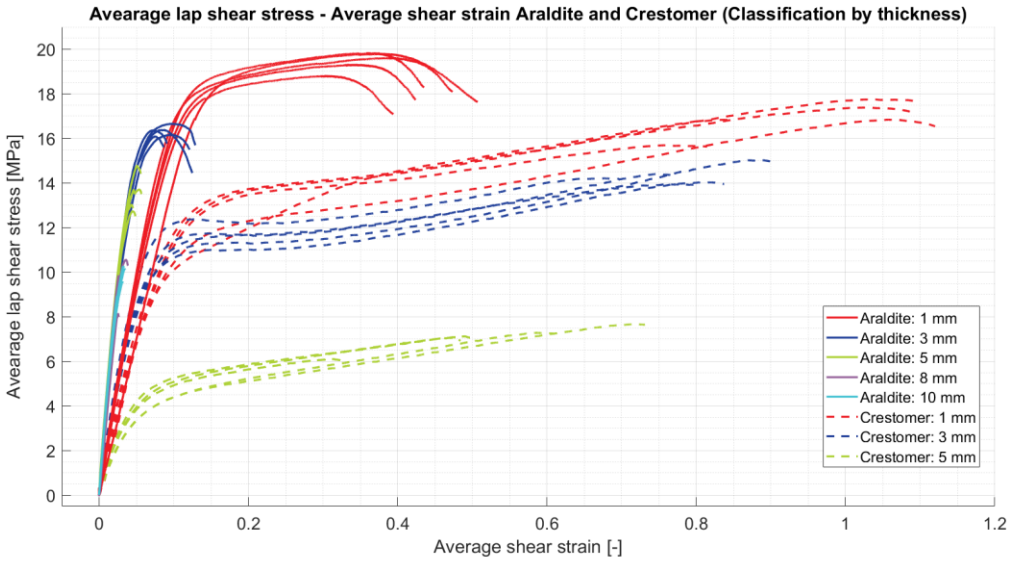

Figure 3.22 Araldite and Crestomer Average lap shear stress – Average shear strain curves. Classification by thickness

3.8.3 Shear modulus and Adhesive Ductility Parameter

The shear modulus is a parameter determined for a bulk material. Although the bulk results of the two adhesives were not available for this thesis, it was studied the possibility that the shear modulus obtained from the joint properties could be related to the bulk properties given in the literature. To determine the shear modulus, the procedure showed below was followed.

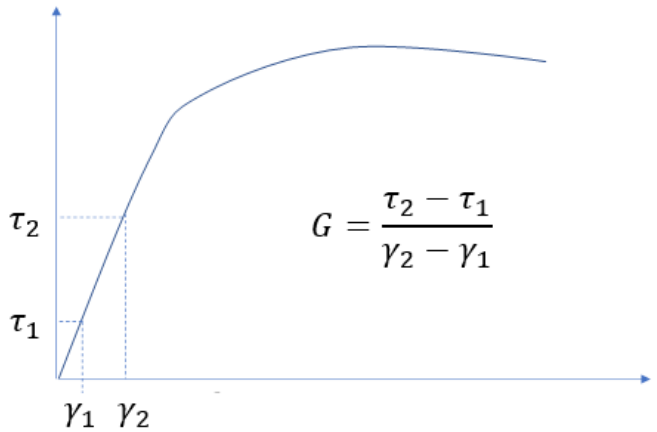

Figure 3.23 Shear stress-strain curve, usually used to calculate the shear modulus

The shear stress – shear strain curve can also be idealized into an elastic-plastic model. It is important that both curves have the same shear strain energy. Thus, the area under the idealized curve should be equal to the area under the actual stress-strain curve [48].

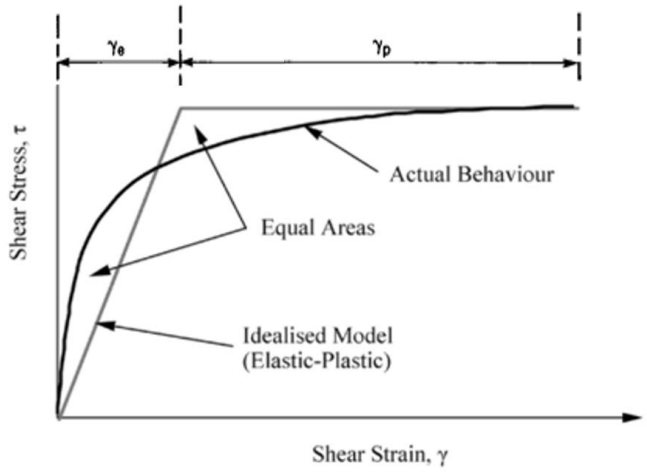

Figure 3.24 Actual and idealized shear stress-strain curve with characteristic parameters [48]

There are three parameters that characterize the properties of an adhesive:

- The plastic shear stress: τ_p
- The plastic shear strain: γ_p
- The elastic shear strain: γ_e

From these parameters it can be derived the following:

- The estimated shear stiffness (E-P): $G = \frac{\tau_p}{\gamma_e}$ (3.4)
- The Adhesive Ductility Parameter: $ADP = \frac{\gamma_p}{\gamma_e}$ (3.5)

The determination of the different elastic-plastic parameters can be achieved by following these steps, which can be found in literature [48].

1. Determine the slope of the initial part of the shear stress-strain curve ($G_{initial}$)
2. Determine the maximum or plastic shear stress (τ_p) and draw an horizontal line at this level.
3. Determine the maximum shear strain (γ_{max})
4. Determine the slope of the line that intersects the horizontal $\tau = \tau_p$ so that it defines two equal areas, above and under the actual curve, (G_{est}). This parameter characterizes the elastic part of the bilinear curve.
5. Calculate the elastic shear strain: $\gamma_e = \frac{\tau_p}{Gest}$ (3.6)
6. Calculate the plastic shear strain: $\gamma_p = \gamma_{max} - \gamma_e$ (3.7)
7. Calculate the shear strain energy, given by the elastic-plastic curve:

$$A = \tau_p \left(\frac{\gamma_e}{2} + \gamma_p\right) \quad (3.8)$$

The following Figure 3.25 shows an example of the obtained bilinear curve for Crestomer 1mm.

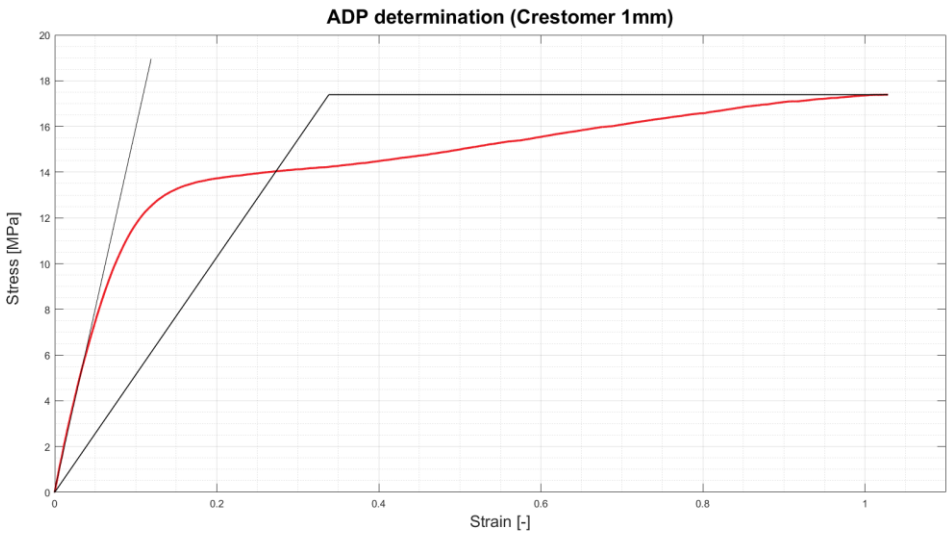

Figure 3.25 Approximation of curve with Elastic-Plastic model for Crestomer 1mm Joint

The obtained results are collected in Table 3.7.

	t	Plastic Shear stress	Max. shear strain	Ginitial	Gest	Elastic shear strain	Plastic shear strain	Shear strain energy (E-P)	Shear strain energy(Actual)	ADP
Units	mm	MPa	-	MPa	MPa	-	-	MPa	MPa	-
CRESTOMER	1	17.388	1.0284	**160**	51	0.3383	0.6901	14.941	14.942	**2.0**
	3	15.034	0.8851	**200**	43	0.3484	0.5367	10.687	10.688	**1.5**
	5	7.286	0.5971	**175**	25	0.2902	0.3069	3.293	3.294	**1.1**
ARALDITE	1	19.836	0.3586	**200**	159	0.1249	0.2337	5.8743	5.874	**1.9**
	3	16.394	0.0846	**533**	331	0.0495	0.0351	0.9812	0.981	**0.7**
	5	14.785	0.0506	**400**	385	0.0384	0.0122	0.4643	0.464	**0.3**
	8	9.866	0.026	**450**	420	0.0235	0.0025	0.1406	0.140	**0.1**
	10	9.577	0.0312	**450**	380	0.0252	0.006	0.1781	0.178	**0.2**

Table 3.7 ADP calculations for Crestomer and Araldite

The ADP is a good indicator of the level of elastic-plastic behavior of the adhesive. For the same thickness, Crestomer shows a more ductile behavior than Araldite, with larger ADP values. Furthermore, it can be seen for both adhesives a tendency of increasing the elastic behavior with thickness since the ADP decreases with thickness. However, note that these parameters are here calculated as for the joint, where in reality they should be obtained from the adhesive bulk test.

The shear modulus can be estimated graphically, determined by the tangent of the curve as shown in Figure 3.23. Since the linear part of the curve slowly decreases, In order to determine the shear modulus from the plots, multiple tangent lines to the test curves are drawn, whose inclination define the G as a function of the shear strain. The results of this procedure are shown in the figures below.

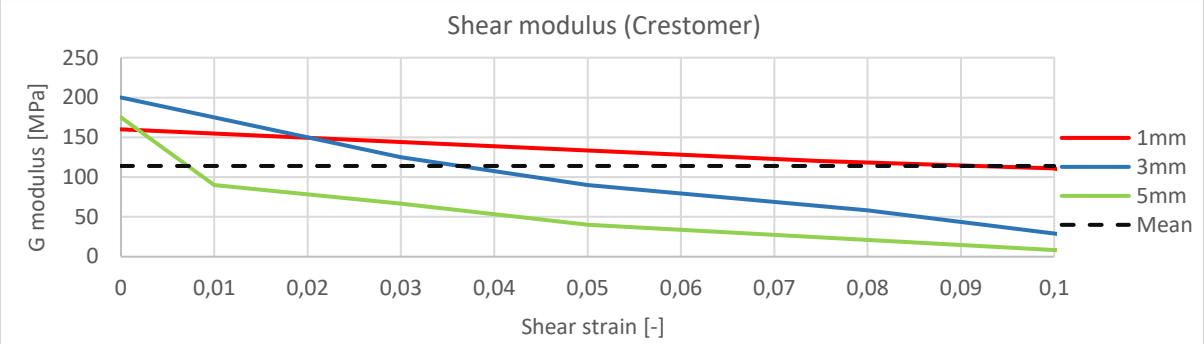

Figure 3.26 Shear modulus determination for Crestomer

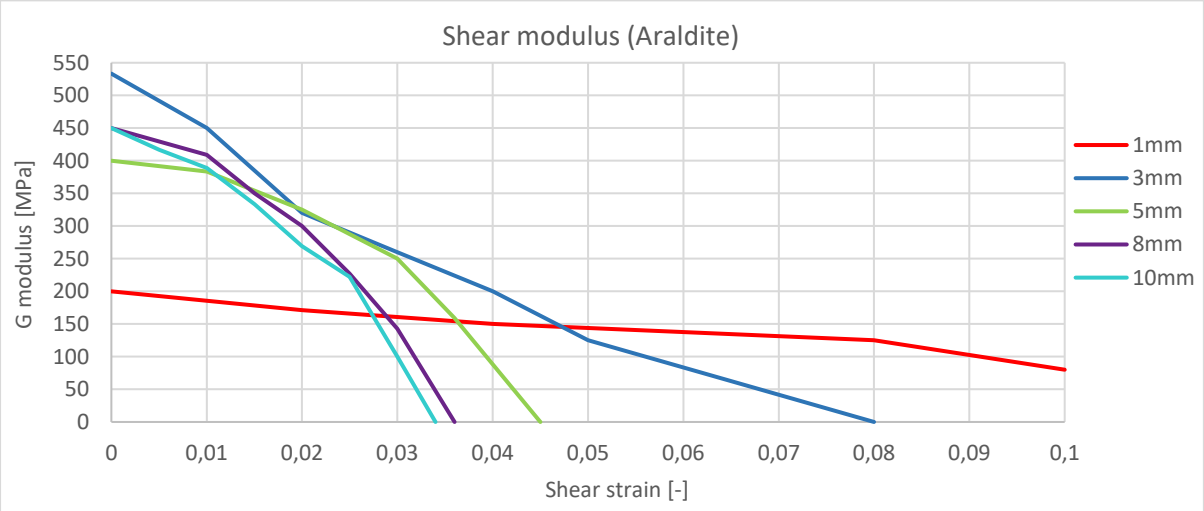

Figure 3.27 Shear modulus determination for Araldite

The obtained mean shear modulus for Crestomer considering all the thickness is 114 MPa. This value, according to the material data should be between 300 and 500 MPa. For Araldite, values vary a lot in thickness and quickly lessen with strain, also differing from the 560 MPa defined in literature.

Thus, it is proven that the parameters obtained with the test curves refer to the joint, but do not give information of the actual shear modulus of the adhesive.

3.8.4 Double lap shear strength

The following figures show the trend of the lap shear strengths that were obtained in the experiments. Also their mean values and standard deviations are given. The lap shear strength decreases with the adhesive thickness by a 52% in case of Araldite (up to 10 mm) and 58% for Crestomer (up to 5 mm).

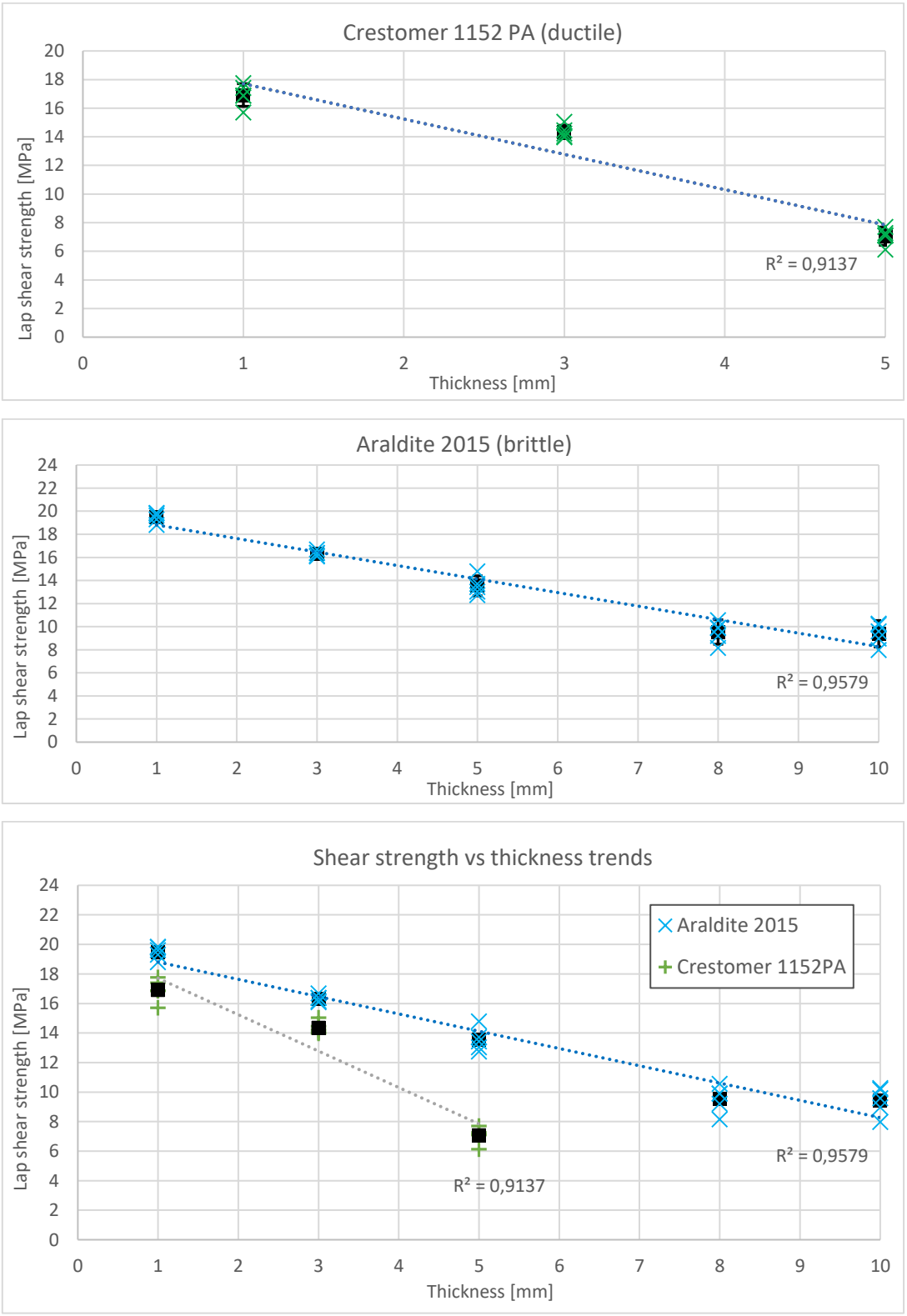

Figure 3.28 Experimental results and linear trends of shear strength vs adhesive thickness (top Crestomer, middle Araldite, bottom both)

The following Figure 3.29 shows a comparison of the experimental results with the data collected in the literature review. In this case linear regression lines are not drawn but lines connecting the dots in order to reproduce the actual data found in the experiments. Linear regression was used in Figure 3.28 for an easier interpretation of the results.

As stated in the literature, the decrease in the shear strength is not linear. In the case of the Araldite, the shear strength decreased almost perfectly linearly up to 8mm thickness. However, it showed a smaller decrease after 8 mm. The difference in the strength decrease of these two adhesives was also expected, since Araldite is an epoxy and in literature epoxies showed a more linear behavior than other adhesives. Crestomer, which is a urethane-acrylic, showed a higher decrease in the shear strength between 3 and 5mm than between 1 and 3 mm. Unfortunately, little information is available in literature about this last type of adhesives to compare with.

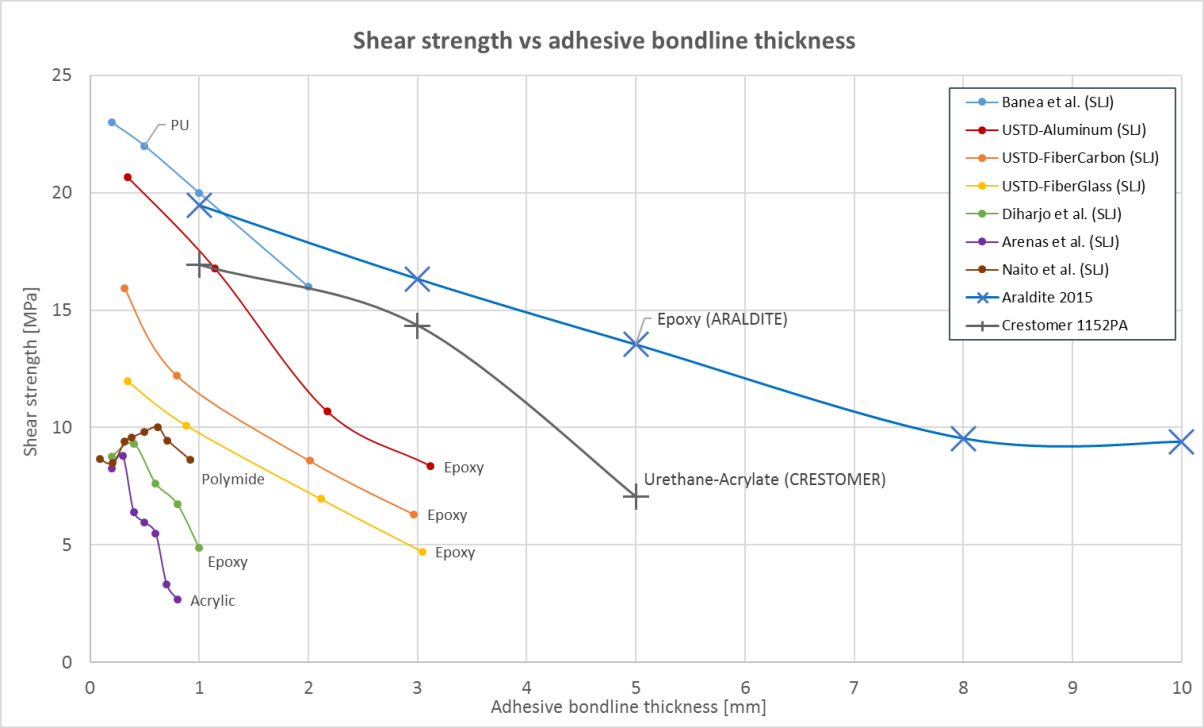

Figure 3.29 Comparison of experimental results and literature review findings

3.8.5 Point of failure initiation and failure direction

Crestomer

All Crestomer samples showed adhesive failure, generally in the interface between the adhesive bondline and the outer adherend (see Figure 3.30). Only in two cases (c35 and c51) out of 15 failure occurred in the interface with the middle plate. Failure initiated on the top next to the adherend and propagated mostly in the interface. In some 1mm cases ((i) in Table 3.8), a portion of adhesive can be seen in the lower part of the outer adherend. Two explanations can be derived from this; either failure also initiated from the bottom part next to the inner adherend or this occurred at the latest stages as a consequence of the impact at the moment of failure or due to the separation of the outer adherend from the initial position. In order to clarify these two assumptions, special attention has to be paid to the High Speed videos.

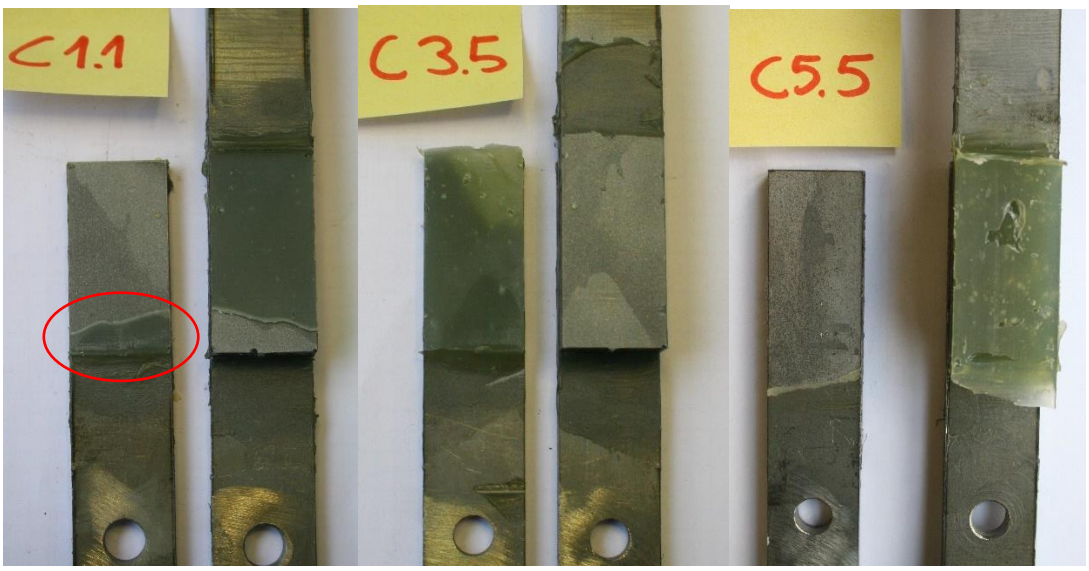

Figure 3.30 Trends in failure (Crestomer). From left to right: 1mm (jump from outer to inner interface), 3mm and 5mm

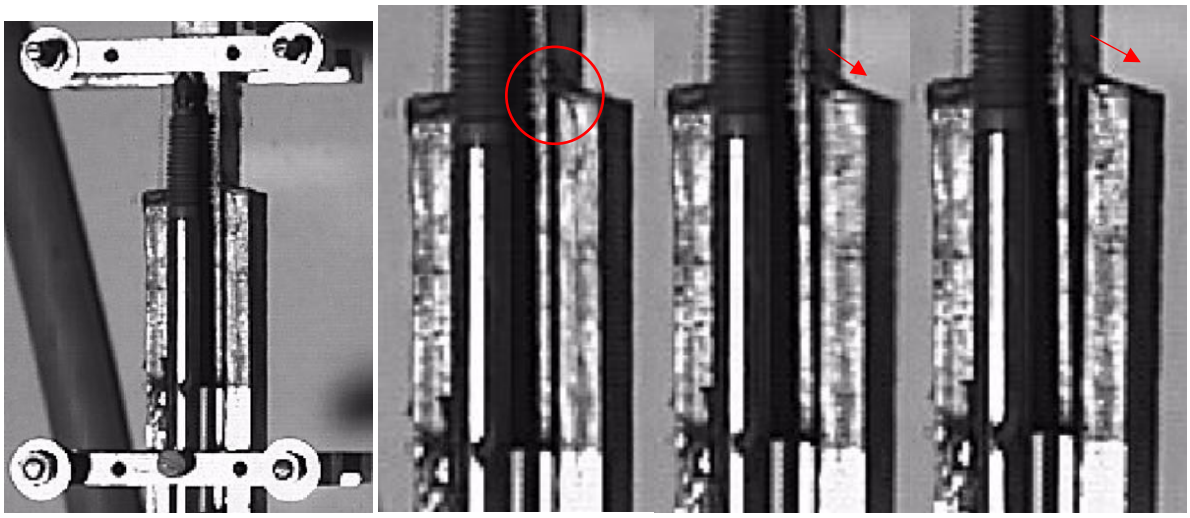

Figure 3.31 Failure initiation and propagation from top to bottom (c13). Frames 345 to 348 at 2000 fps HS video

By analyzing the HS video frame by frame it can be seen that failure starts at the top edge towards the bottom as the outer adherend moves to the side (see Figure 3.31). Therefore, one can conclude that due to the separation of the adherend, which also may introduce bending, the crack might jump into the inner adherend, reason why in some cases the adhesive is present on the top of the outer adherend and on the bottom part of the outer one.

Araldite

Araldite samples, in comparison to Crestomer samples, showed a more cohesive behavior. After analyzing the High Speed videos recorded during the experiments, it can be determined that cracks initiates at the top part of one of the adhesive layers and propagates downwards. A trend can be seen in terms of the exact point of initiation. For thin adhesive layers (1 mm), in most cases the crack starts in the adhesive edge near the outer adherend and propagates diagonally towards the inner adherend. This is proven when looking at the failed cross-section of the outer adherend. It can be seen that steel is visible on the top of the outer adherend, where the crack initiated (see Figure 3.32).

Figure 3.32 Area of Initiation (1mm sample) with visible steel line on top of the outer adherend

Note that the point of initiation explained in the text is marked with a black dot to identify the exact point where the crack initiated.

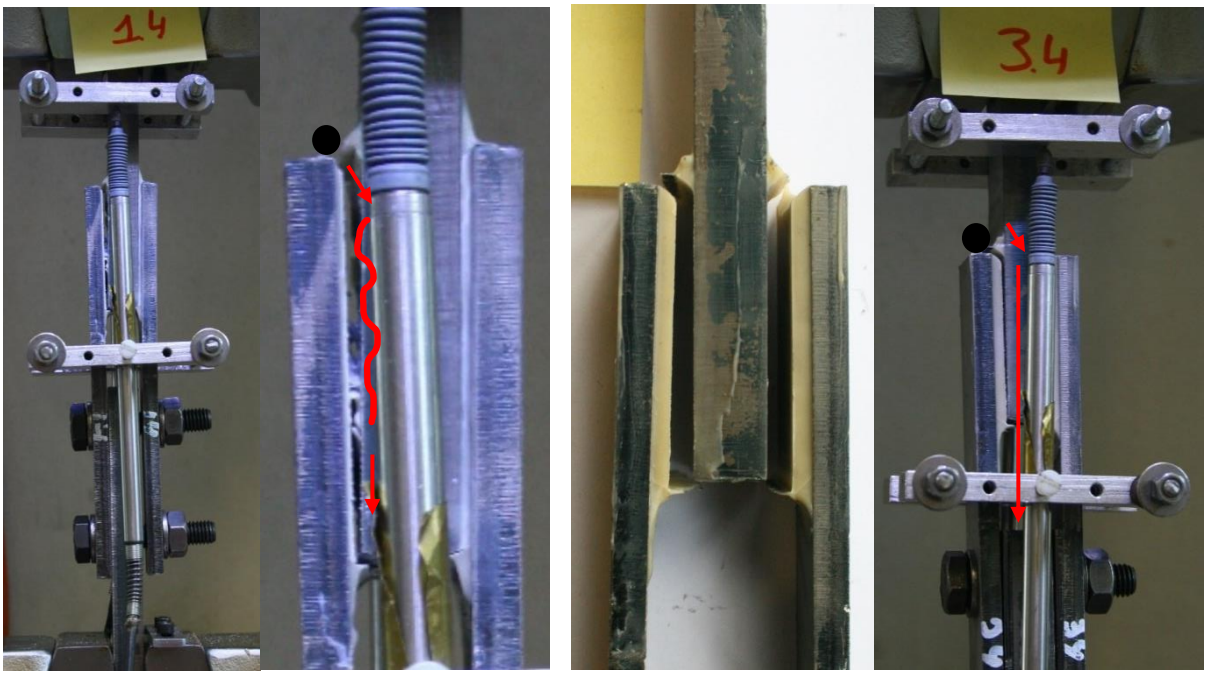

Figure 3.33 (Left)Crack path (1mm) from top outer adherend towards inner adherend, downwards along the adhesive layer. (Right) Trend in failure initiation and crack development for 3mm samples

A similar behavior was observed for the 3 mm adhesive layer. In this case, however, the crack propagated in a straight line downwards after it reached the inner adherend (Figure 3.33, right). Therefore, the failure mode is more adhesive than cohesive.

For larger thicknesses (5 to 10 mm) two trends can be observed. Crack initiated either in the middle of the curved edge (trend A) as cohesive failure and propagated towards the inner adherend to continue there as adhesive failure (see Figure 3.34) or it started already at the mid adherend (trend B) and propagated straight downwards, thus mostly as adhesive failure (see Figure 3.35).

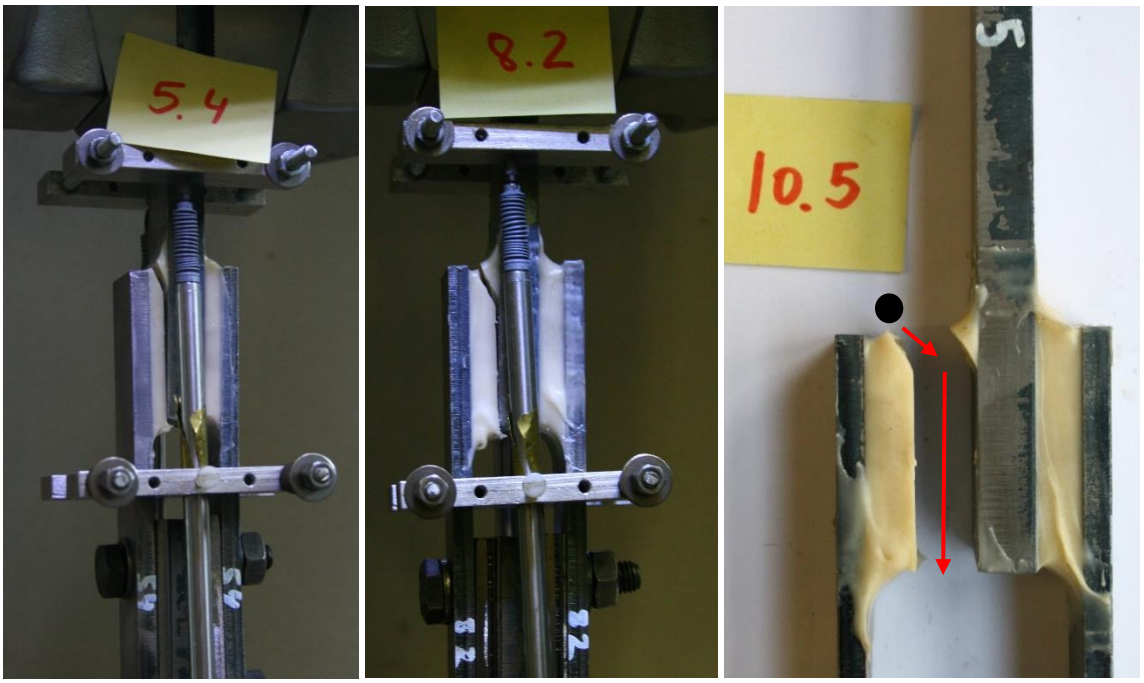

Figure 3.34 Crack initiation in the middle of the edge (trend A). From left to right: 5mm, 8mm and 10mm

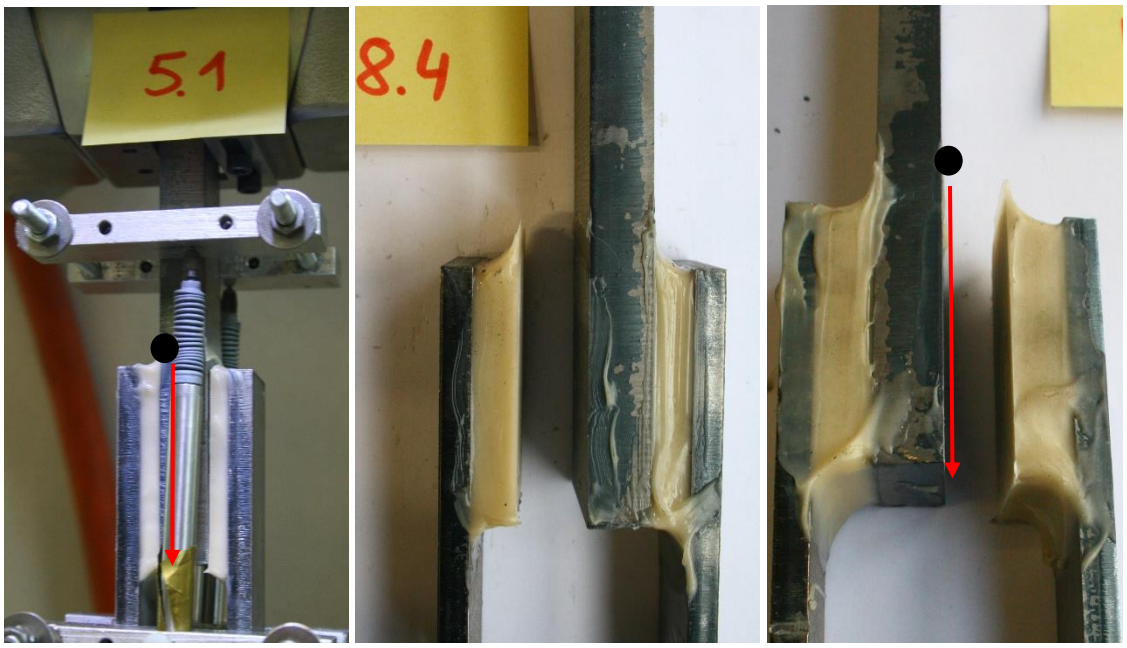

Figure 3.35 Crack initiation next to the mid adherend (trend B). From left to right: 5mm, 8mm and 10mm

By analyzing the high speed videos, it is possible to determine the exact moment when the crack initiates and the time from crack initiation to failure. In all the cases, the crack developed along the bondline within 2 or 3 frames. Thus, since the high speed was set to 2000 fps, it can be assumed that it took less than 2 milliseconds for the crack to propagate till failure.

3.8.6 Failure modes

Two failure modes can be identified in the tests; adhesive and cohesive failure. In the case of the Crestomer, all samples showed adhesive failure. As explained in 3.8.6 (Crestomer section), some samples failed in the outer interface, jumping into the inner adherend at the bottom part ((i) in Table 3.8). For this reason and depending on the geometry of the area in which failure jumped from one interface to the other, a percentage of cohesive failure was determined (2 to 15%). All samples of 3 and 5 mm failed solely in the interface. Note some interesting cases ((ii) in Table 3.8), that showed adhesive failure on both interfaces; outer at the top and inner at the bottom. In these later cases, the interface section cannot be analyzed since the sample did not result in completely separated parts.

For Araldite, failure is mostly cohesive for thin layers and tends to be more adhesive for larger thicknesses. In order to obtain the amount of adhesive that remained on the steel plate and further determine the percentage of each failure mode, the pictures of the failure surface were analyzed with MATLAB. Firstly, the images were cut selecting only the area of the inner adherend. Secondly, the contrast of the images was set to the maximum so colors stand out. Finally, images were converted into a grayscale and thereafter into binary images with color white representing the remaining adhesive and black representing the steel. The different types of images are shown in Figure 3.36.

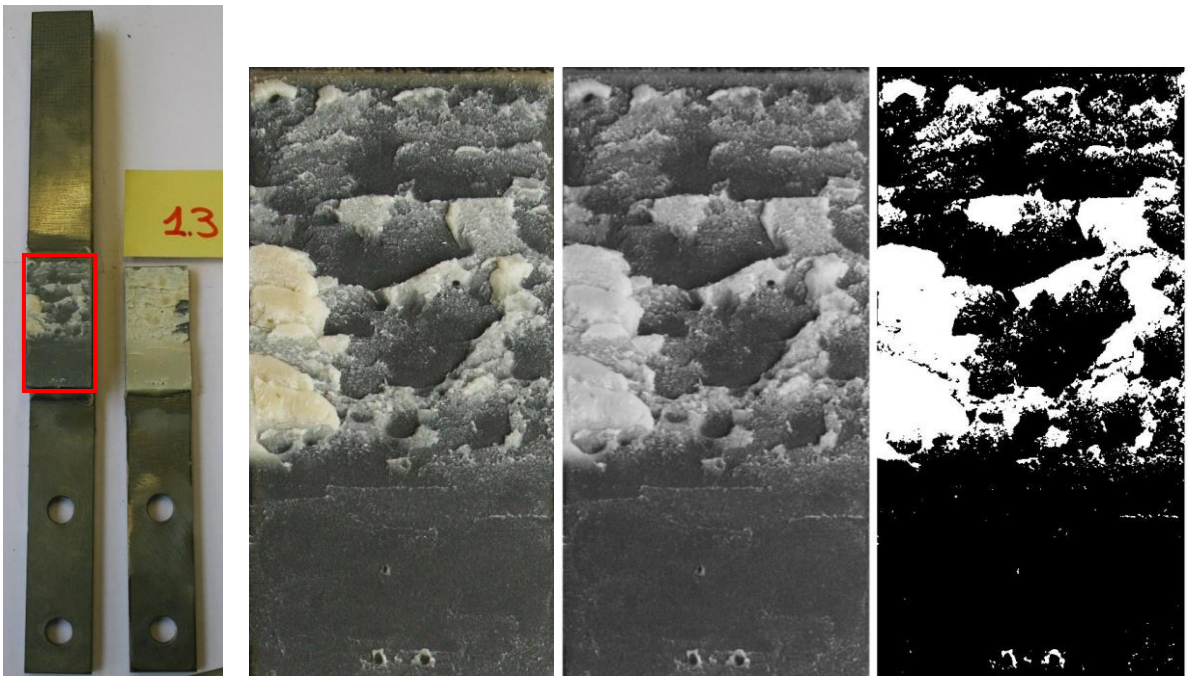

Figure 3.36 From left to right: failed specimen a13 with area of study (red); detailed pictures: initial, grayscale and binary

Using the binary color pictures, an analysis of the pictures with MATLAB provided the percentage of the cross-section in which the adhesive has remained attached in the middle adherend and furthermore, it was used as a tool to determine the type of failure mode.

It was noticed that a change in any parameters such as light and contrast can modify completely the results. For this reason, all the parameters were the same for all the pictures and also all binary pictures were checked so that they accurately represented the failed section. All the detailed pictures used with the method of the photographs can be found in the Appendix 2. The resulting percentages of adhesive and cohesive failure for all specimens, and the average results per adhesive and per thickness, are given in Table 3.8 and Table 3.9.

	Sample	Cohesive failure [%]	Adhesive failure [%]	Obtained FM
1mm	c11	10	90 (i)	10 % CF 90 % AF
	c12	5	95	
	c13	15	85 (i)	
	c14	10	90 (i)	
	c15	10	90 (i)	
3mm	c31	0	100	100 % AF
	c32	0	100	
	c33	0	100 (ii)	
	c34	0	100 (ii)	
	c35	0	100	
5mm	c51	0	100	100 % AF
	c52	0	100 (ii)	
	c53	0	100	
	c54	0	100	
	c55	0	100	

Table 3.8 Failure modes for Crestomer

(i) Adhesive on both adherends
(ii) Failure on both interfaces, but failed section not visible

	Sample	Cohesive failure [%]	Adhesive failure [%]	Obtained FM
1mm	a11	80	20	88 % CF 12 % AF
	a12	100	0	
	a13	60	40	
	a14	100	0	
	a15	100	0	
3mm	a31	40	60	42 % CF 58 % AF
	a32	40	60	
	a33	50	50	
	a34	40	60	
	a35	40	60	
5mm	a51	30	70	32 % CF 68 % AF
	a52	30	70	
	a53	30	70	
	a54	30	70	
	a55	40	60	
8 mm	a81	10	90	18 % CF 82 % AF
	a82	30	70	
	a83	30	70	
	a84	10	90	
	a85	10	90	
10mm	a10 1	20	80	14 % CF 86 % AF
	a10 2	0	100	
	a10 3	0	100	
	a10 4	30	70	
	a10 5	20	80	

Table 3.9 Failure modes for Araldite

As shown in Table 3.8, Crestomer samples' failure mode was mostly adhesive for 1mm thickness and fully adhesive for 3 and 5 mm thickness. In the case of Araldite (Table 3.9), the failure mode was mostly cohesive for the thin adhesive layers. For 3 mm, failure already shifted to a more adhesive mode, which kept gradually increasing with the thickness. Therefore, the change in behavior between cohesive and adhesive failure is expected to occur somewhere between 1 and 3 mm (see Figure 3.37).

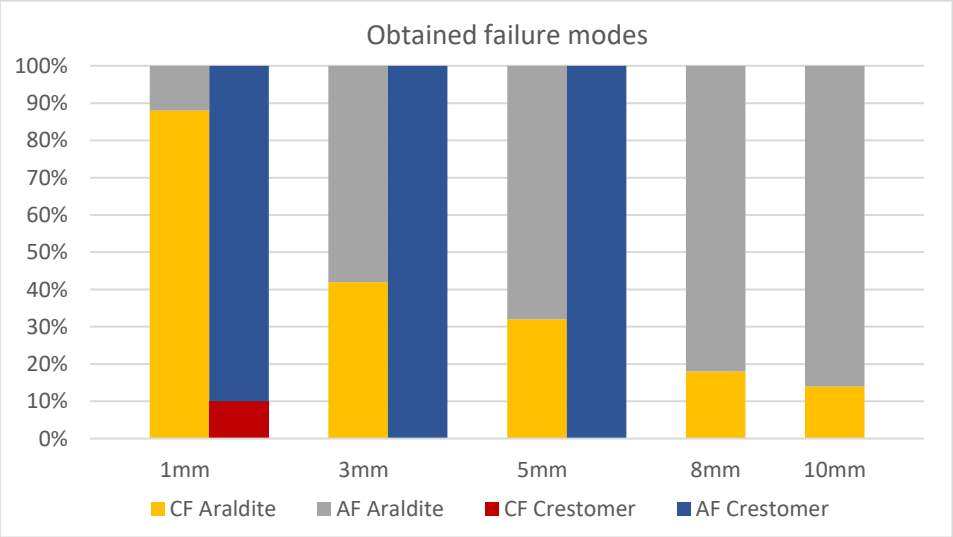

Figure 3.37 Classification by thickness of the obtained failure modes [%], obtained with the photo analysis

Although the Matlab analyses of the failure surface, which are fairly easy to do with standard available equipment, already showed trends, this method is not able to state if adhesive failure was really adhesive failure or cohesive failure very close to the bondline. Therefore, a final action was taken in order to clarify if the adhesive failure actually occured in the interface or in the adhesive bondline but very close to the interface for the thick Araldite specimens. For this purpose, the failure surfaces of the Araldite specimens were analysed with an optical microscope (OM).

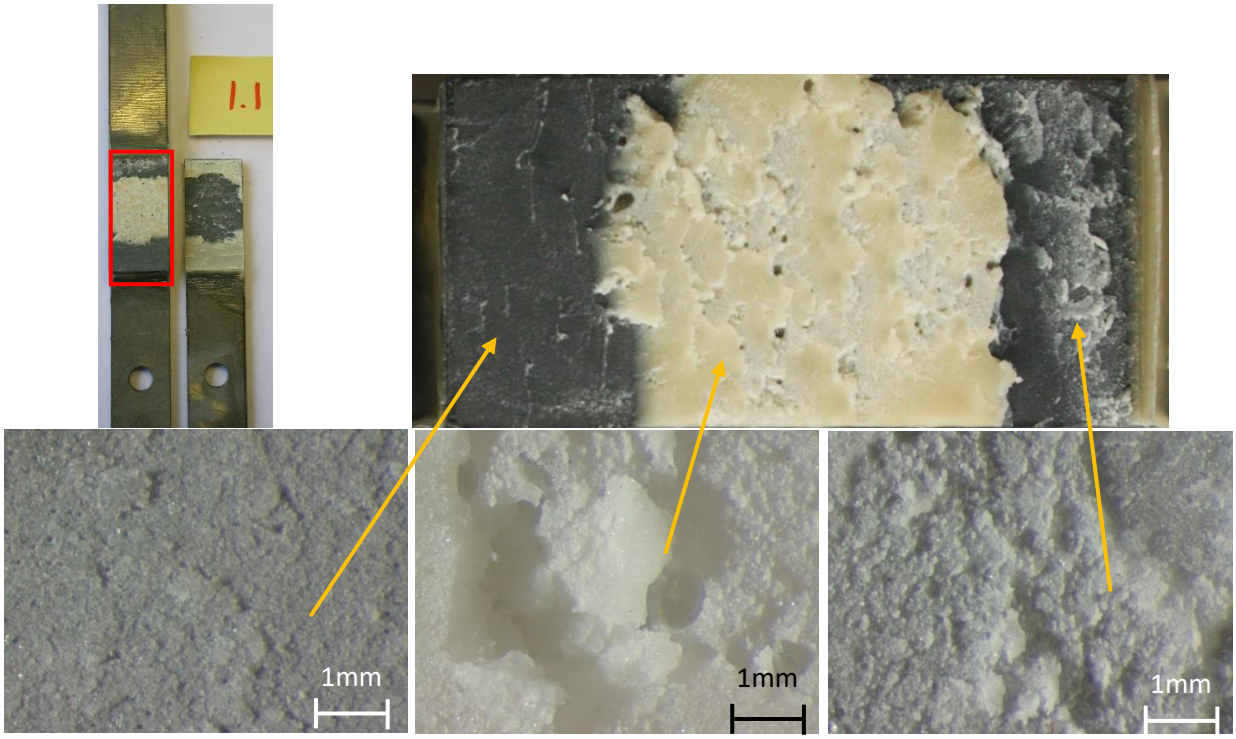

Figure 3.38 Pictures obtained with the microscope, magnification 8x, specimen 1mm (a11)

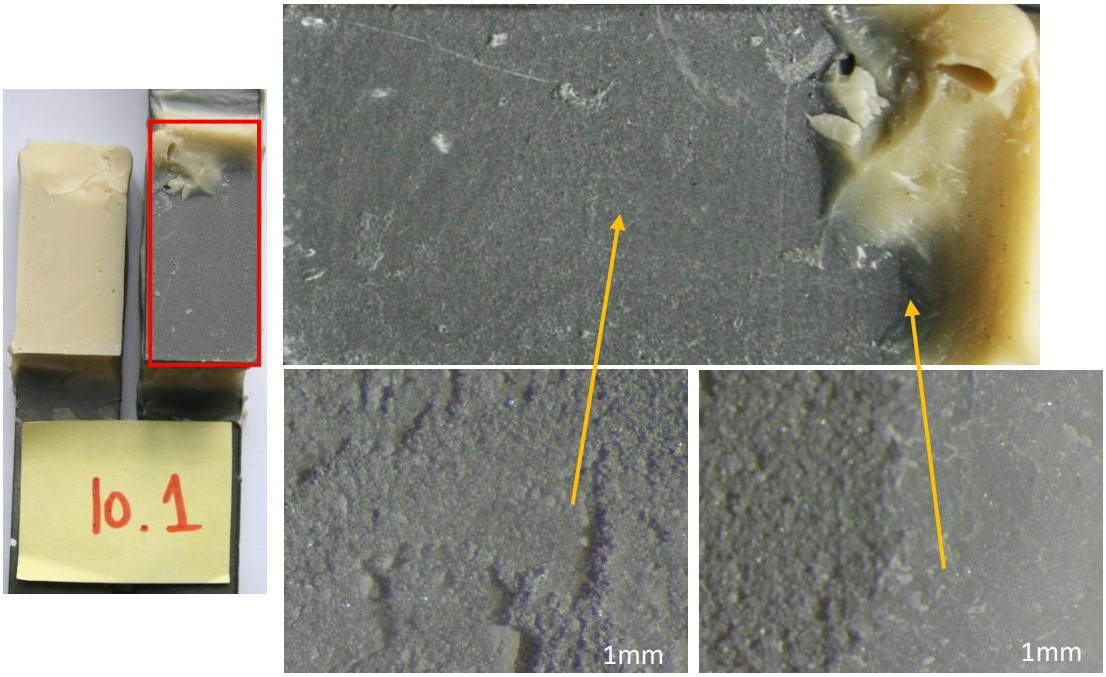

Figure 3.39 Pictures obtained with the microscope, magnification 8x, specimen 10mm (a101)

In all the magnified pictures (see Figure 3.38 and Figure 3.39), the adhesive can be seen, meaning that a thin layer remains on top of the steel plate. Therefore, it can be concluded that what was considered as adhesive failure is actually failure in the adhesive, but very close to the interface.

3.9 DISCUSSION

Load – displacement curves

When assessing the load – displacement curves different conclusions can be drawn. For Crestomer, the trend is an increase of deformation capability (up to 3.6 mm) and decrease of loading capability (from 43.84 ± 2.0 kN to 19.72 ± 1.6 kN) with increasing thickness. The mechanical response agrees with a characteristic curve of a ductile material, with a linear increase of the load at the initiation of the test, up to a certain plateau where the adhesive starts behaving plastically.

For Araldite, the trend is also a decrease of loading capability (from 50.44 ± 1.1 kN to 28.62 ± 2.9 kN) with thickness. However, results showed two different behaviors. Specimens in groups 1, 3 and 5 mm bondline showed a plateau before reaching the failure load, which might correspond to an initiation of failure at a microscale level with formation of microcracks. Specimens in groups 8 and 10 mm bondline showed a similar linear elastic behavior. The length of the plateau seen in the first group does decrease with increasing bondline thickness.

When comparing both materials, Crestomer shows more deformation capability than Araldite, which in turn shows higher loading capability and as such, lap shear strength. The average lap shear strengths, determined by the loading capability and the shear area, decrease with thickness, which is in agreement with literature. A decrease of 58% and 52% was obtained for Crestomer (from 16.92 ± 0.8 MPa to 7.06 ± 0.6 MPa) and Araldite (from 19.47 ± 0.4 MPa to 9.39 ± 0.9 MPa), respectively.

Lap shear strength – shear strain curves

The results are also thickness dependent. As a general statement; for both materials the maximum lap shear strength and maximum shear strain decrease with thickness. For Crestomer a maximum lap shear strength was obtained of 17.8 MPa for the 1 mm sample decreasing with thickness up to 6.1 MPa for 5 mm. The maximum shear strain reached 1.1 [-] for 1 mm bondline and over 0.7 [-] for 5 mm. Note that even if a strain of 1.1 seems very high, it refers to shear and therefore this deformation is related to the thickness of the adhesive layer; actually a shear strain of 1.1 indicates that there is also a longitudinal displacement of 1 mm. The maximum lap shear strength for Araldite is in the order of 19.5 MPa for 1 mm adhesive bondline and 9.4 MPa for 10 mm. The maximum shear strains are in the order of 0.5, which is in agreement with literature. The shear modulus (G) obtained from these curves varies with thickness and does not relate to the values found in literature. Therefore, it is proven that this parameter gives information at a joint level and not about the adhesive itself.

Failure modes

Two failure modes were present in the tests, cohesive and adhesive. All Crestomer samples showed adhesive failure; fully (100%) adhesive for 3 and 5 mm groups and 90% adhesive for 1 mm bondline group, where failure initiated in the curved edge and jumped into the interface. For Araldite, the main failure mode present in the tests was cohesive, which occurred at two levels, either within the bondline, for 1 mm bondline samples, or along a line almost at the interface for all the other thicknesses. Therefore, the change in behavior between mostly cohesive and mostly adhesive failure or ‘‘cohesive next to the interface’’ is expected to occur somewhere between 1 and 3 mm.

4 FINITE ELEMENT ANALYSIS

Within this chapter the Finite Element (FE) Analyses of the double lap joint specimens are discussed. The aim of these analysis is to model the mechanical behavior of these joints. Section 4.1 describes the numerical model, including the mesh modelling techniques used for the bulk material and for the interface modelling. In Section 4.2 the cohesive zone implementation is tested in one element test conditions. Section 4.3 contains the FE results obtained with conventional solid elements. Section 4.4 discusses the results with cohesive zone modelling; Section 4.5, the validation of the models.

The results in this chapter are only given for Araldite, since for this adhesive experimental results showed a cohesive failure mode. This is of interest for this study because thickness plays an important effect on the failure within the adhesive bondline. For Crestomer, failure mode was mostly adhesive, thus, not dependent on the thickness.

4.1 DESCRIPTION OF THE NUMERICAL MODEL

4.1.1 Modelling description

The Finite Element software Abaqus is used for this study. An investigation is done into the behavior of double lap joints (DLJ) in shear loading for increasing adhesive thicknesses.

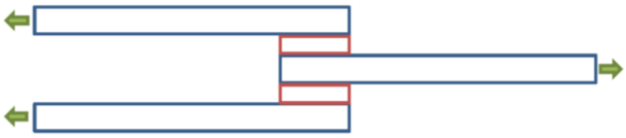

Figure 4.1. Side view schematic representations of a DLJ. Adherends are colored blue, adhesive in red and loading in green

The dimensions of the models are chosen identical to the dimensions of the specimens tested, described in Chapter 3 and in the test plan (see Appendix 1).

Due to the symmetry of a double lap joint through thickness direction, the model is simplified into a single lap joint representing half of the joint. This is possible since same behavior is expected at both adhesive layers. This symmetry is defined when applying the boundary conditions (See Figure 4.2). Therefore, the three boundary conditions applied on the model are the following:

- Uniform displacement on the right hand side of the lower adherend;
- Clamped upper adherend, thus no rotation and no displacements are allowed. In the model, this condition is applied at 75 mm from the center of the adhesive; according to the test set-up, this is the distance at which the specimen was clamped. This distance is large enough so that it does not affect the behavior of the interface;
- Symmetry at the bottom, to reproduce it is a double lap joint

The dimensions of the adhesive joint in the direction normal to the x-y plane (z-direction) are 25.4 mm; the sample width. No boundary conditions are applied to either plane normal to the z-axis. Thus, plane stress conditions apply and all surfaces normal to the z-axis cannot move in the z-direction.

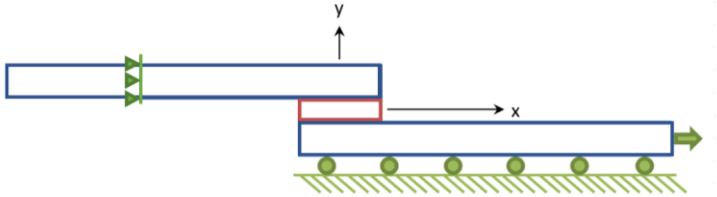

Figure 4.2. Boundary conditions applied in the model

4.1.2 Finite element models

Conventional modelling with solid FE elements is used to model the adhesive layer. The stress-strain curve in Figure 2.35 shows that Araldite behaves linearly up to a certain point after which a large decrease of stiffness occurs. The decrease is probably due to the occurrence of damage in the material. Since the curve resembles an elastic-plastic curve, a representation using a bilinear material curve is used. Three different plasticity models, available in Abaqus, are considered for this.

- Von Mises Model
- Linear Drucker-Prager (Linear D-P) Model
- Exponential Drucker-Prager (Exponential D-P) Model

Drucker-Prager is an extension of Von Mises criterion by including the influence of hydrostatic pressure dependent yielding, for a better representation of the mechanical behavior of the adhesives, whose yielding behavior might differ at different hydrostatic pressure due to their chain chemical structure. This failure criteria was derived from theories of soil mechanics [42].

Of course many other models exist to model the behavior of adhesives such as Smeared Crack Models. These models are very suitable for describing the crack propagation. Since the aim of this thesis is to describe the failure up to failure initiation, these models were not used. Furthermore, in this thesis it was decided to implement both Von Mises and the linear Drucker-Prager plasticity models. Note that for every specific adhesive, it will have to be determined which is the most convenient model to represent the microstructure of that particular adhesive system.

The steel adherends are designed such that no yielding of the material is expected. Therefore, they are modelled using continuum elements with an elastic material behavior.

Cohesive Zone Modeling is also used for strength prediction of adhesive bonded joints as an additional method to the conventional continuum FE models. This method is used for very thin continuum layers or at interfaces between two materials. The Cohesive Zone Models (CZM) follow a 'cohesive law' also known as traction-separation law, to predict crack initiation, propagation and failure. This cohesive law represents the cohesive traction and relates the separation displacement between cohesive surfaces, given as the relative displacement of two associated nodes in a FE model, to the force per unit area, which is named traction.

The coupling of two associated nodes is accomplished by cohesive zone elements (See Figure 4.3). These elements do not necessarily have to represent a physical present material and therefore can be modelled with an initial zero thickness.

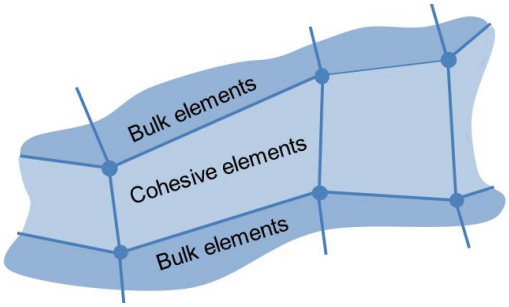

Figure 4.3. Application of cohesive zone elements between boundaries of bulk elements [50]

Thus, by making use of cohesive zone elements, it is possible to model regions of continuous materials with a few micrometers thickness or interfaces of different materials. In the case of thick adhesive layers as in this study, the CZM is suitable only for modelling and investigating the interfaces between the adhesive and the adherends.

There are multiple types of Traction – Separation Laws (TSL). The most commonly used types for strength prediction are the exponential, bilinear (also called triangular) and trapezoidal law. The traction-displacement relationship of these laws is shown in Figure 4.4.

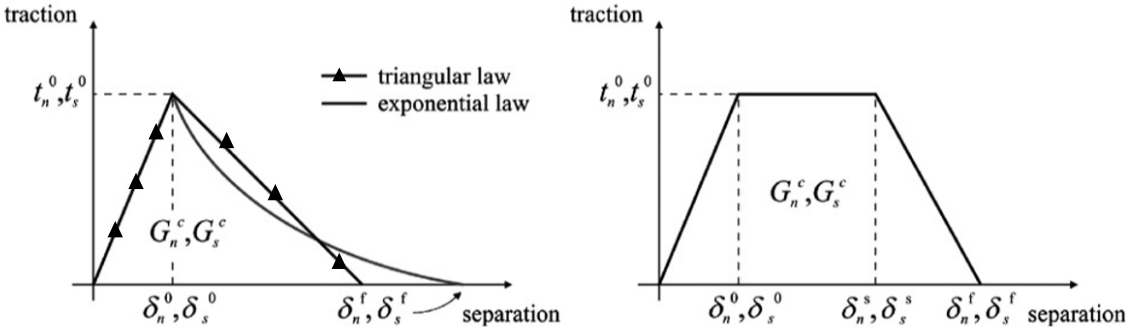

Figure 4.4. TSL with exponential, triangular and trapezoidal shapes available in Abaqus [47]

The maximal allowable traction before degradation of the interface starts, is named the interfacial bond strength, indicated as t_n^0 or t_s^0 for pure mode I (peel) and mode II (shear) loading, respectively. For all traction separation laws, note an initial elastic response of the cohesive zone, until it reaches a critical traction, after which either degradation of the stiffness starts or some plastic plateau is reached. When traction becomes zero, failure occurs. It can be seen that the linear-exponential law is linear up to t_n^0 and t_s^0, the critical cohesive tractions in tension and shear, and afterwards presents an exponential softening up to failure. This shape is an approximation of a full-exponential law, which also has an exponential initial part of the curve, providing in this case a faster stress drop than the bilinear law, after the peak loads are achieved, but a larger separation up to full failure.

These laws are valid for both shear and tension loading. The areas under the CZM laws are the critical energy release rates for mode I and mode II, defined as $G_n(= G_{Ic})$ and $G_s(= G_{IIc})$. The normal and shear maximum displacements are defined as δ_n^f and δ_s^f.

Depending on the geometry and the loading of a bonded joint, a combination of a mode I and mode II loading is present in the cohesive elements. Most FE software are able to combine the pure mode I and mode II CZM and create a mixed mode model. An example of a combination of a bilinear mode I (blue) and mode II (red), forming a bilinear mixed mode CZM (green) is shown in Figure.4.5.

The choice of the CZM law will also depend on the type of adhesive. For brittle adhesives, it is usually recommended to use bilinear laws and for ductile adhesives, trapezoidal laws. In this case, the bilinear CZM law is used since the interface for which the CZM is used has properties of the Araldite, which is assumed to be brittle.

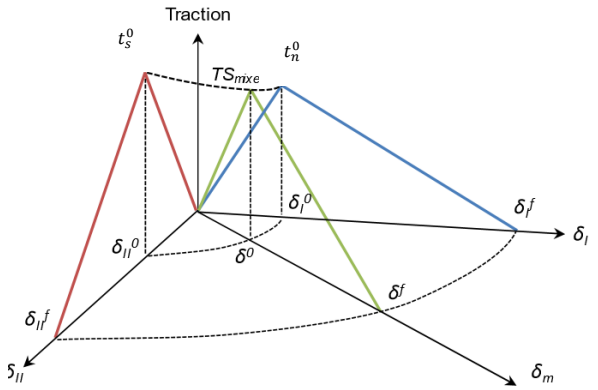

Figure.4.5. Example of bilinear mixed mode cohesive zone model [50]

For mixed mode CZM, combined initiation of failure exists for any of the three CZM laws, defined by the following stress criterion.

$$\left\{\frac{t_n}{t_n^0}\right\}^{\alpha} + \left\{\frac{t_s}{t_s^0}\right\}^{\alpha} = 1 \quad (4.1)$$

Where:

t_n	Mode I interface traction	[Pa]
t_s	Mode II interface traction	[Pa]
α	Exponent	[-]
t_n^0	Mode I interfacial bond strength	[Pa]
t_s^0	Mode II interfacial bond strength	[Pa]

CZM presents a limitation: It is necessary to know in advance the critical zones where damage is prone to occur. However, this is not an issue when using the CZM technique to model interface failure.

4.1.3 Necessary properties for FE modelling of adhesives

The parameters needed for the modelling of thick adhesive layers (thickness varying between 1 to 10 mm) are separated in these two groups:

- Adhesive constitutive and strength parameters of the bulk adhesive material.
- Interface parameters of the adhesive and the adherend material interface.

By obtaining these two types of parameters, one is able to create a FE model where the interface and the adhesive are modeled separately. Therefore, the failure of both zones can also be investigated independently, resulting in a better understanding of the failure process.

4.1.3.1 Adhesive constitutive and strength parameters

As seen in the literature review (Chapter 2), adhesives generally exhibit plasticity. For this reason, it is necessary to differentiate between linear elastic and elastic-plastic analysis. For a linear elastic FE analysis of an adhesive, which is assumed isotropic, only two parameters are required; the Young's modulus of elasticity, E, and the Poisson's ratio, ν. From these, the shear modulus, G, can be derived. For an elastic-plastic FE analysis, besides the elastic material behavior, the plastic material behavior is also required in the analysis. The plastic behavior is described by a "true" stress-strain curve under tension or shear loading, which has to describe the material's behavior until the material failure after the ultimate tensile stress (UTS) is reached. This curve is approximated by a bilinear curve (see Figure 4.6). Even though the stress strain curve introduced in Abaqus is based on true stress, true strain information and as such an ever increasing curve is expected, it does not matter that a straight line is taken as the final part, since this part is only there to enable a last step in the analysis if UTS is reached in between two subsequent displacement steps. Nevertheless, results are only interpreted up to UTS.

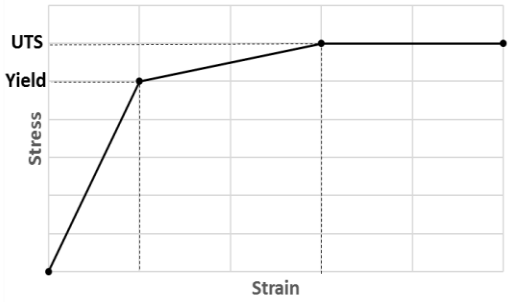

Figure 4.6. Bilinear tension curve that defines the plastic behavior of the adhesive.

Tension	
Stress [MPa]	Plastic strain [-]
σ_y =18	ε_y =0
σ_{UTS} =27.3	ε_{UTS} =0.02
σ_{UTS} =27.3	ε_{max} =1

Table 4.1. Tension curve parameters of Araldite 2015 [32]

A summary of the necessary parameters is given in Table 4.2.

Analysis	Material parameters
Linear elastic	• Young's modulus, E [Pa] • Poisson's ratio, ν [−]
Elastic plastic	• Linear elastic material parameters • True stress-strain curves under tension loading, $\sigma_T\left(\varepsilon_T^p\right)$ or shear loading, $\tau_s\left(\varepsilon_T^p\right)$

Table 4.2. Material parameters required for a FE analysis of adhesives

The shear modulus, for an isotropic bulk material, follows from

$$G = \frac{E}{2(1+\nu)} \tag{4.2}$$

4.1.3.2 Adhesive – adherend interface parameters

An overview of all the needed parameters used for the cohesive zone modelling, with a triangular traction separation law, are given in Table 4.3.

Material parameters
• Normal elastic stiffness, $E_n = E$ • Shear elastic stiffness, $E_s = G$ • Normal interfacial bond strength, t_n^0 • Critical energy release rate mode I, G_{Ic} • Shear interfacial bond strength, t_s^0 • Critical energy release rate mode II, G_{IIc}

Table 4.3. Material parameters required for CZM

4.1.4 Material properties

For the cohesive zone modelling it is important to point out that the cohesive strength used, which have to be obtained experimentally, are not the same in case of bulk adhesives or adhesives as thin layers. The reason behind is that bulk adhesives are homogeneous materials and crack perpendicularly to the maximum principal stress direction, whereas thin adhesive layers are constrained by the two stiffer adherends and the crack growth is characterized by a mixed-mode, shear plus tension, and they crack along the bonding direction. Tests that could be used to determine the required properties are the double cantilever beam test (DCB) for mode I properties and the end notched flexure test (ENF) for mode II behavior (see also Table 2.2).

In this thesis, the DCB and ENF tests are not performed due to time limitations. However, the cohesive parameters are obtained in literature for a specific thickness of 0.02 mm (See Table 4.4). This thickness is assigned to the cohesive elements of "thickness zero" that represent the interface.

Material parameters	Araldite 2015	Crestomer 1152 PA
• Young's modulus, E	1850 MPa	1400 MPa
• Shear modulus, G	560 MPa	
• Poisson's ratio, ν	0.33	0.47
• Normal interfacial bond strength, t_n^0	21.63 MPa	
• Critical energy release rate mode I, G_{Ic}	0.43 N/mm	
• Shear interfacial bond strength, t_s^0	17.9 MPa	
• Critical energy release rate mode II, G_{IIc} $(= G_{IIIc})$	4.7 N/mm	

Table 4.4. Material properties of Araldite 2015 and Crestomer 1152 PA [47, 33]

4.1.5 Mesh description

For the solid elements FE modelling, the mesh size in the adhesive and surrounding areas is relatively fine. For the creation of the mesh, the following properties were fulfilled:

- Different mesh densities. A refined mesh is used at the regions of high stress gradients by progressively biasing the elements.
- Type of elements is C3D8R, linear hexagonal.
- The aspect ratio is as close as possible to 1.
- The technique used to create the mesh is structured.
- A gradual change in the mesh density outside the regions of interest, with elements of dimensions up to 1 mm per side in order to minimize the calculation time.
- Partitioning is used to create the mesh in the curved edges.

In order to choose an adequate size of the elements, a sensitivity study was performed with three proposals. Each proposed model was created assuming first the number of elements along the thickness of the adhesive. For instance, for the model with 1 mm thickness, the options or having 2, 5 or 8 elements per thickness were studied. The corresponding dimensions chosen for the mesh in the central part (see red rectangle in Figure 4.7) are defined in the following table, which also includes the total number of elements in each model.

Number of elements per thickness	Element dimensions *XxYxZ* [mm]	Number of elements
2	1.0 x **0.5** x 0.5	114100
5	1.0 x **0.2** x 0.5	122500
8	0.5 x **0.125** x 0.5	180400

Table 4.5. Element size used in the sensitivity study for the 1 mm model. Bold dimension corresponds to the element height.

After choosing the element density variations in the central part, the remainder of the mesh was created as follows. In the area next to the curved edges, small partitions were created with a finer structured mesh. The size of the mesh at these two regions is conditioned by the height of the elements at the central part of the adhesive, i.e. the larger the height of the elements in the central part, the coarser the mesh in the curved edges will be. All the elements in the model share the nodes with their adjacent elements, leading to a gradual element coarsening.

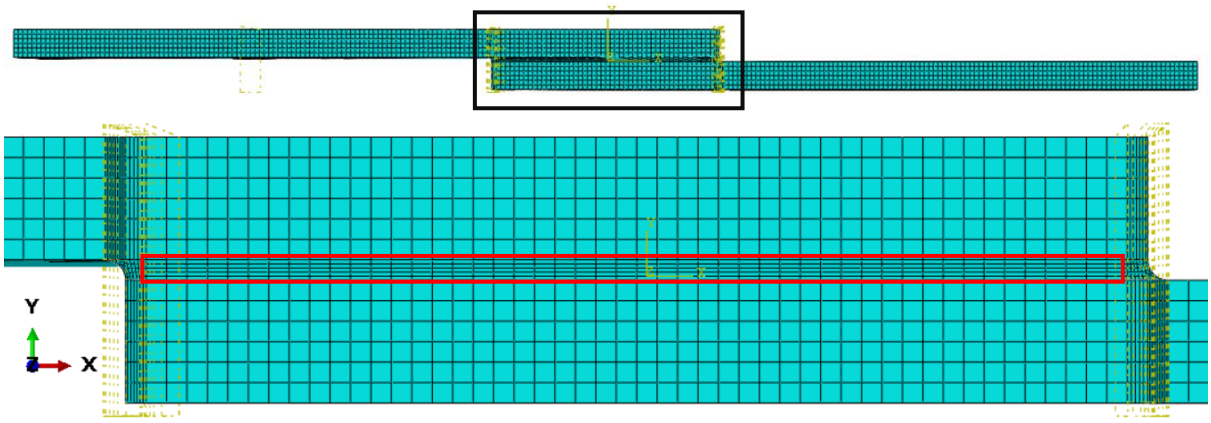

Figure 4.7. Area of interest (black), area of definition of element dimension (red;. 1 mm model with 5 elements per thickness

From the three proposed mesh sizes in Table 4.5, the force-displacement curves that were obtained show a difference of 0.05% in force, with a higher force for the coarse mesh. So it seems that at a global level the analysis is fairly mesh insensitive. However, this does not mean that stress and strain

fields are represented in sufficient detail for each mesh. Therefore, to say which is the optimal mesh, an alternative check is performed which consists in the comparison of the elastic strains contour plots.

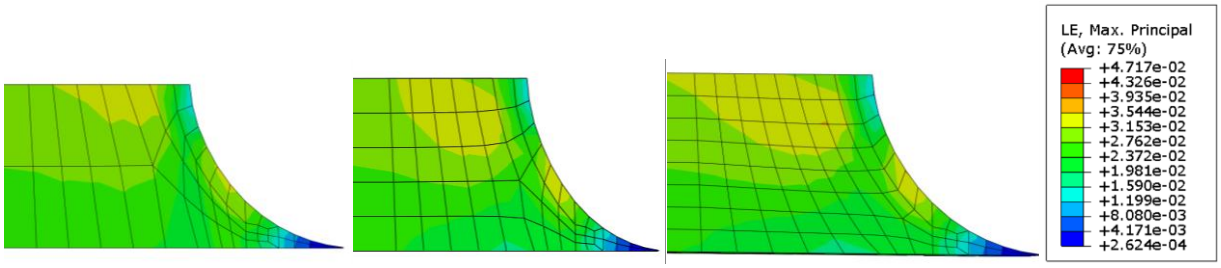

Figure 4.8. Sensitivity study. Comparison of elastic strain (LE) contour plots for different mesh sizes.

The comparison of the three plots (Figure 4.8), shows that the model with 5 elements per thickness provides similar results to the model with 8 elements per thickness. However, the computational time is less due to the fact that the total number of elements is much lower. Therefore, this mesh size is chosen as the optimal to represent the 1 mm adhesive thickness. Besides the qualitative comparison shown in Figure 4.8, a quantitative comparison is also performed by plotting the shear and peel stresses along the thickness for all three mesh sizes (See Appendix 2). A similar procedure is followed for all the five different models in order to determine the mesh size (see Table 4.6).

Model	**Number of elements per thickness**	**Element dimensions *XxYxZ* [mm]**	**Number of elements**
1 mm	5	1.0 x **0.2** x 0.5	122500
3 mm	10	0.5 x **0.3** x 0.5	221500
5 mm	10	1.0 x **0.5** x 1.0	83625
8 mm	12	1.0 x **0.67** x 1.0	79050
10 mm	20	1.0 x **0.5** x 1.0	101000

Table 4.6. FE models size mesh and total number of elements

4.2 COHESIVE ZONE IMPLEMENTATION WITH ONE ELEMENT MODELS

In order to fully understand the functioning of traction-separation laws (TSL) with CZM in Abaqus and the different output fields, some simple models were created. These models consist of one element fully fixed, acting as a rigid solid, and a second element where the displacement in tension or shear or a combination of both is applied.

CZM can be applied in two different ways:

1) As an interaction property which includes the cohesive parameters, which is assigned to the interface that is between the two contact surfaces.
2) As a layer of cohesive elements, created by offsetting the mesh with a layer of thickness zero and sharing the elements' nodes with the two components that are surrounding the cohesive layer.

In this report method 2 is applied. A one element model is created, where the fixed element (blue) is a rigid body with steel properties and the second element (green) is cohesive and has the properties of the Araldite 2015. Firstly, the model is loaded in tension; secondly, in shear (see Figure 4.9). The analysis are displacement controlled with maximum displacements corresponding to the normal and shear maximum displacements.

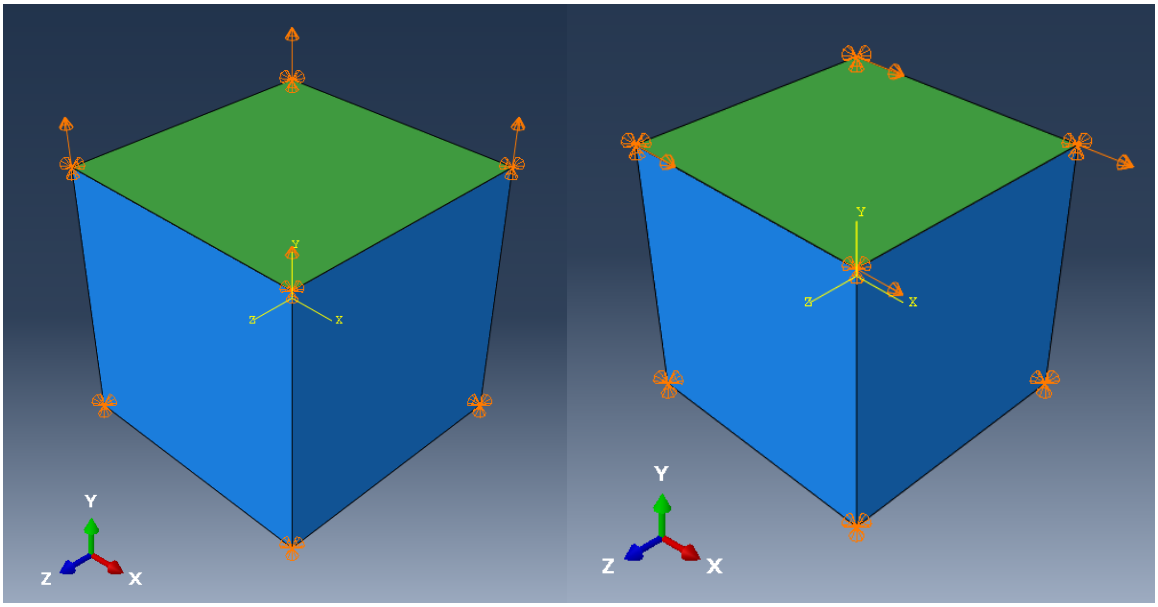

Figure 4.9. One-element models with applied Boundary Conditions for tension (left) and shear (right)

Figure 4.10 and Figure 4.11 show the traction-displacement curves obtained with the one-element models, which agree with the input parameters of Araldite 2015 (see Table 4.4). The output fields that result from a traction separation and their correspondent stress direction are:

$S33 \rightarrow t_n$	Cohesive tensile strength	[MPa]
$S13 \rightarrow t_s$	Cohesive shear strength in first direction	[MPa]
$S23 \rightarrow t_t$	Cohesive shear strength in second direction	[MPa]

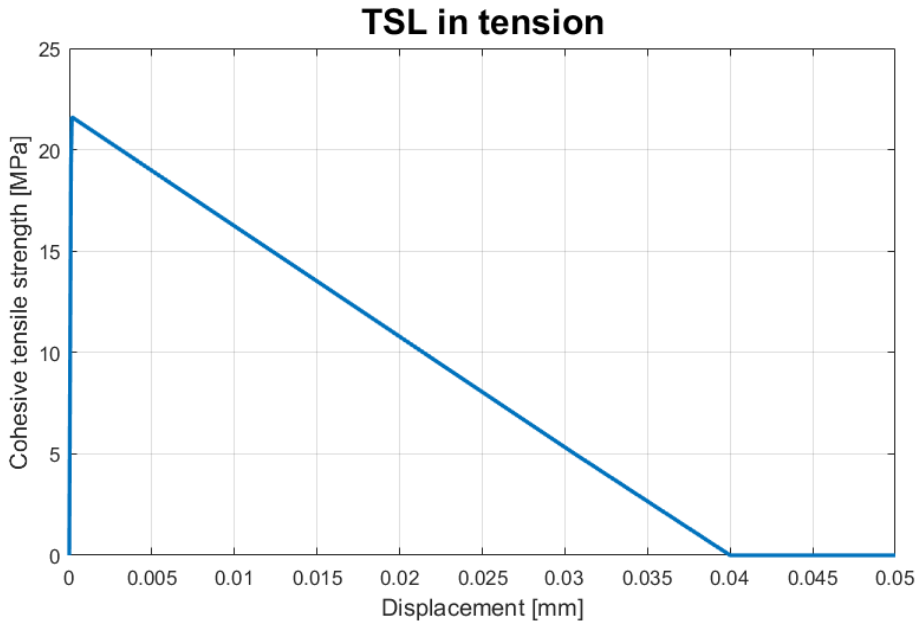

Figure 4.10. Traction displacement curve for one element model loaded in tension

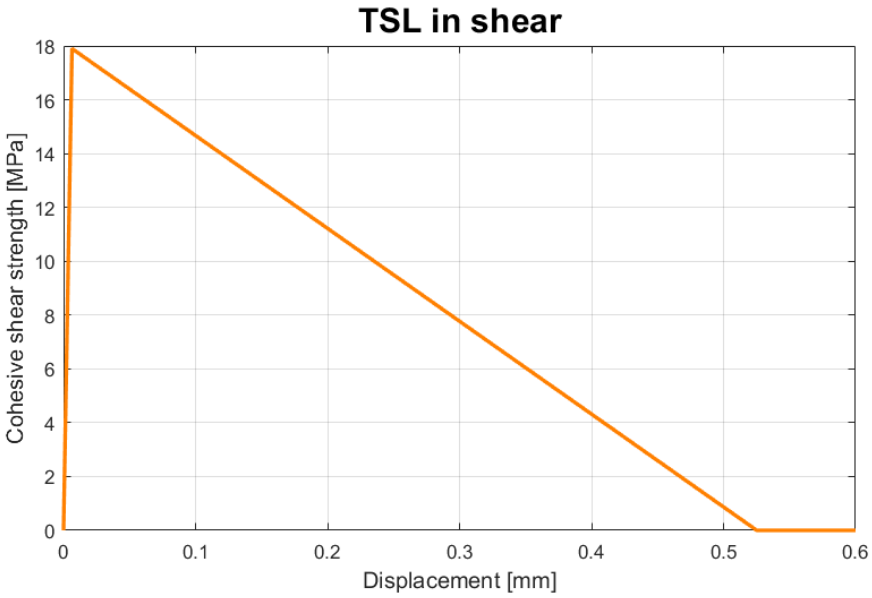

Figure 4.11. Traction displacement curve for one element model loaded in shear

From Figure 4.10 and Figure 4.11 the area under the curve can be calculated (see Table 4.7), which coincides with the critical energy release in mode I (G_{Ic}) for tension and in mode II (G_{IIc}) for shear, thus it confirms that the model follows the cohesive triangular law.

Load	Output parameters	Area under curve	Critical energy release
Tension	t_n^0 =21.63 MPa δ_n = 0.04 mm	$\frac{1}{2} t_n^0 \delta_n = 0.43$ N/mm	$G_{Ic} = 0.43$ N/mm
Shear	t_s^0 =17.9 MPa δ_s =0.525 mm	$\frac{1}{2} t_s^0 \delta_s = 4.73$ N/mm	G_{IIc} =4.7 N/mm

Table 4.7 Check of the output parameters of the Cohesive One-element model

To complete the analysis with the one-element model, the mixed-mode is also analyzed. For this, traction and shear are applied on the element in proportions 1:1. The output of this model is shown in Figure 4.12.

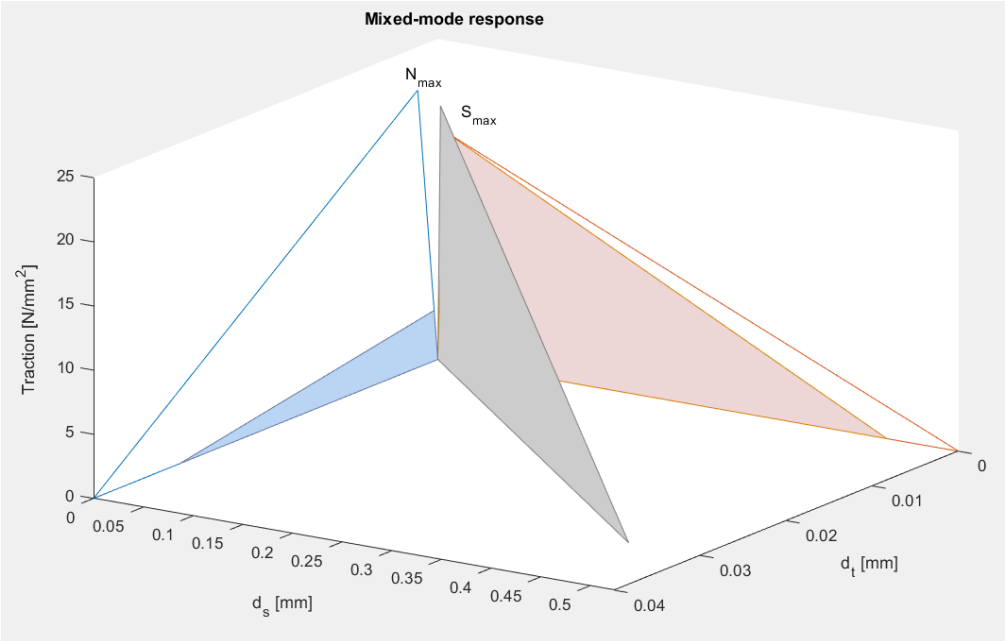

Figure 4.12. Mixed-mode response for CZM, Araldite 2015

4.3 DLJ RESULTS

For the global stresses, next to the overall contour plots that identify areas of high stresses, there are particular locations of interest in the interpretation of the results:

- At the mid thickness.
- At the lower edge of the adhesive, along the overlap length.
- At the upper edge of the adhesive, along the overlap length.
- Over the adhesive layer, at a certain distance from the ends. It is of special interest the lines in which the maximum shear stresses are reached (see Figure 4.15, shear stress).

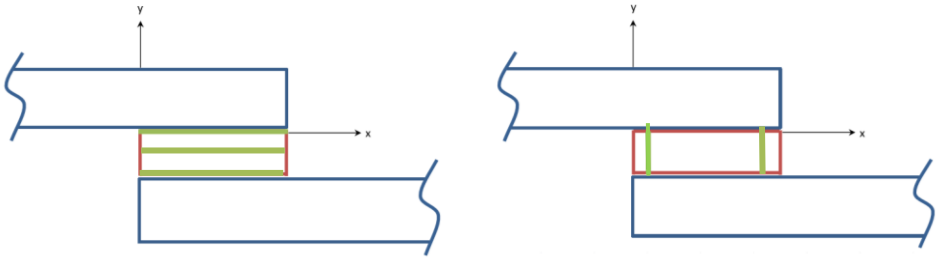

Figure 4.13. Details of adhesive joint showing the location where stresses are analyzed.

The stress behavior over the thickness line (Figure 4.13, right) is placed at *t/2* mm from the right edge of the adhesive bond. The reason of choosing this line is because it starts and ends at two points of interest, since at these points high stress concentrations are observed.

At the locations of interest shown above, two types of graphs are created:

- "State of stress" graphs. It includes the different types of stresses over the overlap length. This type of graph is useful to determine which stress component is dominant.
- "Comparison among variation" graphs. It compares one particular stress component of interest for a range of thicknesses. This type of graph, for example, is used to represent the thickness effect on the peel stresses over the overlap length.

Three different stress components are present in the adhesive layer, which are shear, peel and longitudinal stress. Figure 4.14 shows the direction of the stress components for one single element.

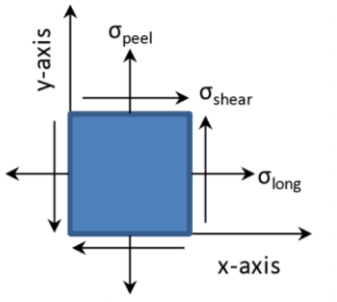

Figure 4.14 Direction of the stress components in an adhesive continuum element [50]

The FE analysis use the displacement applied on the right edge of the steel plate as a boundary condition. This displacement is set beforehand as an initial estimate to approximate the displacement that should be applied. After the first simulation, this displacement is usually adjusted. The output fields are referred to the time step, which coincides with the displacement of the right edge.

The FE analysis with the plasticity models focuses on two instants. It is of importance both the time step in which the yield stress is reached in the adhesive layer, thus the initiation of yield in the material, and the time at which the ultimate stress is reached, which indicates the initiation of the failure in the adhesive. Further on, the progression of failure inside the adhesive cannot be studied with this models because no cracking or element deletion is taken into account. But since it was seen from the experiments that the behavior of Araldite was brittle with only less than two milliseconds between initiation of cracking and failure, taking the initiation of failure as an end point is a fair approximation of the behavior.

4.3.1 State of stress

For the Araldite 10 mm thickness the state of stress is determined along the overlap length, at three locations; at the upper edge, at mid-thickness and at the lower edge, prior to first yield stress is reached. The lower edge and the mid-thickness locations are chosen because in the experiments, for the 10 mm samples, failure started either on the curved edge or in the interface with the middle plate, which is the lower edge in the FE model. The check at the upper edge is done because as shown in the figure below, for S12 stress distribution, the maximum stresses occur in a diagonal direction across the thickness, which indicates there are high shear stress concentrations present at the upper edge. These results are used to determine which stress component contributes more to the total stress state, right before yield starts, because after that point there might be a redistribution of the stresses.

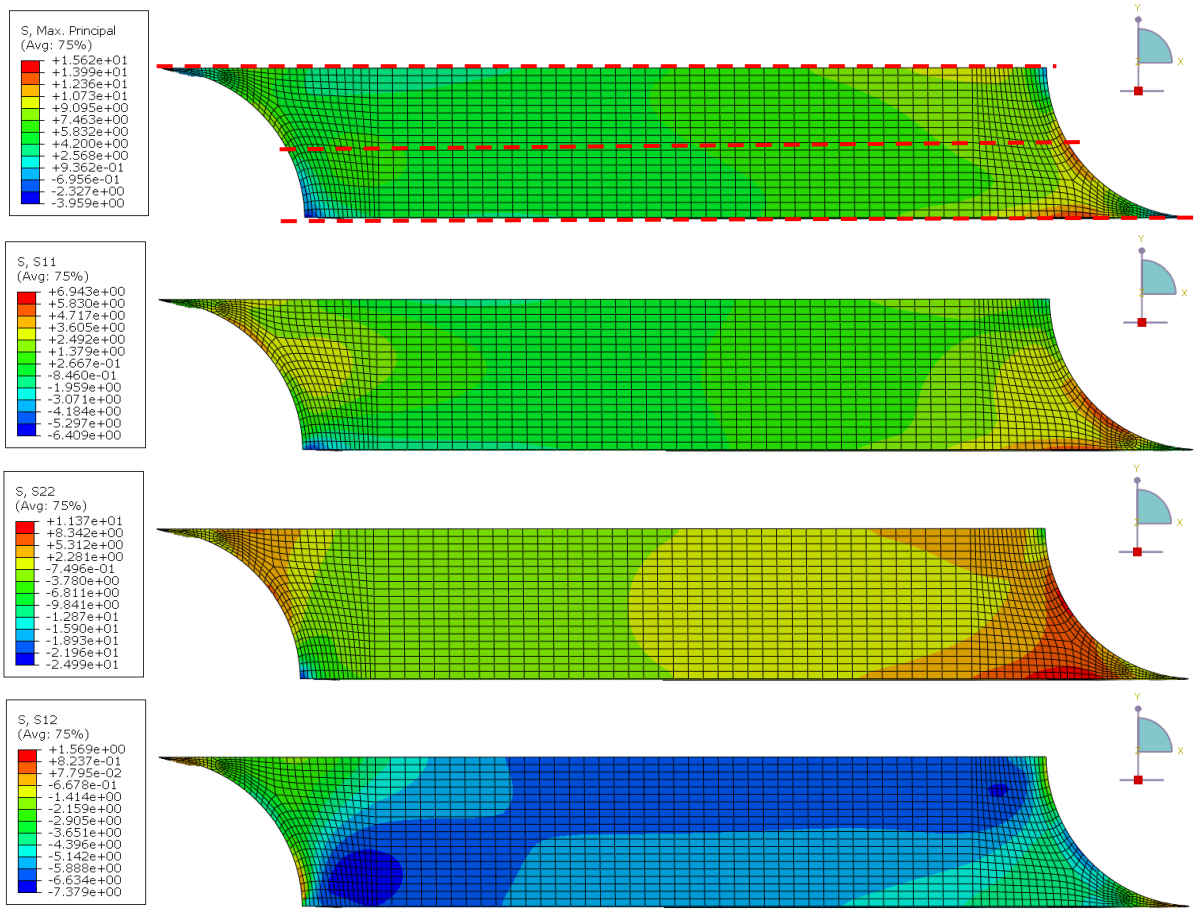

Figure 4.15 Contour plot of Maximum principal stress, tensile stress (S11), peel stress (S22) and shear stress (S12) prior to yield, Araldite 10mm. Dashed red lines indicate the lines along which the stresses are analyzed.

The maximum principal stress is given for the following expression:

$$\sigma_1 = \frac{\sigma_x+\sigma_y}{2} + \sqrt{\left(\frac{\sigma_x-\sigma_y}{2}\right)^2 + {\tau_{xy}}^2} \quad (4.3)$$

First, the state of stress is analyzed for the 10 mm model (Figure 4.16). Along the mid-thickness (Figure 4.16, left) both shear and peel are the most dominant components. Note that it has to be considered the absolute value of all the components. At the lower edge (Figure 4.16, right), the component that contributes the most to the total stress state is the peel stress (S22) towards both ends. It is important to notice that at the left end there is a singularity. However, this is not an inconvenience since failure does not initiate in that end. The alternation between peel and tension (S11) occurs at around 20 mm from the right edge.

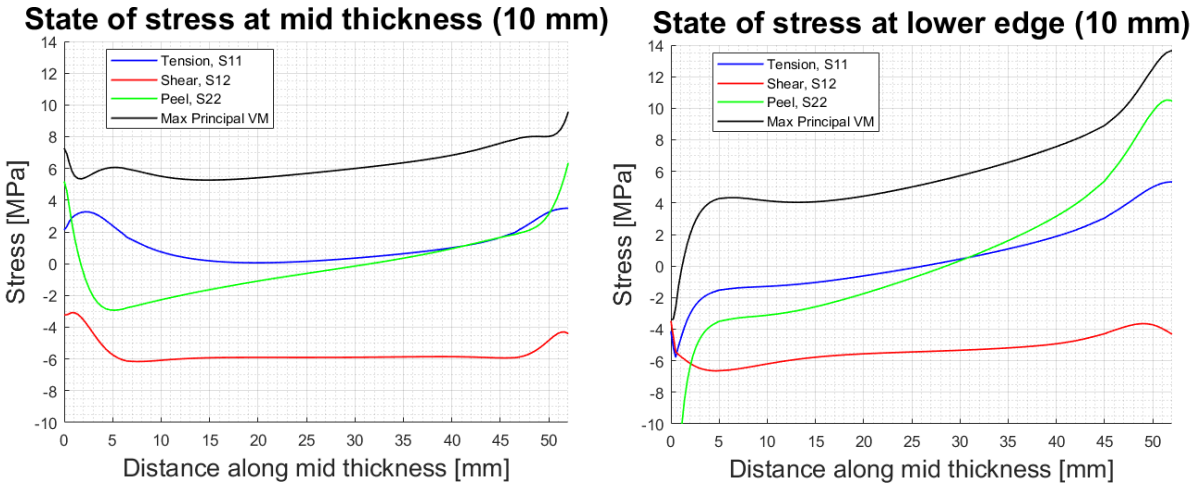

Figure 4.16 State of stress at mid thickness (left) and at lower edge (right), prior to yield. Araldite 10 mm

The equivalent figures are plotted for the 1mm model. Along the mid-thickness, (Figure 4.17, left) the most dominant components at the ends (where failure starts) are also shear and peel stresses. Along the lower edge, right end, all three components are approximately zero. Therefore, it can be concluded from this that for the 1 mm model it is expected that failure initiation does not occur next to the adherend (lower edge), but more to the curved edge (mid-thickness, right end) or to the upper edge. For this, it is also the stresses along the upper edge are checked for 1 mm (Figure 4.18).

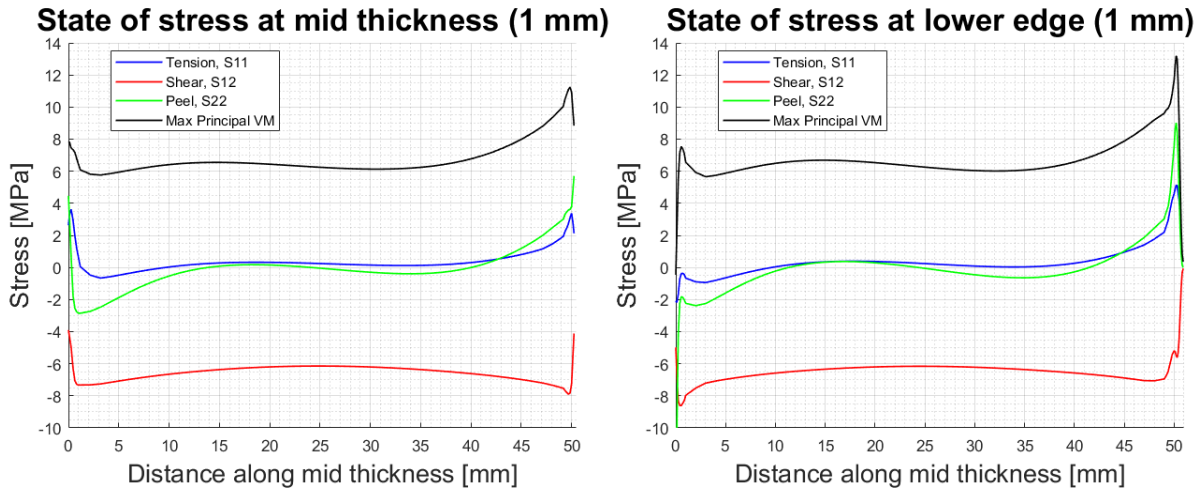

Figure 4.17 State of stress at mid thickness (left) and at lower edge (right), prior to yield. Araldite 1 mm

One difference between Figure 4.16 and Figure 4.17 is that in the 1 mm model (Figure 4.17), peel and tension are practically zero in the central part on both locations, but peel is not zero for the 10 mm model (Figure 4.16. Thus, by increasing the bondline thickness, the higher the peel stresses become.

By analyzing the stresses along the upper edge for 10 mm (Figure 4.18, left), it is seen than the three stress components are close to zero at the left end but increase towards the right end, with a shear stress that appears to be higher than in the lower edge, which is in agreement with Figure 4.15. For the 1 mm thickness, no big difference is seen between the lower and the upper edge stress states.

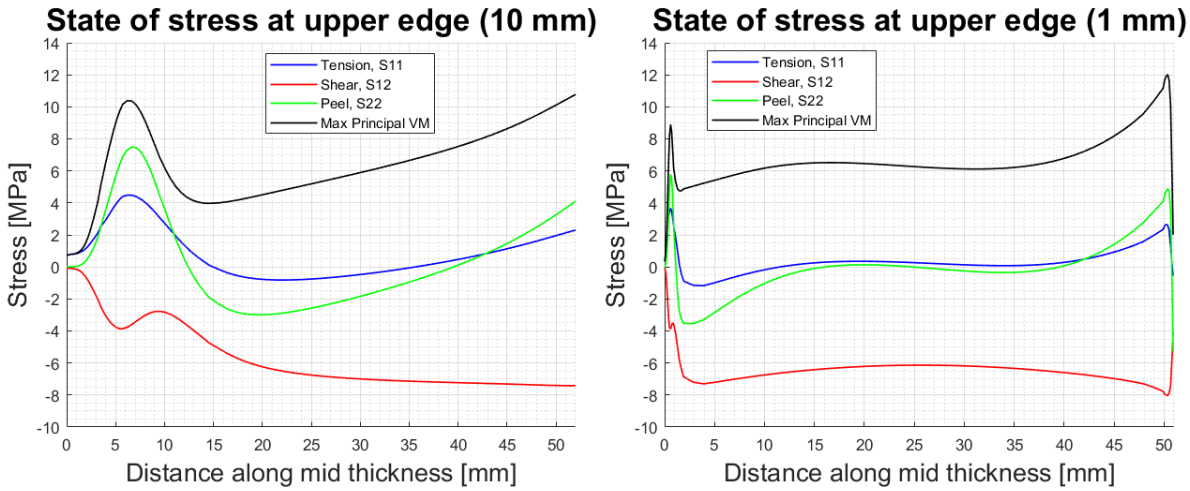

Figure 4.18 State of stress at upper edge, Araldite 10 mm (left) and at upper edge, Araldite 1 mm (right), prior to yield

4.3.2 Shear and peel stresses

The distribution of the shear and peel stresses is determined along a path at mid-thickness for all the models, from the left to the right curved edge. Note that the tensile force is applied from the right side, which is in concordance with the fact that peel stresses increase towards the right end of the path (see Figure 4.19). Peel stresses increase show their maximum values at both ends and show an increase towards the right end. Note that this increase is not linear for the 1 mm and 3 mm models, compared to all the other thicknesses, where a clear constant linear increase can be observed.

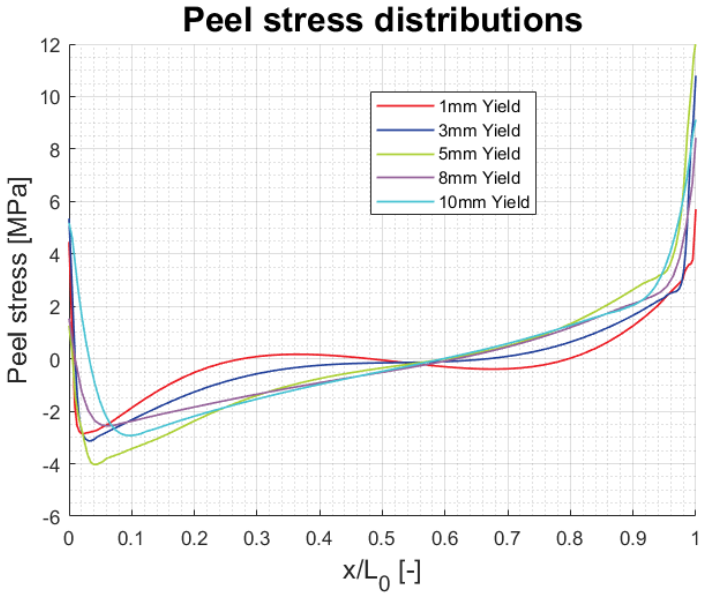

Figure 4.19 Peel stress distribution at Yield, Araldite all thicknesses

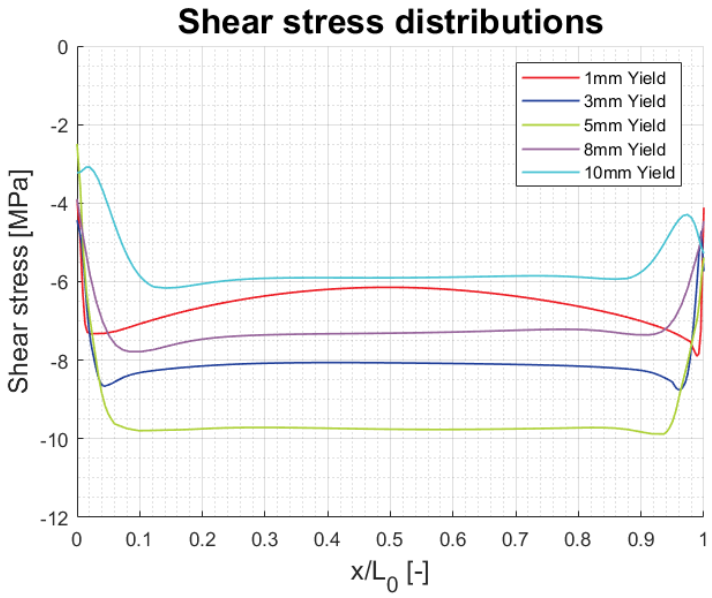

Figure 4.20 Shear stress distribution at Yield, Araldite all thicknesses

For all thicknesses, both shear and peel stresses show the maximum value at the ends of the path, i.e. at the curved edges, points where the stress concentrations occur and in the experiments failure initiates. Note from Figure 4.20 that for thicknesses 3 to 10 mm shear stresses remain constant in the central part of the overlap length (from 0.1 to 0.9 of the normalized overlap length), whereas for the 1 mm model, the stresses show a gradual small decrease towards the middle. As a result of the different trend in peel and shear for the 1 mm model, the ratio between peel and shear stresses is expected to follow also a different trend for the 1mm model compared to the other thicknesses.

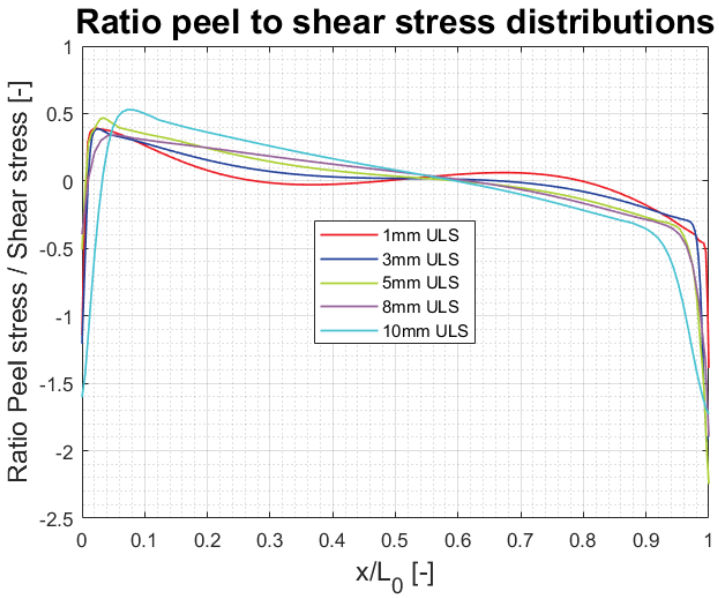

Figure 4.21 Ratio peel stress to shear stress distribution at Yield, Araldite all thicknesses

In Figure 4.21 the 1 mm clearly shows a nonlinear decrease in *x* whereas the 5, 8 and 10 mm show a linear decrease. The 3 mm also shows a bit of nonlinearity, but much less pronounced than the 1 mm. The difference in the ratio peel to shear can be an explanation for the different failure behavior observed in the experiments. For this reason, this maximum ratio is determined for every thickness and for the same load level (applied load on the steel plate of 54 MPa). This loading is chosen after observing that yielding on the adhesive is first reached for the model 1 mm thick, at this load level. Thus, it is ensured that at this loading level, in all the other models the adhesive has not yet reached

the yielding; therefore the linear behavior applies. The obtained peel to shear ratios for the same load level are collected in the following Table 4.8, where values S22 and S12 are determined at the node in which the maximum principal stress is reached. Note that this values are determined at the same load level by interpolation and may not coincide with the maximum values shown in Figure 4.21, which shows the ratio of each specimen at the load where the Yield is reached for that specific thickness.

Thickness [mm]	S22 [MPa]	S12 [MPa]	Ratio S22/S12 [-]
10	11.01	7.73	1.42
8	10.64	7.45	1.43
5	10.57	7.48	1.41
3	10.95	7.75	1.41
1	10.85	8.31	1.30

Table 4.8. Ratios peel to shear for the same load level [54 MPa], prior to Yield

When looking at the previous table the peel to shear ratio for all thicknesses are very close, although the 1 mm is about 8% lower than the others. From this it can be concluded that at least for thicknesses of 3 mm and thicker, the peel to shear ratio does not change and offers no explanation to the differences seen in the failure behavior. However, the 1 mm does show a difference and this could explain the more cohesive failure seen in the tests on this thickness compared to more cohesive failure very close to the adhesive seen on the other thicknesses. The 1 mm specimens failure onset is slightly more influenced by shear compared to the other thicknesses. Overall it is seen that peel is more dominant than shear in all thicknesses, with ratios well above 1.

4.3.3 Location of failure initiation

In the following figures the maximum principal stress field at ULS is shown. ULS is taken to analyze the failure initiation locations. From these contour plots the point in which failure will initiate can be determined. By analyzing Figure 4.22, two stress concentration areas are seen at the right end side: at the middle of the curved edge and at the edge, at an appropriate distance of 5 mm from the end. Comparing this to Figure 4.16, at the curved edge the high stress concentration is due to both shear and peel, whereas at the lower edge, it is mainly due to peel. When studying the results in more detail the absolute maximum principal stress is found in the middle of the curved edge. This is in agreement with the experimental results in which failure initiated at the middle of the curved edge.

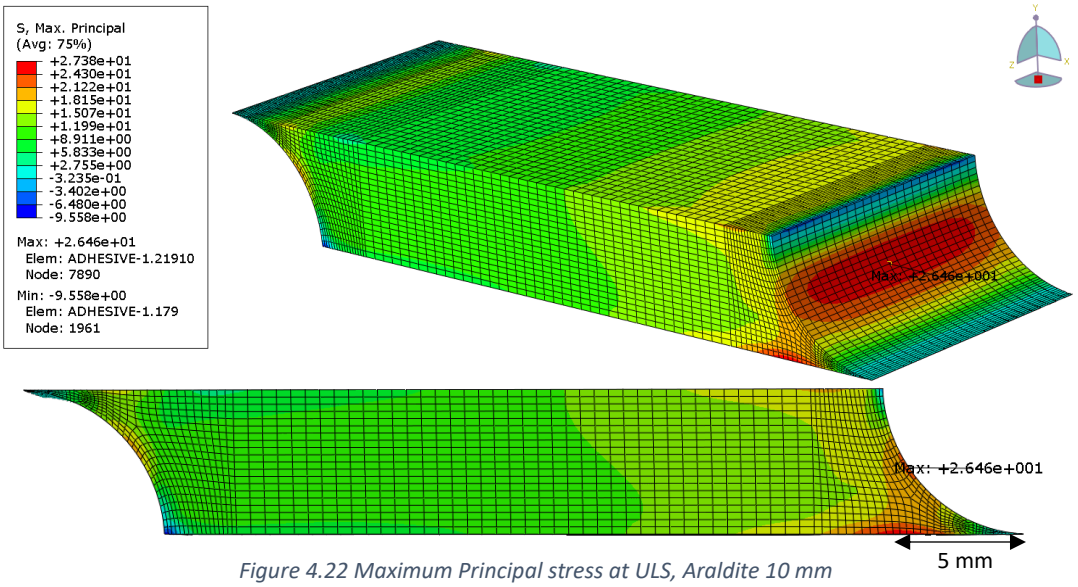

Figure 4.22 Maximum Principal stress at ULS, Araldite 10 mm

The point of initiation occurs solely at the middle of the curved edge for the 1 mm bondline model (see Figure 4.23), which is in agreement with the state of stress (Figure 4.17) which showed shear as the only component influencing the state of stress along the lower edge. This is another difference of the 1 mm model with respect to other thicknesses.

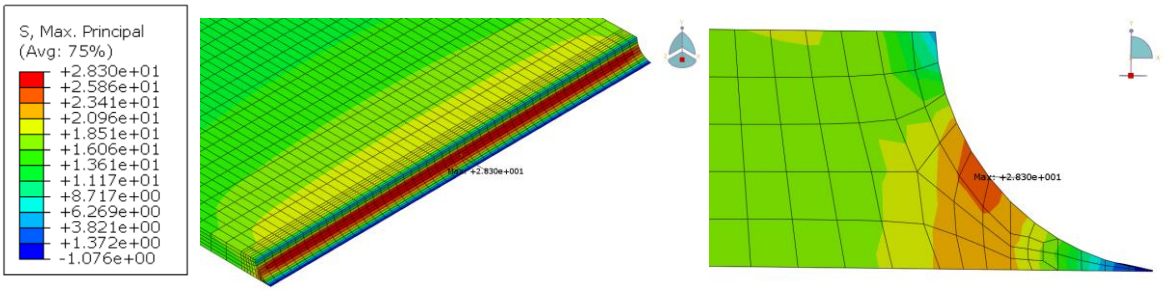

Figure 4.23 Maximum Principal stress at ULS, Araldite 1 mm

Thus, it can be concluded that according to the models failure is expected to occur in the middle of the curved edge for all the thicknesses.

4.3.4 Pressure

Using the von Mises plasticity model, the hydrostatic pressure is not taken into account. To study if there is need to switch to Drucker Prager, the pressure for different thicknesses is plotted. The following contour plots show the maximum pressure values in the edges, which are the area of interest of the models, because as it was observed, it is the area where maximum stress concentration occurs.

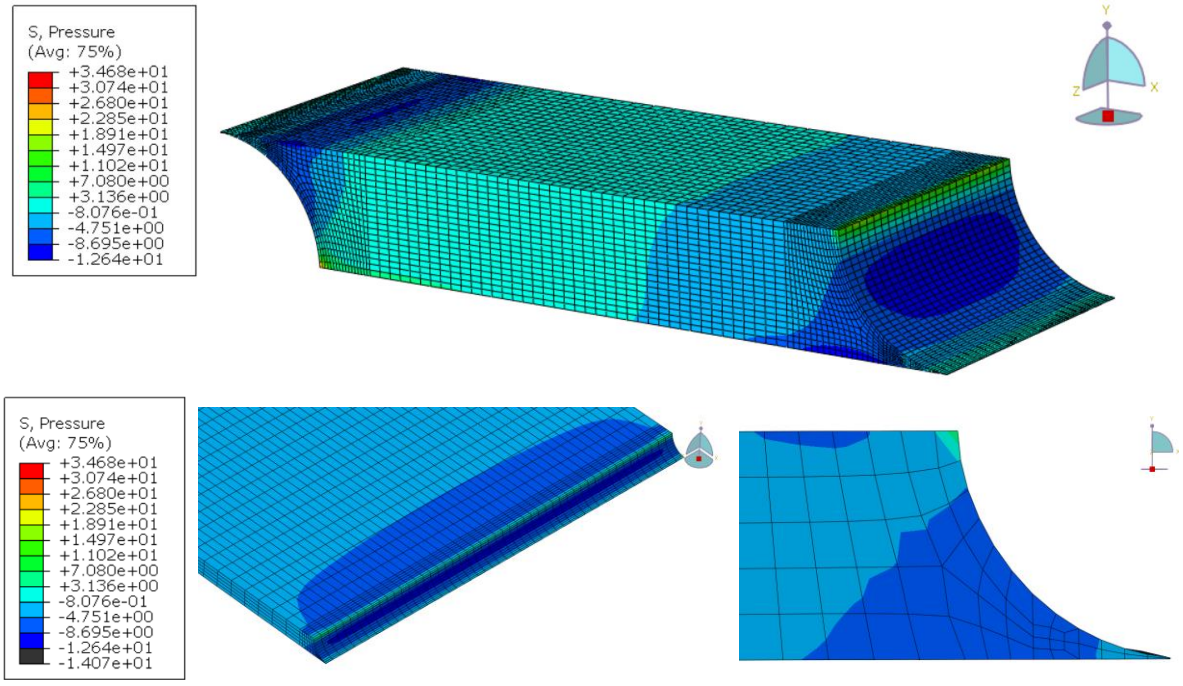

Figure 4.24 Pressure contour plots at ULS, Araldite 10 mm (up) and Araldite 1mm (down)

In Figure 4.24, the maximum pressure is compared for the 10 mm and 1 mm models. Pressure is zero for most of the central part, in both cases. The maximum values reach 12.6 MPa for the 10 mm model, and higher values (14.1 MPa) for the 1 mm model (see Figure 4.24). Although the difference is not big, still analyses were rerun using Drucker Prager model to study the possible influence of the hydrostatic pressure. Table 4.9 includes the parameters that are used to define the Drucker Prager model, which

are to be used in addition to the bilinear curve parameters presented initially in Table 4.1. These parameters were calculated based on the material data available and the method described in literature [52].

Angle of friction	30°
Flow stress ratio	1 [-]
Dilatation angle	26°

Table 4.9 Parameters that describe the linear Drucker Prager [52]

4.4 COHESIVE ZONE MODELLIING

This FE method was applied as an interaction property (see Section 4.2) to see how failure occurs along the interfaces. One of the output fields that can be obtain and is presented here is the cohesive damage, which ranges from 0 to 1. It is 1 in case the element is fully damaged and 0 in case it is undamaged. As it can be observed in Figure 4.25, the failure starts at the regions where maximum stress concentration were found along the edge. One important finding is the elliptical shape of this region, which indicates that the third dimension (z-axis) is also of importance.

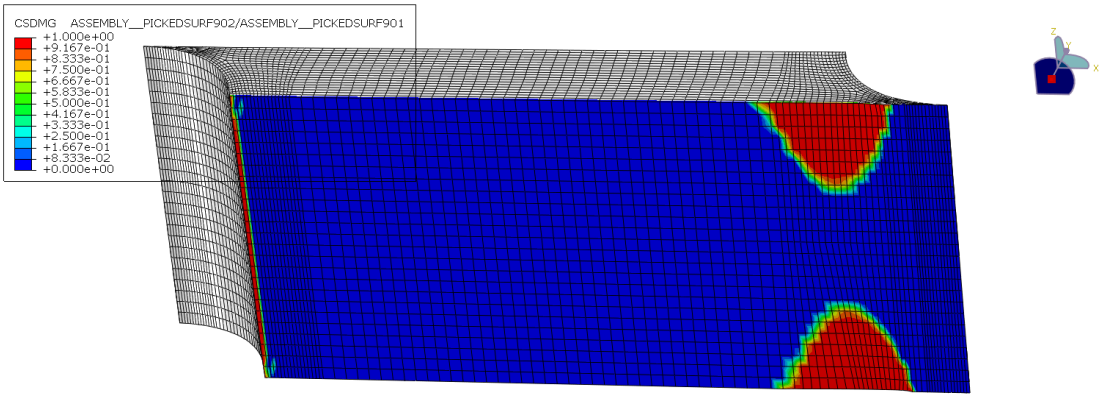

Figure 4.25 Damage in the lower interface. Araldite, 10 mm

Due to the complexity of this method and the fact that multiple test should have been performed in order to use the exact material data as input, it was decided to not make further use of this method. A list of recommendations and some advises for future work with this method are included in the recommendations.

4.5 VALIDATION OF THE FE ANALYSIS

The results obtained with the numerical predictions have to be in agreement with the experimental results. The FE models were validated with experimental results by comparing the force-displacement curves and the point of failure initiation. The comparison of the FE and the experimental results is given in Chapter 5.

4.6 LIMITATIONS OF THE FEA

The Finite Element models suggested in Section 4.1 present some limitations that are stated below.

- The material model chosen is only suitable up to failure initiation.

- No crack propagation is described.
- The material data is obtained from the data sheet, which is probably a lower bound.
- The perfect geometry in the FE model compared to the experiment which might contain voids and at which the edge is not perfectly shaped.
- The input data is in tension (as obtained from literature), while adhesive loading is in shear. Therefore, better would be to apply the shear input.

Furthermore, a parametric study would have shown the importance of the different parameters such as the overlap length and the width among other geometrical parameters. A reason why this was not performed is because the numerical modelling was performed as a first step into looking in different possible causes for the effects seen in the experiments. A parametric study would provide an inside to the importance of the different parameters, but only with respect to the assumptions made for the model. Since these assumptions in this case still had a number of uncertainties in them, the results of the parametric study might say more about these parameters for these models, than for the actual phenomena observed in the experiments. Therefore, after studying the assumptions of the models more carefully and coming to models with less uncertainties, it is strongly recommended that a parametric study is performed.

5 COMPARISON OF RESULTS

The experimental results (Chapter 3) are compared in this chapter to the numerical results (Chapter 4). This is necessary in order to validate the finite element analysis, which in turn determinates whether the selected models predict the behavior of the double lap joints when loaded in tension. Once more, this comparison is done with emphasis on the adhesive thickness and its effect on the stresses along the bondline and the elongation of the joint.

There are in general two checks that can be done, one in the elastic regime and one in the plastic regime. The first will give the best indication if the mesh, modelling choices and elastic properties are chosen correctly. After first yielding in the adhesive, stress redistribution will take place, which can largely influence the results. The comparison after yielding is therefore much more prone to differences. The FE models presented in Chapter 4 do not include damage propagation. Therefore, they do not allow to estimate how the failure propagates along the interface or the adhesive after the first element has reached the ultimate failure stress. After the first element reaches the ultimate stress defined, this element is not deleted from the analysis and therefore, results at a later stage in the analysis are not meaningful. As a consequence the models predict failure initiation, not failure propagation.

In Section 5.1 a first comparison is done with respect to the relative displacement of the joint at yield. Section 5.2 compares the force – displacement curves obtained with the FE models to the test curves. In Section 5.3, the comparison is done in terms of the location of failure initiation. In Section 5.4 the plastic strains are analyzed which may be a good indicator of the direction of the crack at failure.

5.1 RELATIVE DISPLACEMENT AT YIELD

To compare numerical and experimental results in the elastic phase, the relative displacement before the maximum stress reaches the yield stress (18 MPa, Araldite) in the models is compared to the relative displacement obtained from the test. The relative displacement from the test is taken from the force-displacement curve, given by the point in which the curves start deviating from the linear elastic line (see Figure 5.1).

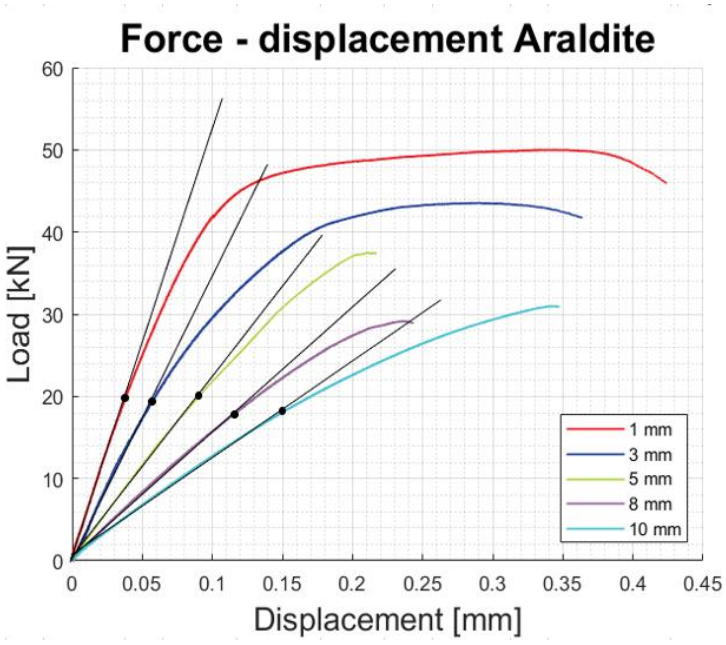

Figure 5.1 Determination of the relative displacement from the test, Araldite all thicknesses

The comparison between the test relative displacement and relative displacement from the model is shown in the following figure.

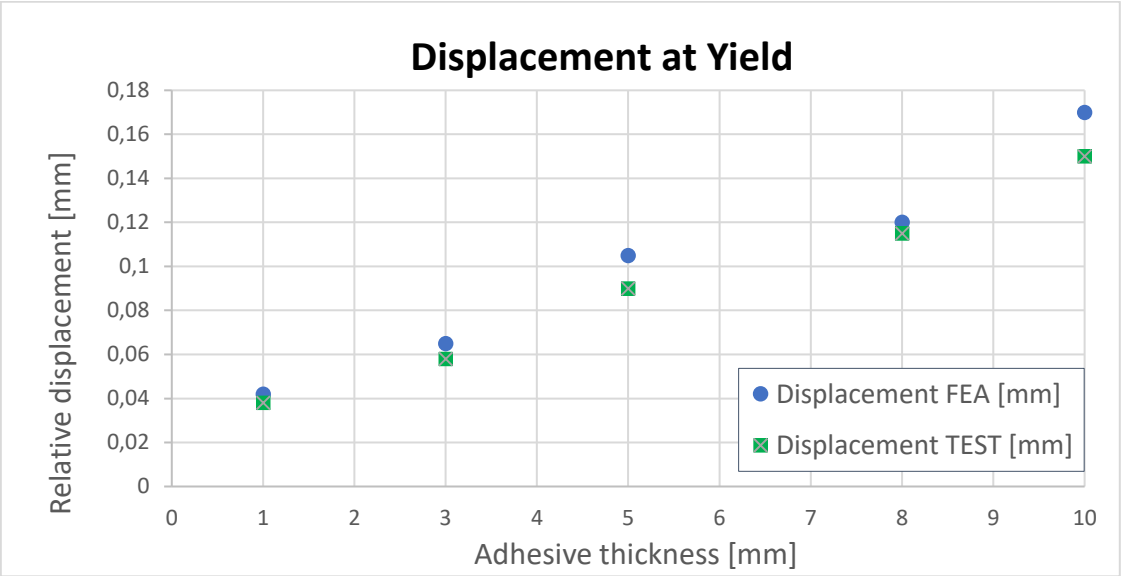

Figure 5.2 Comparison between numerical and experimental results in terms of relative displacement at yield as a function of adhesive thickness, Araldite

As it can be observed in Figure 5.2, the relative displacements obtained in the experiments are lower than in the FE analysis. Therefore, in the model deformations are higher than in reality. It can also be stated that up to the yield there is a trend that deformation increases with thickness, which is in agreement with the experimental results for Araldite.

5.2 FORCE DISPLACEMENT UP TO FAILURE INITATION

The test results were plotted together with the results from the models using the material data, for both von Mises and Drucker Prager plasticity models. The force - displacement curves obtained in the models were determined by plotting the force of a free body at a plane perpendicular to the tensile force direction at the end of the steel plate, where the load cell was placed in the experiments. The relative displacement is obtained by substracting the displacement of two nodes that are at 100 mm distance, corresponding to the initial +50 and -50 mm x positions from the center of the adhesive. It was observed that the node at +50mm from the origin, thus at the plate that is being pulled, shows a much larger displacement than the note at the other plate. For the 8 and 10 mm models, the displacement of this second node is none, whereas for the other models with thinner thickness, these displacements increase up to 0.015mm.

A check is done at this point to see whether the relative displacements measured in the joint correspond to the displacement of the adhesive or whether the steel plates also show a displacement; in such case the plate displacements should be substracted from the relative displacement to obtain the displacement in the adhesive. For this, the linear strains are plot for both adherends and for the adhesive prior to yield (see Figure 5.3). These check is done for the 10 mm model since Is the one that showed the highest displacements before the yield.

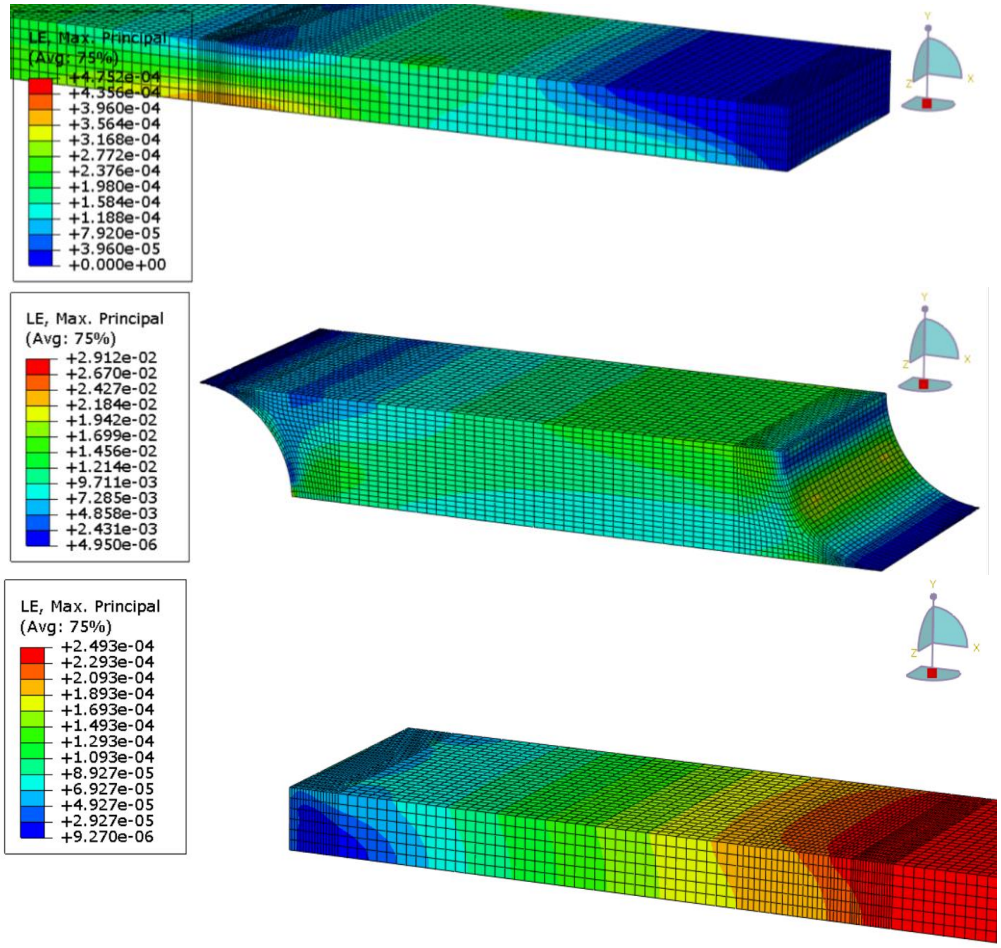

Figure 5.3 Linear strains in the adherends and the adhesive prior to yield. Araldite, 10 mm

As seen in Figure 5.3 the maximum strains in the steel plates are in the order of 100 times smaller than in the adhesive. Therefore, the effect of the relative displacement of the plates is not taken into consideration for the calculation of the displacement nor for the calculation of the shear strains.

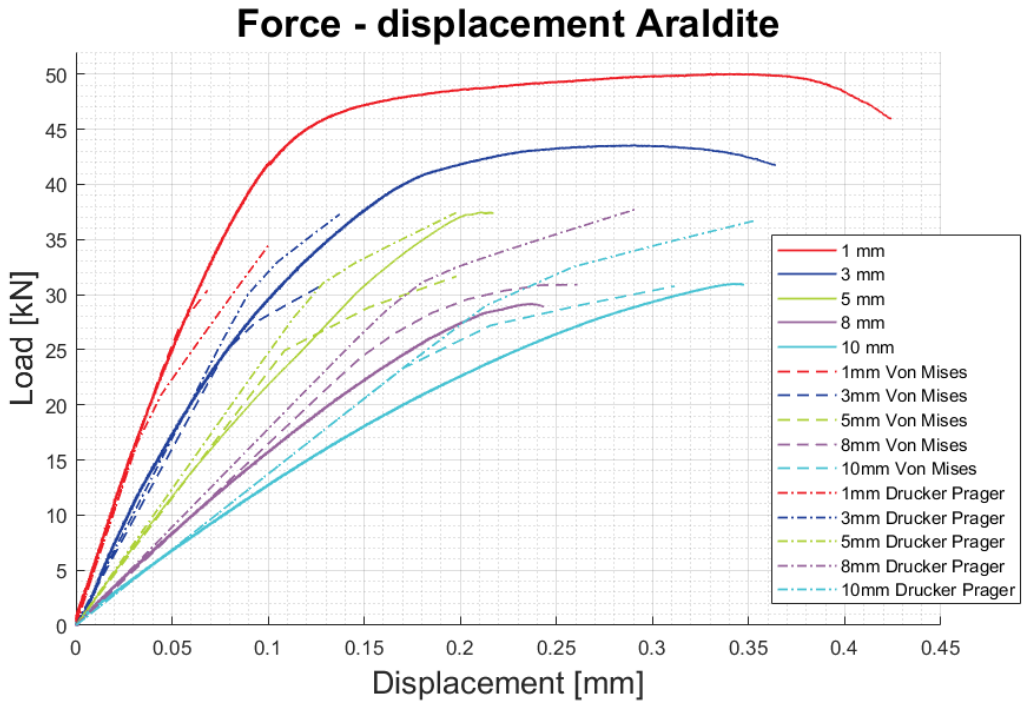

Figure 5.4 Comparison test and model with Von Mises and Drucker Prager. Araldite, all thicknesses

The FE analysis showed for all thicknesses a good representation up to the first yield (see Figure 5.4). For larger thicknesses (5, 8 and 10 mm) the experiment does not show a plateau but mainly elastic behavior, meaning that there is little time between failure initiation and full failure. In those cases, a fair agreement exists with the FE results. For smaller thicknesses (1 and 3 mm), the plateau is not captured since the FE model does not include propagation. Thus, for 1 and 3 mm the curve is not well captured after the elastic behavior. This could be due to:

- For 1 mm, clearly due to a different behavior. For this reason, the thickness 1 mm is disregarded.
- For the thin bondlines (3 and 5 mm), when a higher UTS than 27.3 MPa is taken, then the result is with closer agreement with the experimental curve, since the last part of the curve will show a more pronounced slope.
- For the thick bondlines (8 and 10 mm), when a lower UTS than 27.3 MPa is taken, the result is with closer agreement to the experimental curve. This can be expected because in these two cases the load In the model is larger than in the test.

Note that the UTS might be thickness dependent. Thicker bondlines might have more voids and other defects which might result in a lower UTS. The experiments showed that the lap shear strength decreased with increasing thickness, so that it seems logical that for thicker joints the material parameter UTS will also become lower, thus giving proof to the fact that better results are obtained when decreasing the UTS for larger thicknesses.Therefore, given the limitation of not knowing the bulk shear strength, this model is applicable for thick adhesive layers (thickness higher than 5 mm).

The results from Drucker Prager and von Mises are compared to the test by thickness. In all the cases the model with Drucker Prager shows a curve that deviates more from the test than with von Mises. In every case, it is determined the point in the curve where the yield stress and the ultimate stress are first reached (see Figure 5.5). In the figure, it can be observed that the point of yield is coincident for both models. After this point, plasticity in the adhesive initiates. For this reason, the two curves show different trend after yield. Drucker Prager provides a higher deformation capability and also higher failure load (Figure 5.5). In this case, von Mises approximates better to the test results.

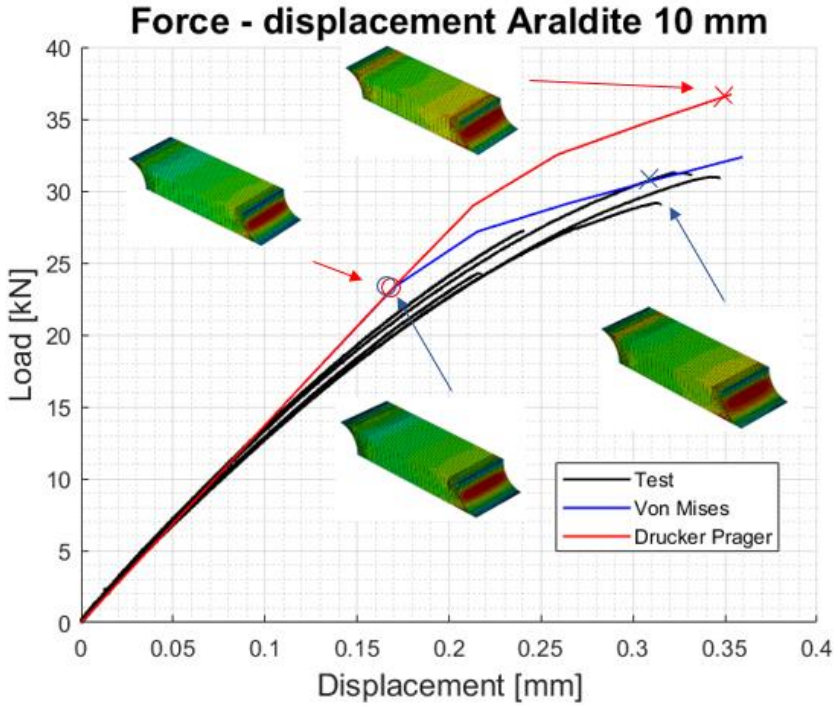

Figure 5.5 Comparison of points of yield and ultimate stress with von Mises and Drucker Prager. Araldite, 10 mm

5.3 POINT OF FAILURE INITIATION

In the experiments, different trends were visible. For 1 mm samples, failure mostly initiated in the edge, close to the outer adherend and then the crack propagated diagonally to the inner adherend. A similar point of initiation was seen for the 3 mm samples. For higher thicknesses, the point of initiation was either in the middle of the curved edge or in the edge with the middle adherend (See Figure 5.6).

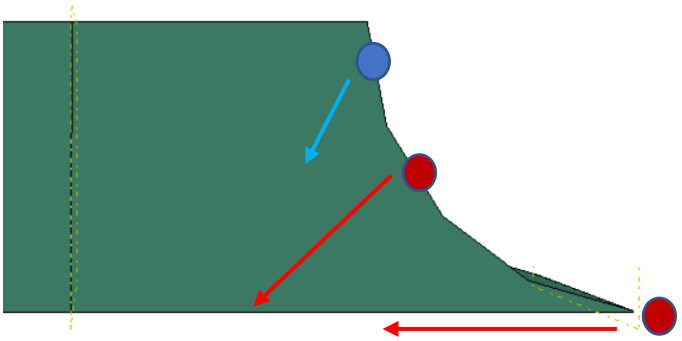

Figure 5.6 Point of initiation observed in the experiments. In blue: 1 and 3 mm; in red: 5, 8 and 10 mm

In the FE models, for 1 mm the models did not show the failure towards the upper edge but in the middle of the curved edge. For the 10 mm models, the highest stress concentration was found in the middle of the curved edge, which is in agreement with the experiments, if it is supposed that the weakest component has to be the adhesive and not the interface.

5.4 PLASTIC STRAINS

After having determined the point of failure initiation in the models, which is in fair agreement with the tests for thicknesses larger than 5 mm, another interesting parameter to analyze in the models of thickness 5 mm and thicker is the paths determined by the plastic strain fields. As it can be observed in the following figure, the maximum plastic strains at ULS occur at the curved right edge and at the left bottom corner. The contour plot suggest that the failure will occur along the diagonal that connects this two points (dashed line in Figure 5.7).

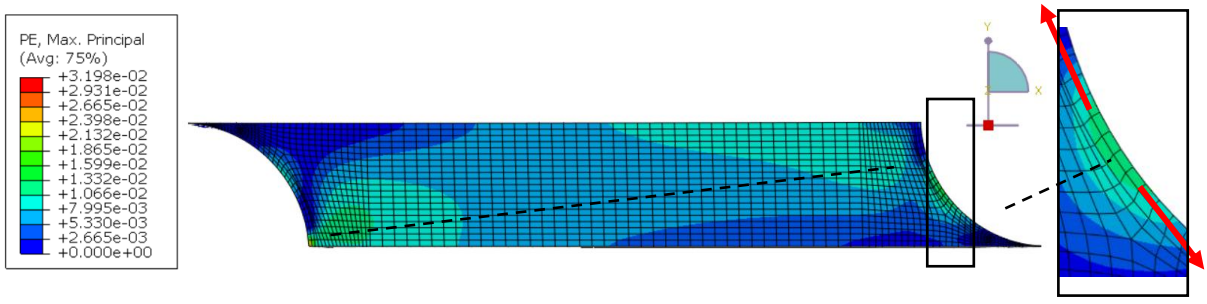

Figure 5.7 Maximum principal Plastic Strains at UTS. Red arrows indicate the direction of principal strain. Araldite, 10 mm

By looking at the principal strain directions it is observed that the arrows in Figure 5.7 point in the direction of the curved edge. Therefore, it can be assumed that the crack will occur perpendicular to this direction, thus, towards the interface, as shown in Figure 5.6.

6 DESIGN OF DOUBLE LAP JOINTS

This chapter focuses on the design resistance of double lap joints determined from the test results. The main goal is to obtain the design factor for the resistance of these joints that takes into account the accuracy of the strength of the joint and the material and geometrical uncertainties. The procedure followed, which is in compliance with the Eurocode 3 and also described in literature [51], is presented below. This procedure was applied to the test results of Araldite 2015, since it covers thicknesses up to 10 mm, and the method is intended to cover any thickness up to 10 mm. This method is meant to be as interpolation but note that it cannot be extrapolated to higher thicknesses. Furthermore, it should be noted that the methodology described in the Eurocode ideally is based on a large number of test results and independent variables with a log normal distribution. If these assumptions are not met some correction to the method has to be done. In this project only a very limited number of tests are available and variables in the system are not all independent (e.g. the shear strength in thickness dependent). However, the methodology is used to give a first indication of the partial safety factors.

The rules in Eurocode are based on a limit state, in which design effects of the actions cannot exceed the design resistance.

$$S_d \leq R_d \tag{6.1}$$

Based on the observations of the actual behavior in tests and on theoretical considerations, for instance the effect of the shear area on the lap shear strength, a ‘‘design model’’ is created. Then, by doing a regression analysis, the efficiency of the model is checked. The model is accepted once the correlation between the theoretical values and the experimental values is sufficient; i.e. the ratio R is around 0.8 and 0.9.

The model is based on the samples of thickness 3 to 10 mm which showed a similar failure behavior. The suggested design model for the joint resistance was chosen as shown below. It was determined by knowing that the resistance of a double lap joint is related to the shear area and decreases with thickness. In order to adjust the dimensions of the equation, the thickness is divided by a nominal thickness.

$$R = \frac{2 \cdot f_s \cdot l \cdot w}{\left(\frac{t}{t_0}\right)^{0.3}} \qquad [N] \tag{6.2}$$

Where:

f_s is the mean shear strength of the adhesive $[MPa]$

l is the overlap length $[mm]$

w is the width of the adhesive bondline $[mm]$

t is the thickness of the adhesive bondline $[mm]$

t_0 is the reference thickness of the adhesive bondline, set as 1 $[mm]$

Thus, the variables included in this model are geometrical (l, w, t) and from the material (f_s). Information of the variation of the geometrical variables was obtained by measuring them from the actual samples, before testing (Appendix 2). Since no measurement for the material data was available, it was taken as the average value; hence, a shear strength of 18 MPa. All the measured geometrical data and the average shear strength were introduced in the design model to obtain all

the values of the characteristic resistance (Rt). These were plotted together with the data obtained in the tests, referred as realizations (Re) (see Figure 6.1).

By comparing the results from the tests and the model, the variation in the prediction the design model is determined, known also as the variation of the mean value of the observed error.

The design resistance of this type of double lap joints for real applications has to be determined in the serviceability limit state. For this reason, the test values are determined at a same deformation for all the thicknesses, 0.2 mm (mean relative displacement of the LVDTs), which is far from the failure displacement.

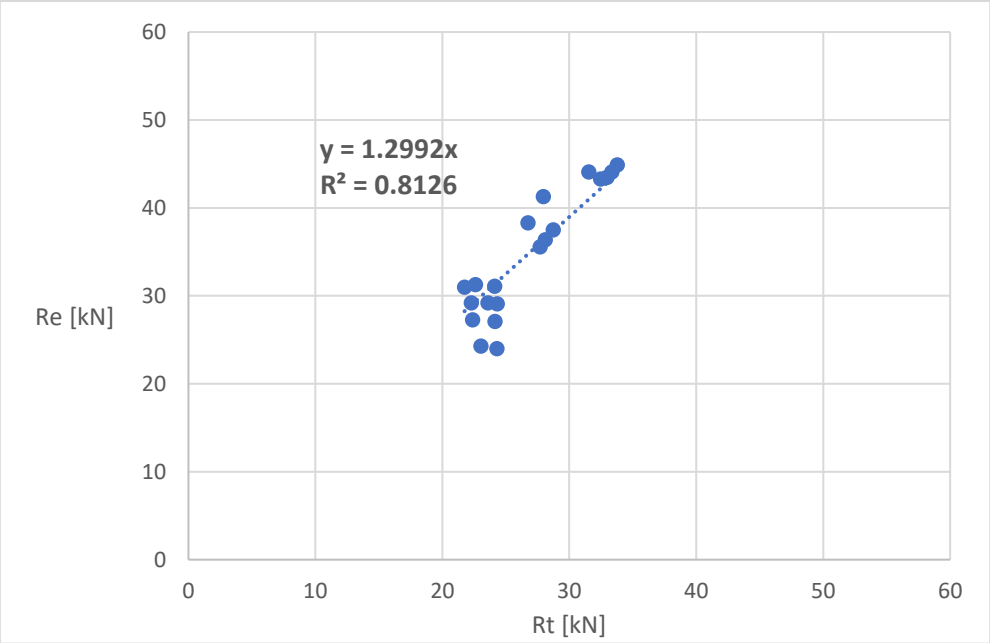

Figure 6.1. Comparison of model and test resistance

If the design function was exact, the trend line would be the bisector of the angle between the two axis. As expected, this is not the case. Therefore, it is necessary to determine if the correlation is sufficient by analyzing the correlation factor (ρ). This parameter, which is obtained from the tendency line, is 0.9, which according to the Eurocode, is considered sufficiently high.

The next step is the calculation of the mean value correction (b). For each specimen *i,* the relationship between the test and the model results in the term b_i. The mean of all these terms renders the mean value correction.

Correction term: $$b_i = \frac{R_{e,i}}{R_{t,i}} \quad (6.3)$$

Mean value correction: $$\bar{b} = \frac{1}{n}\sum_i b_i = 1.052 \quad (6.4)$$

Therefore, the corrected resistance function is:

$$R_m = \bar{b} \cdot 0.002 \frac{f_s \cdot l \cdot w}{\left(\frac{t}{t_0}\right)^{0.3}} \quad [kN] \quad (6.5)$$

The next step is to determine the coefficient of variation of this new model, as follows.

Error terms: $$\delta_i = \frac{R_{e,i}}{\bar{b} \cdot R_{t,i}} \quad (6.6)$$

Assuming that the Coefficient of variation (Var_g) is small the mean error, standard deviation and Coefficient of variation are given by the equations below.

Mean error: $$\bar{\delta} = \frac{1}{n}\sum_i \delta_i = 0.99 \quad (6.7)$$

Standard deviation: $$\sigma_\delta = \sqrt{\frac{1}{n-1}\left(\sum_i {\delta_i}^2 - n\,\bar{\delta}^2\right)} = 0.154 \quad (6.8)$$

Coefficient of variation: $$Var_\delta = \frac{\sigma_\delta}{\bar{\delta}} = \sigma_\delta = 0.156 \quad (6.9)$$

This results in a variation of 0.156 for the model. Following a similar procedure with the measurements, it is possible to determine the variation for all the geometrical variables.

- Thickness coefficient of variation: $Var_t = 0.0530$
- Overlap length coefficient of variation: $Var_l = 0.0171$
- Width coefficient of variation: $Var_w = 0.0173$

Once all these parameters are determined, it is possible to apply Monte Carlo to increase the number of tests other than having only five tests per thickness. To do so, it is chosen a log-normal probability distribution that creates random variables for a given mean and coefficient of variation. It is chosen this distribution because it has the advantage that no negative values can occur, which is beneficial since all the geometrical variables must be positive.

In order to determine the design value of the strength and the design factor, as stated in the Eurocode, it is necessary to determine the 5% fractile coefficient of the resistance distribution and substitute it by a k_d design fractile, which is related to a new probability of failure. According to the Eurocode the fractile 3.04 corresponds to an acceptable safety factor (β) 3.8. Thus,

$$k_d = 0.8 \cdot \beta = 0.8 \cdot 3.8 = 3.04 \quad (6.10)$$

Thus, the fractile 3.04 leads to a probability of failure of $p_f = 10^{-3}$, that should not be exceeded. Therefore, in the modeled data it is determined the design resistance as the resistance corresponding to the 3.04 fractile. Then, the design factor is calculated as the ratio between the nominal resistance and the design resistance.

$$\gamma_M = \frac{R_{nom}}{R_d} \quad (6.11)$$

The model is applied for n=10, 100 and 1000 tests in order to predict the minimum number of test that would necessary to be performed in an ideal case so that the safety factor could be determined. It is observed that for small number of tests, the randomly created variables result in distributions that continuously change its shape and the design factor also shows variations for every simulation. These variations decrease for higher sample sizes (see Table 6.1).

Sample size *n*	**Safety factor γ_M**
10	0.9 – 1.8
100	1.13 – 1.49
1000	1.30 – 1.45
5000	1.35 – 1.41
10000	1.4

Table 6.1. Safety factors for increasing sample sizes

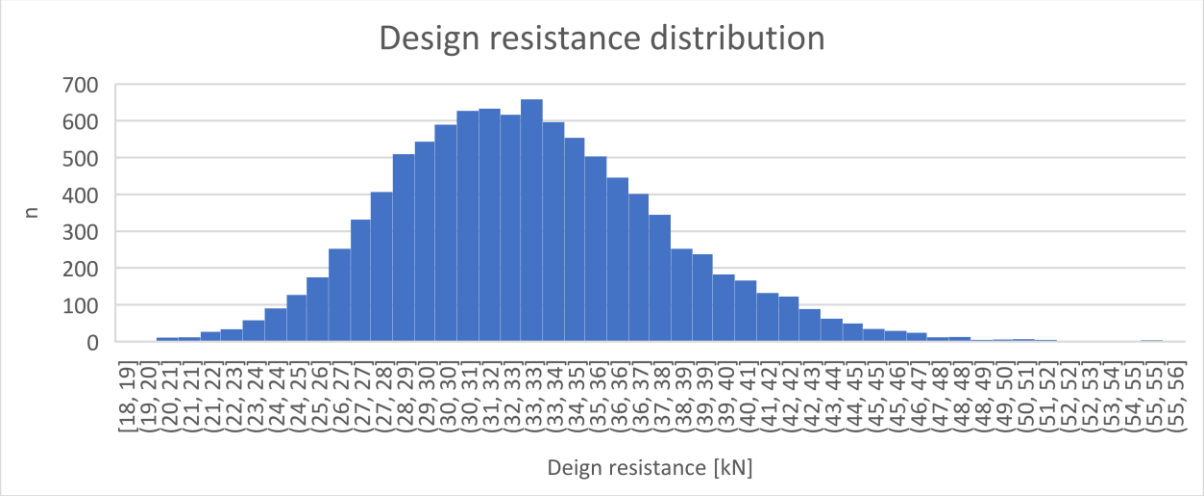

Figure 6.2. Log-normal distribution of the model, n=100000

As it can be seen in Figure 6.2, the modeled data represents the shape of a log-normal distribution.

To summarize, it can be concluded that the higher the number of samples, the more accurate obtaining of the safety factor will be. Furthermore, for small scale double lap joints with an adhesive of up to 10 mm thickness, it is suggested that the safety factor that might be used in the design is 1.40. From the information collected in Table 6.1, it is suggested that a sample size of 100 would be large enough to obtain a safety factor of 1.50; thus on the safe side.

This is in agreement with the values found in literature (see Table 6.2). For instance, the ECDH provides some safety factors to be used for structural adhesives, which individually range from 1.0 to 2.0, depending on different aspects. The overall safety factor (γ_m) is the product of four partial safety factor, which consider the properties of the adhesive ($\gamma_{m,1}$), the method of application of the adhesive ($\gamma_{m,2}$), the type of loading ($\gamma_{m,3}$) and the environmental conditions ($\gamma_{m,4}$). Note that the study above only can be compared to the first two partial safety factors mentioned in the table where even the second one is already set during the manufacturing (1.25 due to the mold used). Thus, the comparison with the factor 1,50 obtained is to be made with the factors 1.25 and 1.5 of the first factor, which would have to be multiplied by the second factor for thickness controlled manufacturing (1.25), resulting in a maximum value of 1.88.

Aspect	**Partial safety factor γ_i**
Source of adhesive properties ($\gamma_{m,1}$)	
- Textbook values	1.5
- Values obtained by testing	1.25
Method of adhesive application($\gamma_{m,2}$)	
- Manual, no thickness control	1.5
- Manual, thickness controlled	1.25
- Established procedure with controlled parameters	1.0
Type of loading ($\gamma_{m,3}$)	
- Long-term loading	1.5
- Short-term loading	1.0
Environmental conditions ($\gamma_{m,4}$)	
- Service conditions outside the test conditions	2.0
- Properties in service conditions	1.0

Table 6.2 Partial safety factor for adhesively bonded joints [Eurocomp Design Code and Handbook]

7 CONCLUSIONS AND RECOMMENDATIONS

This chapter contains the principal conclusions and answers to the research questions of this thesis, stated in Section 1.2, aim and objectives. It also provides a list of recommendations for future experimental work related with adhesively bonded joints and a list of topics that were not addressed in this thesis and could be studied as a continuation since it is believed they would give valuable extension to the findings of this research.

7.1 CONCLUSIONS

The experimental results provided information on the mechanical behavior of the double lap joints for increasingly adhesive thicknesses up to 10 mm. The effect of the increasingly thickness on different parameters is contained in the following table.

	Crestomer	**Araldite**
Thickness	↑	↑
Failure lap shear strength	↓	↓
Loading capability	↓	↓
Deformation capability	↑	↓
Failure shear strain	↓	↓
Young's modulus	≅	≅

Table 7.1. Trends on different parameters for increasingly bondline thickness

It is concluded that there are multiple parameters that are thickness dependent, such as the lap shear strength, the load at failure, the deformation capability and the strains at failure. It was found that the average lap shear strength decreases with thickness, which is in agreement with the information described in literature.

The assessment of the load-displacement curves resulted in different conclusions depending on the adhesive. On one hand, Crestomer showed an increase of the deformation capability and decrease of the loading capability with thickness. Its response is characteristic of a ductile materials, with a linear increase of the load with displacement up to a certain plateau where the adhesive started behaving plastically. On the other hand, the trends for Araldite were also a decrease of the loading capability but a decrease of deformation capability with thickness. For both materials, the average failure shear strains decreased with thickness.

Not much change was seen in Young's modulus. It can be concluded that this parameter is thickness independent.

Two failure modes were present in the tests, cohesive and adhesive. All Crestomer samples showed mostly adhesive failure. For Araldite, the main failure mode present in the tests was cohesive, which occurred at two levels, either along the bondline, for 1mm bondline samples, or along a line almost at the interface for all the larger thicknesses, 3 to 10 mm. Therefore, it is concluded that for brittle adhesives such as epoxies the expected failure mode is cohesive, with a crack occurring very close to the interface for increasing thicknesses.

The mechanical behavior of thick bondlines can be modelled using finite element methods. The methods applied in this thesis are elasto-plastic material models that consider the material as a material that exhibits a linear behavior up to a certain stress state. Afterwards, it deforms plastically till it reaches a ultimate limit stress. In the models it can be determined thus, the point of initiation of the failure, given by the first element that reaches such level of stress. These locations vary with thickness. For thin models, it is more common to see the initiation at the middle of the curved edge, whereas for thicker models, the initiation points can be determined at two points; at the middle of the curved edge and at the interface with the middle plate, exactly under the location at the curved edge. This fact can be observed as one of the reasons why for thick bondlines, failure occurred either starting at the curved edge and propagating towards the interface or solely on the interface.

Another reason to explain the different behavior between the 1 mm and the other thicknesses is the stress state along the interface and at mid thickness. For the thicker bondlines, both the shear and the peel stress distribution showed a linear behavior along the overlap length. In the case of the 1 mm thickness, those distributions were not linear. Therefore, it can be concluded that for thicknesses higher than 3 mm the distribution of stresses is more constant along the overlap length. Furthermore, in the case of 1 mm, the stress distributions at mid thickness and along the lower edge were very similar. For the other thicknesses it can be observed that the peak stress concentrations that occur at the ends are larger at mid thickness than at the interface, which explains the crack path observed in most of the experiments.

A limit assessment was made to determine the partial safety factors needed for the design of double lap joints. Since only a limited number of tests were available and variables studied were not all independent, no complete assessment can be done. The effect of the limited number of tests was overcome by performing Monte Carlo simulations. It was seen that using 100 simulations (or test) a good convergence is already seen towards a material partial safety factor of 1.5. This value is also in the range found in literature.

7.2 RECOMMENDATIONS

A list of recommendations is briefly explained below, to follow in case some similar experiments with adhesively bonded joints have to be performed in a future.

- The use of digital image correlation (DIC) techniques. This technique would be beneficial, on one hand, to gather input for FE comparison of strain fields; on the other, to identify the failure mode (cohesive or adhesive) that is governing in each case.
- The use of acoustic emission (AE) technique for the detection and location of the cracks that create and propagate through the adhesive layer. With this technique it would also be possible to determine the cracks that occur at micro-level, which were not visible in the experiments and it is assumed that they occurred.
- The use of another ductile adhesive other than Crestomer 1152 PA. Due to the poor performance of this adhesive in terms of failure that occurred entirely in the interface, and also the lack of material information that in literature, it is recommended to use another ductile adhesive. For instance, a polyurethane such as SikaForce, which is widely used in wind turbines and other civil applications.

Furthermore, some recommendations are listed below for future work that could be done as a continuation of this thesis and to further extend the research on adhesively bonded joints.

- The analysis of the damage propagation in adhesive layers. It is suggested an study of the crack propagation using elasto-plastic models and smeared crack approaches.
- The analysis of the cohesive failure mode for the thin models (1 mm). Since the experiments showed a very different failure behavior for the 1 mm samples, compared to the 3 to 10 mm, it is proposed here the study of the cohesive behavior for thin adhesive layers in terms of the strain and stress distributions along the adhesive layer and the method how this results can be approximated by use of FE cohesive zone modelling.
- The study of the design of double lap joints applied to a real application. Since the design safety factors in this study are based on a small scale design and due to the fact that the values found are very much in line with values already given in regulations, it is suggested that the results obtained here could be used to study the design for a real application with previous knowledge of the loading and the geometry conditions.
- The mechanical behavior and resistance of double lap joints when subjected to both tension and bending. In this case, the loading was pure in tension. However, it is more realistic to think that in real applications these types of joints will be under different types of loadings. Therefore, an interesting research is to see how properties change and the suitability on applying such a design or which modification should be done in that case.
- Study of the degradation of the adhesively bonded joints in case the ambient conditions change, for instance if submitted to high temperatures and/or high moisture contents.

8 DISCUSSION

This research provides knowledge about the mechanical behavior of adhesively bonded joints for increasingly thickness, up to 10 mm. Up until this research was started, information was available for small thicknesses, mostly up to 2 mm, but very little was known for thicknesses higher than 2 mm. Furthermore, after this research it is possible to know in which failure mode the thick bonded joints are expected to fail.

The major implications of this research are, on one hand, the possibility of using thick bondline layers in double lap joints by knowing the expected resistance of such joints. As a consequence, in case the capacity of the joint is high enough, there will be no need of using any additional fasteners such as bolts and no drilling will be necessary. This latter will make a big change specially when using adherends of FRP, since the structure of the fibres might be prejudiced and affect the mechanical properties of the material when drilled. Thus, it will be possible to lessen the price of the double lap bonded joints, which in return will be more commonly used. Furthermore, if the capacity is determined beforehand, it will be possible to determine the maximum thickness of the bondline that can be used in the design.

However, it is important to remark that the strength of the joint can be lessened up to 50 % for large thicknesses (10 mm In the case of Araldite, 5 mm for Crestomer). For the 10 mm bondline joints, failure occurred in the adhesive but propagated in a line very close to the interface. Thus, to some extent, the increase of the thickness might result in a test of the properties of the interface and the surface preparation other than to the adhesive properties itself.

On the other hand, the obtained finite element, which matched the experimental results in terms of location of the failure initiation for thick bondlines, can be used as a tool to determine the stresses in the adhesive layer, the strains and the expected location of the initiation of the failure. However, these models do not assign damage propagation neither within the adhesive layer nor in the interface. Thus, they do not allow to predict the development of the crack that was observed in the experiments. Currently, some new tools for modelling crack propagation are being used in FE analysis such as XFEM. However, this method is still in research, at a very initial stage. Other available methods to study the crack propagation are the smeared crack method, which requires more input parameters than those normally known during design, and the cohesive zone modelling, in which case the crack path has to be predefined.

REFERENCES

[1] P. N. H. Wright, Y. Wu, and A. G. Gibson, *Fibre reinforced composite-steel connections for transverse ship bulkheads*, Composites:PartA,vol.29,no.10,pp.549–557,2000.

[2] Çiçek Özes and Nurhan Neser, *Experimental Study on Steel to FRP Bonded Lap Joints in Marine Applications*, Dokuz Eylul University, Turkey, 2015.

[3] M. Heshmati, R. Haghani and M. Al-Emrani, *Environmental durability of adhesively bonded FRP/steel joints in civil engineering applications: State of the art,* Chalmers University of Technology, Sweden, 2015.

[4] X. Jiang, M.H. Kolstein, F.S.K. Bijlaard, *Study of mechanical behaviours of FRP-to-steel adhesively-bonded joint under tensile loading,* Delft University of Technology, The Netherlands, 2012.

[5] T. Vallee, J.R. Correia and T. Keller, *Probabilistic strength prediction for double lap joints composed,* Swiss Federal Institute of Technology EPFL, Lausanne, 2006.

[6] J.R. Vinson, *Adhesive bonding of polymer composites*, Polymer engineering and science, Vol. 29, No. 19, University of Delaware, US, 1989.

[7] I.J. van Straalen, *Development of design rules for structural adhesive bonded joints – A systematic approach.* Delft University of Technology, The Netherlands, 2001.

[8] M.D. Banea and L.F.M. da Silva, *Adhesively bonded joints in composite materials: an overview.* Institute of Mechanical Engineering (IDMEC), Porto, 2008.

[9] M. Afendi, *Study on effect of bond thickness upon adhesive strength and fracture characteristics of brittle epoxy adhesively bonded dissimilar joints.* University of Tsukuba, Japan, 2011.

[10] M.J. Davis and D. Bond, *Principles and practice of adhesive bonded structural joints an repairs.* Directorate General of Technical Airworthiness, Royal Australian Air Force, Australia, 1999.

[11] V. Mara, *Development of connections for fiber reinforced bridge elements and an analysis of sustainability* (Unpublished doctoral thesis). Chalmers University of Technology, Gothenburg, 2015.

[12] G. Ji, Z. Ouyang, G. Li, S. Ibekwe and S. Pang, *Effects on global and local Mode-I interfacial fracture of bonded joints,* Louisiana State University, US, 2010.

[13] R.Haghani, *Analysis of adhesive joints used to bond FRP laminates to steel members – A numerical and experimental study,* Chalmers University of Technology, Gothenburg, 2010.

[14] K. Diharjo, M. Anwar, R.A.P. Tarigan and A. Rivai, *Effect of adhesive thickness and surface treatment on shear strength on single lap joint Al/CFRP using adhesive of epoxy/Al fine powder,* Sebelas Maret University, Indonesia, 2016.

[15] J.M. Arenas, J.J. Narbon and C. Alia, *Optimum adhesive thickness in structural adhesives joints using statistical techniques based on Weibull distribution,* Technical University of Madrid, 2010.

[16] J.P.-H. Belnoue and S.R. Hallett, *Cohesive/adhesive interaction in ductile adhesive joints Part I: A smeared-crack model for cohesive failure,* University of Bristol, UK, 2016.

[17] J.P.-H. Belnoue, S. Giannis, M. Dawson and S.R. Hallett, *Cohesive/adhesive interaction in ductile adhesive joints Part II: Quasi-static and faigue analysis of double lap-joint specimens subjected to through-thickness compressive loading,* University of Bristol, UK, 2016.

[18] Y. Zhu and K. Kedwards, *Methods of analysis and failure predictions for adhesively bonded joints of uniform and variable bondline thickness.* Department of Mechanical and Environmental Engineering, University of California, US, 2005.

[19] J.S. Tomblin, C. Yang, and P. Harter, *Investigation of thick bondline adhesive joints.* Wichita State University, US, 2001.

[20] A.A. Taib, R. Boukhili, S.Anchiou and H. Boukehili, *Bonded joints with composite adherends. Part II: Finite element analysis of joggle lap joints,* Polytechnique Montreal, Canada, 2005.

[21] L.F.M. da Silva and R.D. Adams, *Measurement of the mechanical properties of structural adhesives in tension and shear over a wide range of temperatures,* Department of Mechanical Engineering and Industrial Management, University of Porto, Portugal, 2004.

[22] D.A. Dillard and A.V. Pocius, *The mechanics of adhesion,* Elsevier Science B.V., 2002.

[23] B. Broughton and M. Gower, *Measurement good practice guide n.47. Preparation and testing of adhesive joints*, National Physical Laboratory, UK, 2001.

[24] B. Broughton, *Measurement good practice guide n.28. Durability performance of adhesive joints*, National Physical Laboratory, UK, 2000.

[25] ISO 15166-1/2: 2000 (En), Adhesives – Methods of preparing bulk specimens, ISO, 2000.

[26] ISO 527-2: 2012, Plastics – Determination of tensile properties – Part 2: Test conditions for moulding and extrusion plastics, ISO, 2012.

[27] ASTM D5379, Standard test method for shear properties of composite materials by the V-Notched beam method, ASTM International, West Conshohocken, PA, 2005.

[28] ISO/DIS 11003-2 (2000-03-00) (E), Adhesives – Determination of shear behaviour of structural bonds, Part 2: Thick-adherend tensile-test method, ISO, 1993.

[29] ISO 604: 2002, Determination of compressive properties, ISO, 2002-03.

[30] ASTM D695, Standard test method for compressive properties of rigid plastics, ASTM International, West Conshohocken, PA, 2015.

[31] ASTM D5573-99, Standard practice for classifying failure modes in fiber-reinforced-plastic (FRP) joints, ASTM International, West Conshohocken, PA, 2012.

[32] HUNTSMAN (2013), Araldite 2015. Technical data sheet. Switzerland, Huntsman advanced materials

[33] SCOTT BADER (2014), Crestomer 1152PA. Technical data sheet. UK, Scott Bader Company Limited

[34] PROSPECTOR (2014), Epoxy typical properties Generic epoxy, Technical data sheet, Germany, Prospector.

[35] LOCTITE (2011) Design guide for bonding plastics Volume 6. US, Henkel Corporation Engineering Adhesives

[36] 3M, *Choosing and using a structural adhesive*, Industrial adhesives and tapes division, 2012.

[37] Y. Najeeb Ali, *Failure analysis of bonded steel/CFRP laminate connections*. PhD thesis, University of Glasgow, UK, 2015.

[38] G. Kelli, *Joining of carbon fibre reinforced plastics for automotive applications,* Royal Institute of Technology, Stockholm, 2004.

[39] C. Syn., S. Gil, J. Yoon and M. Kim, *Lap shear strength of adhesively bonded composites,* Korea Aerospace Industries, 2011.

[40] J.Van Bitterswyk, D.Backman, J. Laliberte and R.Cole, *Application of Digital Image Correlation to the Thick Adherend Shear Test,* In: Cloud G., Patterson E., Backman D. (eds) Joining Technologies for Composites and Dissimilar Materials, Volume 10. Conference Proceedings of the Society for Experimental Mechanics Series. Springer, Cham, 2017.

[41] L.F.M. da Silva, R.A.M. da Silva, J.A.G. Chousal and A.M.G. Pinto, *Alternative methods to measure the adhesive shear displacement in the Thick Adherend Shear Test,* In: Journal of adhesion Science and Technology 22, Department of Mechanical Engineering and Industrial Management, University of Porto, Portugal, 2008.

[42] B. Xu, *Fracture mechanisms and failure criteria of adhesive joints and toughened epoxy adhesives*, School of Engineering and Materials Science, Queen Mary, University of London, UK, 2010.

[43] G. Pesquet, L.F.M. da Silva and C. Sato, *The use of thermally expandable microcapsules for increasing the toughness and heal structural adhesives,* Department of Mechanical Engineering and Industrial Management, University of Porto, Portugal, 2014.

[44] S. Teixeira de Freitas and J. Sinke, *Adhesion properties of bonded composite-to-aluminium joints using peel tests,* The Journal of Adhesion, Delft University of Technology, The Netherlands, 2014.

[45] S. Teixeira de Freitas and J. Sinke, *Test method to assess interface adhesion in composite bonding,* Faculty of Aerospace Engineering, Delft University of Technology, The Netherlands, 2015.

[46] H. Hadavania, L. Kawashita, A.J. Kinloch, D.R. Moore and J.G. Williams, *A numerical analysis of the elasto-plastic peel test*, Department of Mechanical Engineering, Imeprial College London, 2006.

[47] R.D.S.G. Campilho, M.D. Banea, J.A.B.P. Neto and L.F.M. da Silva, *Modelling adhesive joints with cohesive zone models: effect of the cohesive law shape of the adhesive layer,* Oporto Polytechnic Institute, Portugal, 2013.

[48] R. B. Heslehurst, *Design and analysis of structural joints with composite materials*, University of New South Wales, Australian Defence Force Academy Canberra, USA, 2013, p. 47-48.

[49] Mecmesin, Types of peel test, photograph, viewed July 2017, <http://www.mecmesin.co/peel-test-adhesion-testing>

[50] S. Dragt (TNO), F. van Eeden (TNO), I. Schipperen (TNO), C. Verhaeghe (DSNS) and A. Ruitenberg (DSNS), *DTP Bonded Joints; WP1; Literature study.* TNO_2016_R11802 [Draft report], 2017.

[51] F. S. K. Bijlaard (TNO), G. Sedlacek (RWTH) and J.W.B. Stark (TNO-IBBC), *Procedure for the determination of design resistance from tests; Eurocode 3.* BI-87-112, 1988.

[52] National Physical Laboratory, *Manual for the calculation of Elastic-Plastic materials models parameters.* NPL [Electronic Guide], 2007.

APPENDIX 1. TEST PLAN

Adhesives are often used in structural applications as a joining material. However, not much is yet known of bonded joints with adhesive thicknesses between 1 and 10 mm. To learn more about the effect of increasingly adhesive thickness on the mechanical properties of the adhesive bonded joints and how they behave in shear; a set of adhesively bonded double-lap joints are tested in shear loading. Once the tests are finalized, the obtained data will be analyzed and the outcome will be compared to the results obtained with finite element modelling.

The test proposed consist of small scale test with a simplified geometry. Thus, experience is gained and can be used for the development of large scale test which might be performed in a future.

These tests will constitute the experimental part of the thesis "The thickness effect in hybrid bonded joints", which is written as part of the research project C*omposite Joints*. This project consists of a Joint Industry Project (JIP) in which TNO is involved.

The performance of these tests has two main goals. On one hand, the goal is to determine the load related to the applied displacement with special importance on the load at failure. On the other hand, to determine the strain fields and displacements in the adhesive layer, which are also related to the relative displacement of the adherends.

1 Test set-up

The tensile shear strength test for double lap joints is performed based on the Standard Test Method ASTM D 3528. This test method is designed to determine the shear strength of adhesives in a peel-free standard specimen. The double lap joint specimen is placed in the test machine and loaded in tension at a constant rate.

1.1 Test specimens

The test specimens have the layout shown in figures 1 and 2. The dimensions of the specimens were chosen in accordance with the dimensions of the joints tested in the Composite Joints JIP project. The dimensions reproduce in small scale the dimensions suggested in the standard.

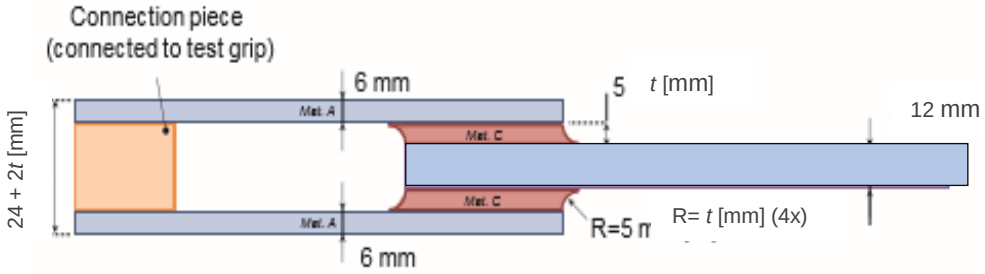

Figure A.1.1. Side view of a small scale test specimen with a generic thickness t adhesive layer

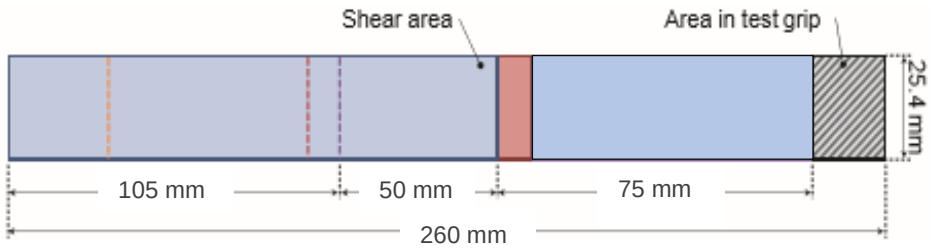

Figure A.1.2. Front view of a small scale test specimen with a generic thickness t adhesive layer

There are two types of specimens, a maritime specimen and a civil specimen. The specimen's name is related to the adhesive material used, which is Araldite 2015 for the maritime and Crestomer 1152PA for the civil specimen. For both the maritime and civil types, different thicknesses of adhesives are tested, which will condition the overall dimensions of the specimen. It is important to point out that the same layout holds for both specimens. As shown in figure 1, the overall thickness is determined as (24 + 2*t*) mm, being *t* the adhesive thickness.

In order to reduce the amount of variables in the study of the thickness effect of adhesive layer, these parameters are kept constant for all the variations of the adhesive thickness:

- Overall length of 260 mm
- Adhesive length of 50 mm
- Adherend thickness of 6 mm for the outer sheets and 12 mm for the inner sheet
- Overlap length of 50 mm

The design of these specimens was done by simplifying the large scale specimens that are used in real applications. Therefore, the DLJ tests as described in ASTM D 3528 is followed where possible.

The properties of the different components are:

- Maritime specimen
    - Steel adherends
        - Material: Steel – S355
        - Dimensions: Length: 155 mm; thickness: 6 mm (outer), 12 mm (inner); width: 25.4 mm.
        - Pre-treatment: TBD
    - Adhesive layers
        - Material: Epoxy – Araldite 2015
        - Dimensions: Overlap length: 50 mm; thickness: t, width: 25.4 mm.
        - Adhesive tip shape: fillet with *t* mm radius (x4)
    - Connection piece
        - Material: Steel – S355
        - Dimensions: One plate of 12 mm thickness and multiple thin plates of 1, 2 or 4 mm covering the total thickness of (12 +2*t*) mm.
        - Re-usable. Multiple layers adjusted upon specimen layout.

- Civil specimen
    - Steel adherends
        - Material: Steel – S355
        - Dimensions: Length: 155 mm; thickness: 6 mm (outer), 12 mm (inner); width: 25.4 mm.
        - Pre-treatment: TBD
    - Adhesive layer
        - Material: Urethan Acrylate – Crestomer 1152 PA
        - Dimensions: Overlap length: 50 mm; thickness: t, width: 25.4 mm.
        - Adhesive tip shape: fillet with *t* mm radius (x4)
    - Connection piece
        - Material: Steel – S355
        - Dimensions: One plate of 12 mm thickness and multiple thin plates of 1, 2 or 4 mm covering the total thickness of (12 +2*t*) mm.
        - Re-usable. Multiple layers adjusted upon specimen layout.

1.2 Instrumentation

A front view of the test set-up is shown in Figure 3. Tests are performed using a 25 ton hydraulic universal testing machine, where the specimens are held by a pair of self-aligning grips. On one end (upper end in the figure) the grip holds the specimen inside the LVDT load cell and has to move into alignment as soon as the load is applied. On the other end (lower end in figure) the adherends are held by another grip and also fixed by two bolts, used in combination with the connection piece. Thus, the adherends are perfectly aligned with the direction in which load is applied and any lateral displacement or rotation is avoided.

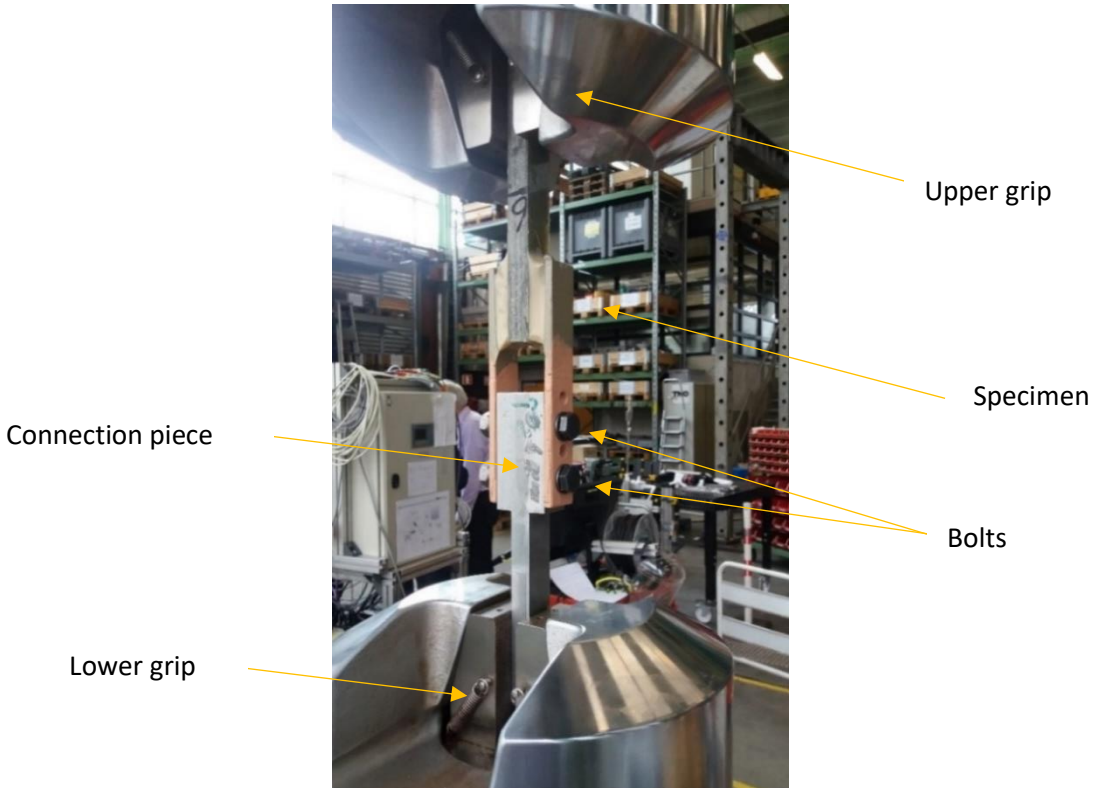

Figure A.1.3. Test device layout

The connection piece will be adjusted to the thickness of the specimen. It consists of one piece of 12 mm thickness and small plates of 1, 2 and 4 mm. These plates are placed symmetrically at both sides of the main piece, covering the total thickness of (12 + 2*t*) mm. Both the tick and all the thin plates have two holes in the same position. Thus, two perfectly aligned bolts are placed connecting the connection piece to the outer adherends and ensuring that bending is not introduced.

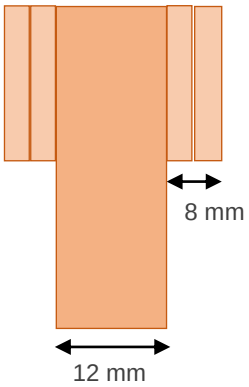

Figure A.1.4. Connection piece, steel S355. Example for specimen with 8 mm adhesive layer

1.3 Measuring equipment

The specimen is connected with two sensors, located in the positions showed in Figure 5 in order to measure the relative displacement of the adherends. It Is important to note that a distance of at least 100 mm has to exist between the two clamps that hold the sensors.

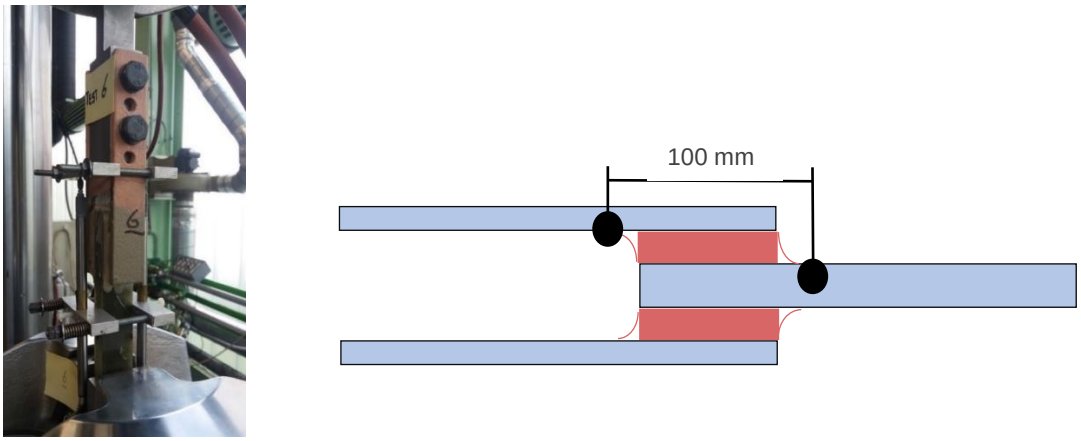

Figure A.1.5. Sensors layout and detail of the positioning of the sensors.

Additionally to the sensors, a high-speed video camera is used to record the crack initiation and propagation. The speed of the high-speed camera will be 2000 fps.

1.4 Specimen classification and parameters

The two types of tested specimens are built for several adhesive thicknesses. The maritime specimen is tested for five different thicknesses whereas the civil, only for three. The thicknesses to be tested were chosen according to the typically used in bonded joints in the two application areas, which suggested some upper boundaries. For the Araldite 2015, the upper boundary was set to 10 mm and for the Crestomer 1152PA; to 5 mm. The lower boundary was set to 1 mm because with this thickness information is available in the literature for Araldite 2015. Thus, the test results will be compared to the findings in the literature. Due to the tolerances in the production, it was decided to leave a gap of at least 2 mm between the different thicknesses. Therefore, the thicknesses to be tested are 1, 3, 5, 8 and 10 mm. For each thickness, 5 equal specimens are tested, giving a total of 40 specimens.

Adhesive	**Adherend**	**Test method**	**Bondline thickness [mm]**	**Number of tests**
Crestomer 1152PA	Steel S355	Tensile shear	1	5
			3	5
			5	5
Araldite 2015	Steel S355	Tensile shear	1	5
			3	5
			5	5
			8	5
			10	5
				40

Table A.1.1. Test matrix

1.5 Preparation of specimens

Note that the preparation of the specimens is done externally by MOCS. The specifications on the fabrication process will be explained in this section as provided by the producer.

1.6 Loading and test conditions

The specimens are tensile loaded under displacement control conditions. The *Testing Machine* has to maintain a rate of loading by applying a crosshead motion of 1.27 mm/min (0.05 inch/min) as stablished by the ASTM D 3528 standard.

The capacity of the testing machine was determined with the finite element results, which are also used to check the dimensioning of the specimens, i.e. the thickness of the adherends. Since the focus of this thesis is on the behavior of the adhesive layer when varying its thickness, it is very important to note that the specimen should not fail due to failure of one of the adherends.

The tests are conducted at room temperature (23 ± 2^{o} C). To ensure this approximate temperature condition, all specimens have to be kept in the lab for at least 24 hours before testing. No specific requirements are set to the humidity condition.

2 Test program

The tests and all the procedures prior and post testing will be performed at the TNO laboratory.

2.1 Before testing

The first step in the test program is to do a quality control of all the specimens. The purpose of this step is to ensure that the specimens were prepared correctly and fulfill the specified requirements. The quality control consist of:

- Measurement of dimensions with special attention to the adhesive layer thickness; the width and the overlap length to determine the shear areas.
- Supervision of the surface finishing of the adhesive.
- Identification that there are no voids in the adhesive layer.
- Supervision that the holes in the outer adherends are in the same line to avoid asymmetrical loading.

The specimens are numbered and coded according to the adhesive thickness. The code used for this experiments will be determined as follows: *A-X-Y*, where:

- *A* refers to the type of specimen. *C* stands for civil, *M* for maritime.
- *X* refers to the thickness of the adhesive layer. *X* will be 1,3,5,8 or 10.
- *Y* refers to the number of sample, from 1 to 5.

The numbering has to be present on the three adherends so afterwards the numbers can be used for the reconstruction of the failed specimen.

Specimens are photographed including a front and side view. By doing so, evidence of the quality remains available in case any inspection is required after the finalization of the experiments.

2.2 Measurement during testing

During the test the following parameters are measured:

- Applied load (also specify the load at failure), measured with the load cell;
- Displacement of the crosshead, measured with the LVDT;
- Displacement of adhesive layer at two points (back and front), measured by the sensors;
- Strain and displacement fields in the adhesive layer, measured with DIC.

- Starting location of the specimen failure, obtained by a high-speed video recording a front and side vie of the specimen.

2.3 Post-measurements

After the test program is run, the post-measurements consist of:

- Inspection of the specimens. Determination of the nature of failure (cohesive or adhesive). In case a mixed failure is visible, determination of the percentage of each failure mode.
- Photography of the specimens including side view and front view of the surfaces.
- Storage of the specimens under lab conditions (constant temperature and humidity). Hereby, inspection of the specimens after testing is possible if need.

2.4 Detailed test program

In total, five samples of each specimen type are prepared, giving a total of 40 tests to be performed. In average, it is expected that 10 to 12 specimens are tested per day. Therefore, test are expected to be performed within 3 to 4 days.

Table A2 shows the detailed test program as performed.

Action	**Time required**	**Timeline of testing**
Production of specimens (Prior)	6 – 8 weeks	
Quality control of specimens	Hours	Day 1
Photography	Hours	Day 1
Number the specimens	Hours	Day 1
Testing	4/5 days	Day 1 – 3/4
Inspection and photography	Hours (or while testing)	Day 3/4
Processing of results	3 – 4 weeks	Day 5 - 30

Table A.1.2. Test program

3 Time schedule

	17	18	19	20	21	22	23	24	25	26	27	28	29	30	31	32
	3-jul-17	10-jul-17	17-jul-17	24-jul-17	31-jul-17	7-aug-17	14-aug-17	21-aug-17	28-aug-17	4-sep-17	11-sep-17	18-sep-17	25-sep-17	2-okt-17	9-okt-17	16-okt-17
Approval of test matrix																
Order the specimens																
Production of specimens																
Pre-processing																
Testing (4 days)																
Processing of results																

Table A.1.3. Test timeline

In total, the work at the laboratory is expected to take 5 days.

Thus, 5 days are required including half a day of preparation, 4 days of experiments (considering that 10 specimens are tested per day) and half a day more as extra time in case of testing is not finished or there are still remaining activities to be done.

APPENDIX 2. TABLES AND FIGURES

Figure A.2.1. Araldite, failure surfaces of all samples

Parameters at failure

This table includes the experimental results at failure, i.e. the maximum load and the calculated double lap shear strength. For every series also the mean value and the standard deviation was calculated.

Mean shear stress: $\bar{\tau} = (\sum \tau_i)/n$

Standard deviation: $S = \sqrt{\frac{\sum(\tau_i - \bar{\tau})^2}{n-1}}$

	Sample	Max force [kN]	Mean F_{max} [kN]	STDV	Lap Shear strength τ [MPa]	Mean τ [MPa}	STDV
1 mm	c11	45.1	43.84	2.01	17.41	16.92	0.77
	c12	40.7			15.71		
	c13	43.7			16.87		
	c14	46			17.76		
	c15	43.7			16.98		
	a11	51.4	50.44	1.12	19.84	19.47	0.43
	a12	50.8			19.61		
	a13	51.3			19.80		
	a14	50			19.30		
	a15	48.7			18.80		
3mm	c31	38.3	38.62	1.16	14.23	14.34	0.43
	c32	38.9			14.45		
	c33	40.5			15.04		
	c34	37.8			14.04		
	c35	37.6			13.97		
	a31	43.5	43.98	0.63	16.16	16.33	0.23
	a32	44.9			16.68		
	a33	44.1			16.38		
	a34	44.1			16.38		
	a35	43.3			16.08		
5mm	c51	20.3	19.72	1.61	7.27	7.06	0.58
	c52	21.5			7.69		
	c53	19.9			7.12		
	c54	19.8			7.09		
	c55	17.1			6.12		
	a51	36.4	37.82	2.20	13.03	13.54	0.79
	a52	37.5			13.42		
	a53	38.3			13.71		
	a54	41.3			14.78		
	a55	35.6			12.74		
8 mm	a81	27.1	28.10	2.69	9.20	9.53	0.91
	a82	31.1			10.56		
	a83	29.2			9.91		
	a84	24			8.15		
	a85	29.1			9.88		
10 mm	a10 1	31.3	28.62	2.90	10.27	9.39	0.95
	a10 2	24.3			7.97		
	a10 3	27.3			8.96		
	a10 4	29.2			9.58		
	a10 5	31			10.17		

Table A.2.1. DLJ experimental results at failure

	Sample	Max force [kN]	Time to failure [s]	Time [s] Mean ± STD	Displacement at failure [mm]	Displ. at failure [mm] Mean ± STD
1 mm	c11	45.1	120	111.6 ± 9.8	1.093	1.0 ± 0.1
	c12	40.7	97		0.816	
	c13	43.7	114		1.117	
	c14	46.0	120		1.093	
	c15	43.7	107		0.841	
3mm	c31	38.3	159	178 ± 12.7	2.089	2.4 ± 0.2
	c32	38.9	184		2.311	
	c33	40.5	193		2.718	
	c34	37.8	180		2.513	
	c35	37.6	174		2.348	
5mm	c51	20.3	194	180.7 ± 32.8	3.045	2.9 ± 0.6
	c52	21.5	221		3.649	
	c53	19.9	156		2.513	
	c54	19.8	152		2.428	
	c55	17.1	EXCL. 106		EXCL. 1.631	

Table A.2.2. Maximum force, Failure-time and maximum displacement for Crestomer

The sample c55 was excluded from the group Crestomer 5mm since it failed much earlier than the samples in the same group and with lower strength than the mean. As a consequence the mean failure-time has changed from 166 to 181 seconds and the standard deviation, from 44 to 32.8.

	Sample	Max force [kN]	Time to failure [s]	Time [s] Mean ± STD	Displacement at failure [mm]	Displ. at failure [mm] Mean ± STD
1mm	a11	51.4	76.5	87.9 ± 8.1	0.435	0.45 ± 0.04
	a12	50.8	96.2		0.473	
	a13	51.3	95.3		0.507	
	a14	50.0	84.7		0.424	
	a15	48.7	87.0		0.394	
3mm	a31	43.5	76.7	88.9 ± 8.6	0.364	0.33 ± 0.06
	a32	44.9	84.1		0.387	
	a33	44.1	90.9		0.375	
	a34	44.1	98.7		0.274	
	a35	43.3	93.9		0.261	
5mm	a51	36.4	57.4	76.1 ± 13.3	0.227	0.26 ± 0.03
	a52	37.5	EXCL.143		0.217	
	a53	38.3	76.2		0.283	
	a54	41.3	84.2		0.279	
	a55	35.6	86.8		0.243	
8 mm	a81	27.1	50.6	54.2 ± 9.1	0.221	0.24 ± 0.04
	a82	31.1	70.2		0.310	
	a83	29.2	51.2		0.244	
	a84	24.0	47.9		0.211	
	a85	29.1	51.0		0.208	
10mm	a10 1	31.3	60.2	76.2 ± 17.9	0.332	0.29 ± 0.06
	a10 2	24.3	67.8		0.217	
	a10 3	27.3	71.3		0.241	
	a10 4	29.2	106.6		0.315	
	a10 5	31.0	75.3		0.347	

Table A.2.3. Maximum force, Failure-time and maximum displacement for Araldite

The sample a52 was excluded from the group Araldite 5mm for the calculation of time-to-failure, since the machine was not properly connected for the first half of the test. However, maximum force and displacement were recognized.

Crestomer – all samples

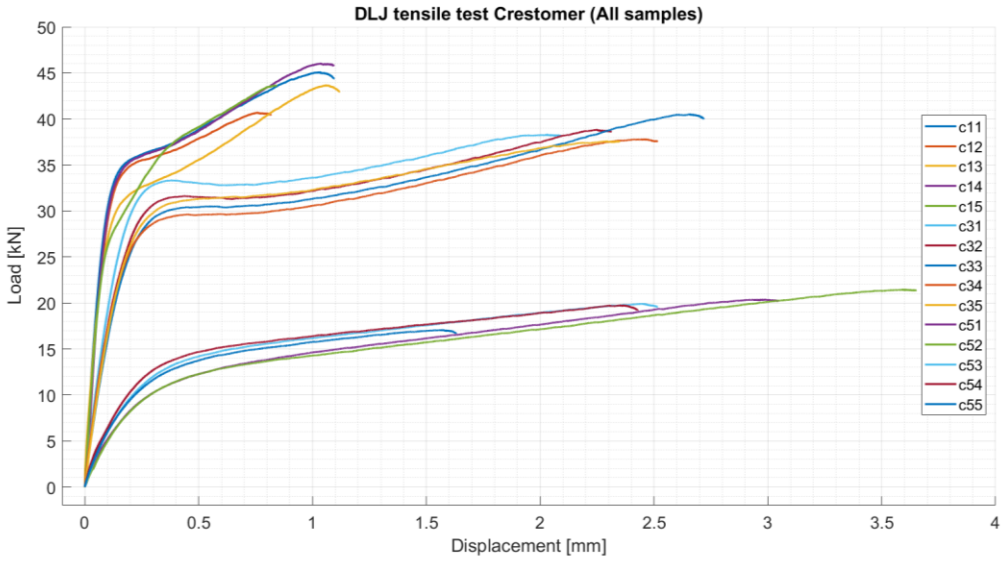

Figure A.2.2. Crestomer Load – displacement curves obtained in the DLJ tests

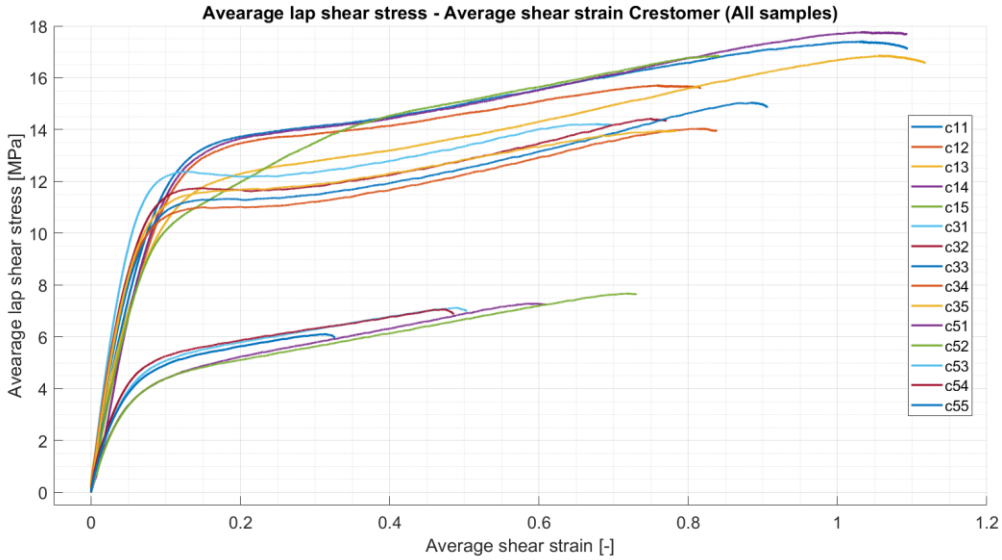

Figure A.2.3. Crestomer Average lap shear stress – Average shear strain curves obtained in the DLJ tests

Araldite – all samples

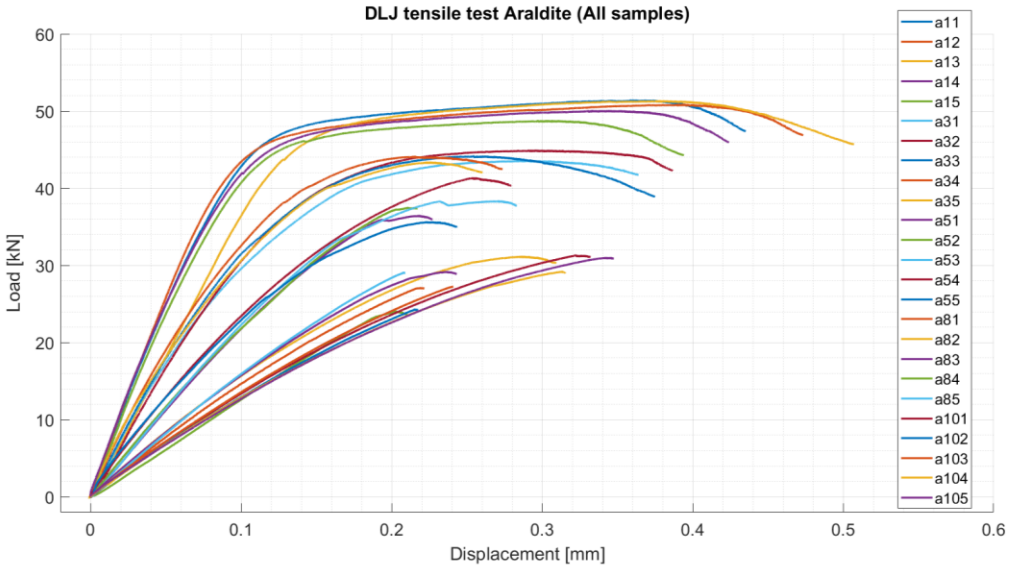

Figure A.2.4. Araldite Load – displacement curves obtained in the DLJ tests

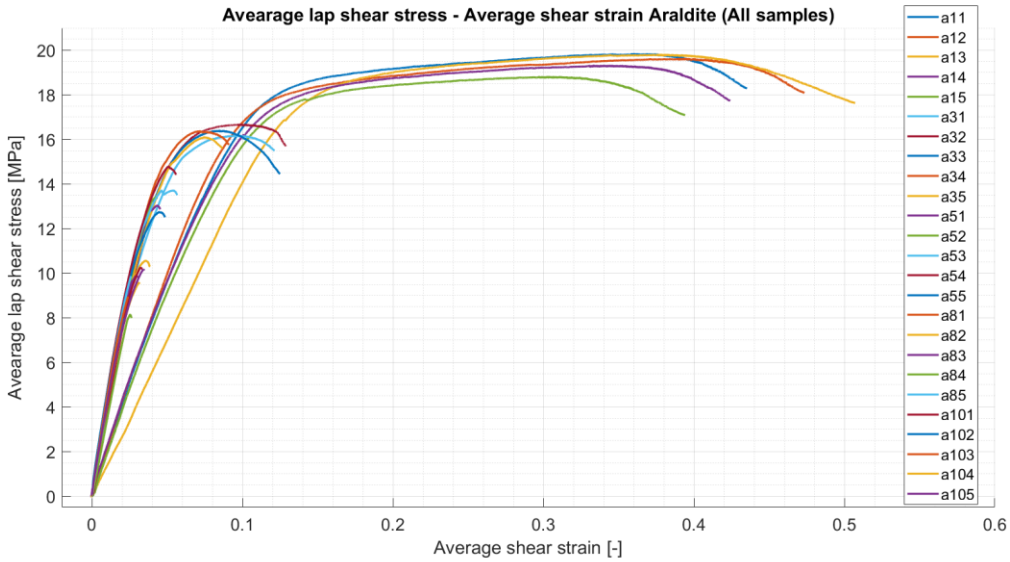

Figure A.2.5. Araldite Average lap shear stress – Average shear strain curves obtained in the DLJ tests

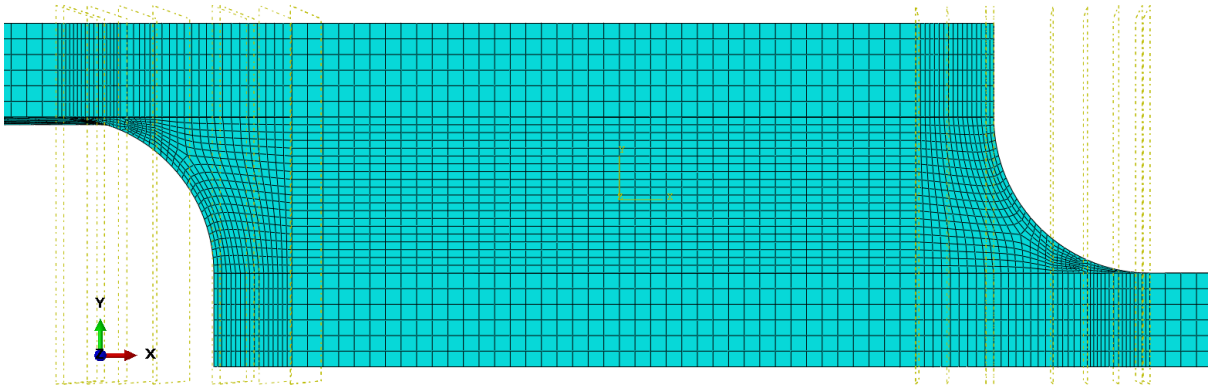

Figure A.2.6. Detail mesh 10 mm thickness

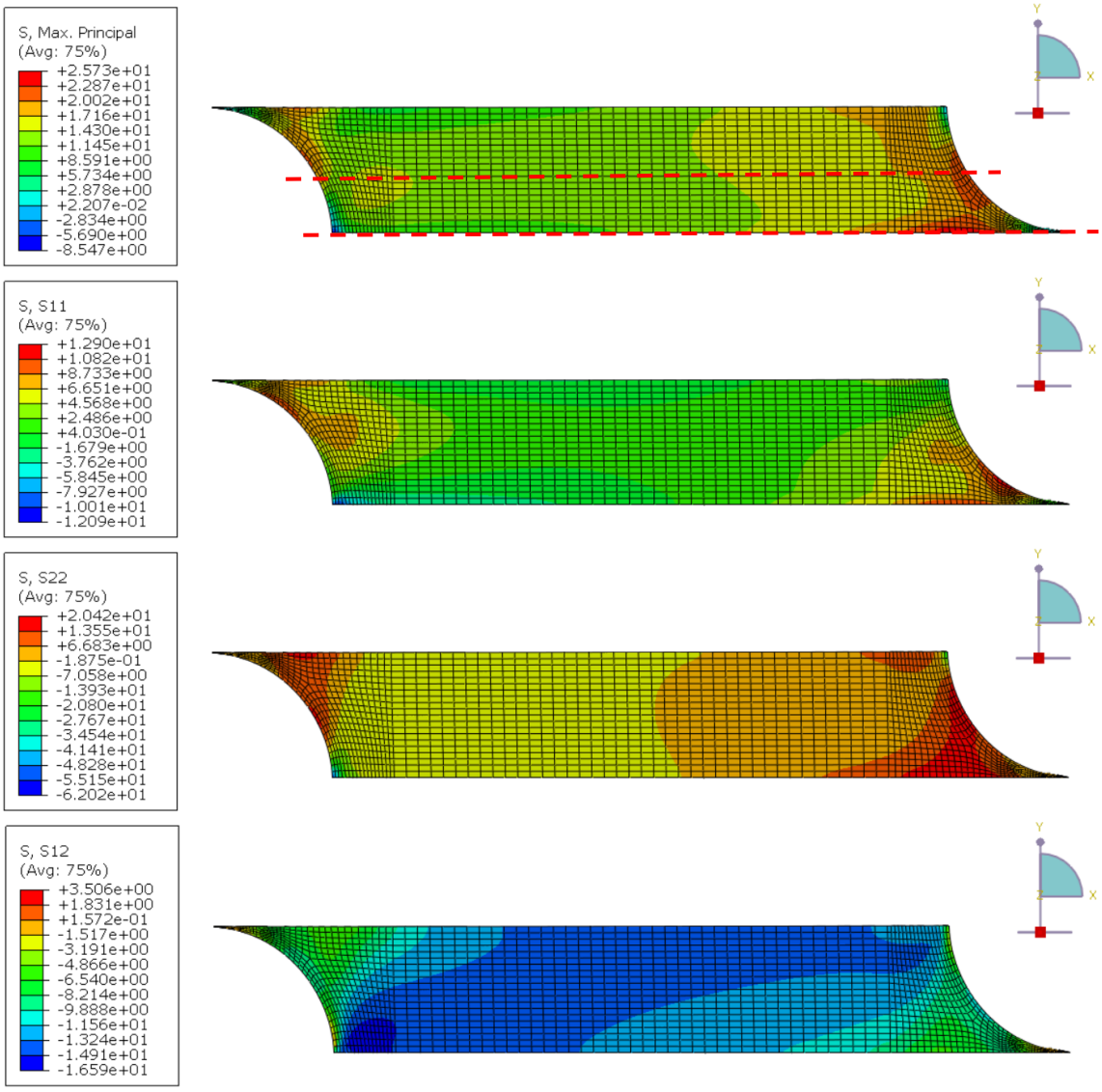

Figure A.2.7. Contour plot of Maximum principal stress, tensile stress (S11), peel stress (S22) and shear stress (S12) at ULS, Araldite 10mm. Dashed red lines indicate the lines along which the stresses are analyzed

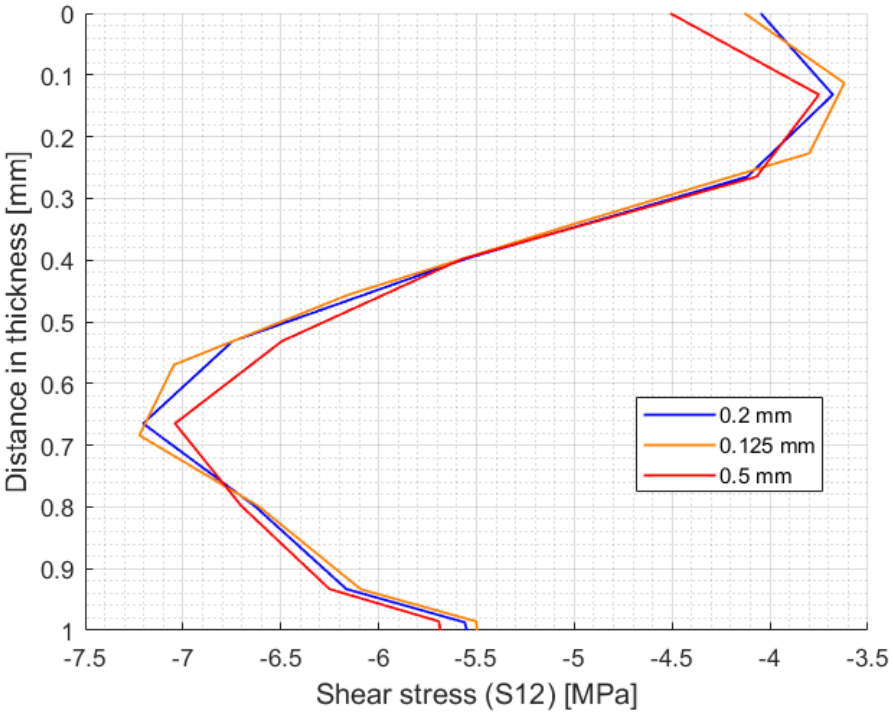

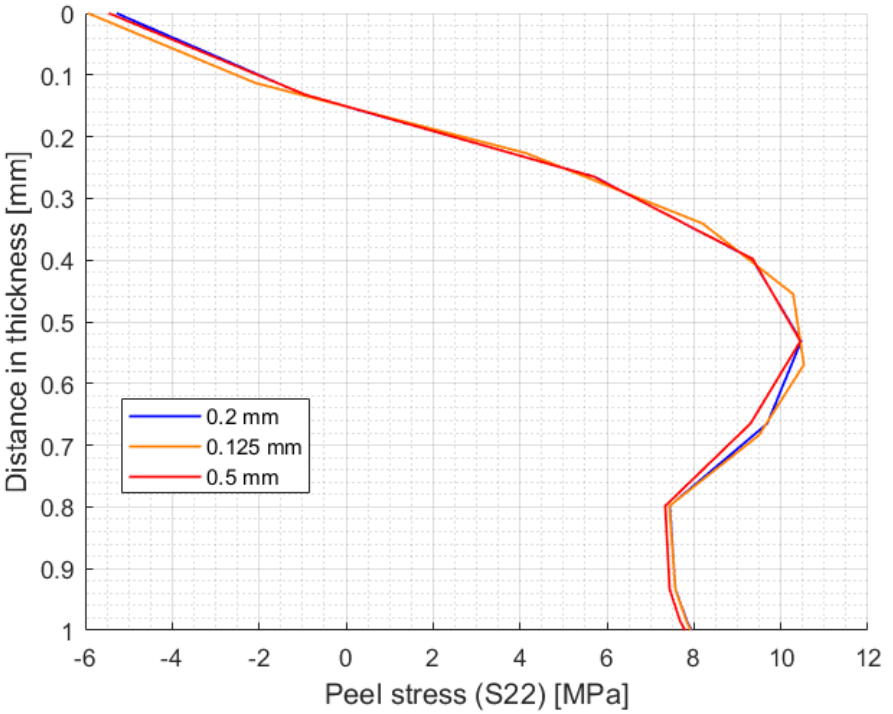

Figure A.2.8. Mesh sensitivity study. Shear stress (S12) and peel stress (S22) for different mesh sizes along thickness prior to Yield, Araldite 1 mm.

Measurements from samples

	Sample	Thickness [mm]	Width [mm]	Overlap length [mm]	Mean ± STD Thickness	Mean ± STD Width	Mean ± STD Overlap length
1mm	a11	1.2	25.5	51.5	1.26 ± 0.17	25.53 ± 0.11	50.5 ± 0.68
	a12	1	25.55	50.6			
	a13	1.4	25.4	50.5			
	a14	1.4	25.7	50.3			
	a15	1.3	25.5	49.6			
3mm	a31	2.9	25.2	53.5	3.24 ± 0.22	25.92 ± 0.61	53.7 ± 0.68
	a32	3.2	26.6	54			
	a33	3.3	26.5	54.1			
	a34	3.5	25.5	54.3			
	a35	3.3	25.8	52.6			
5mm	a51	4.8	25	54	5.12 ± 0.44	25.22 ± 0.38	54.74 ± 1.09
	a52	4.7	25.4	53.9			
	a53	5.6	24.9	54.6			
	a54	4.9	25	54.6			
	a55	5.6	25.8	56.6			
8 mm	a81	8.3	25.3	59	8.06 ± 0.31	25.02 ± 0.23	58.62 ± 0.70
	a82	8	25	58.5			
	a83	8.4	24.8	59.6			
	a84	7.6	24.8	57.8			
	a85	8	25.2	58.2			
10mm	a10 1	10.2	25.2	59	10.12 ± 0.19	24.92 ± 0.52	59.74 ± 1.48
	a10 2	10.1	25.6	59.7			
	a10 3	9.8	24.65	62			
	a10 4	10.3	24.9	58			
	a10 5	10.2	24.25	60			

Table A.2.4. Measured thickness, width and overlap length of Araldite samples

	Coef. Var. Thickness	Coef. Var. Width	Coef. Var. Overlap length
1 mm	0.132803	0.004291	0.013503
3 mm	0.06762	0.023688	0.012698
5 mm	0.086689	0.014942	0.019911
8 mm	0.03884	0.009114	0.011966
10 mm	0.019007	0.020687	0.02476

Table A.2.5. Coefficient of variation for thickness, width and overlap length of Araldite samples